FUNDAMENTAL STUDIES IN X-RAY ASTROPHYSICS

Grant NAGW 246

Semiannual Progress Report No. 1

For the period 15 October 1981 through 14 April 1982

Principal Investigators

Dr. Donald Q. Lamb

Dr. Alan P. Lightman

Prepared for

National Aeronautics and Space Administration
Washington, D. C. 20546

April 1982

Smithsonian Institution
Astrophysical Observatory
Cambridge, Massachusetts 02138

The Smithsonian Astrophysical Observatory
and the Harvard College Observatory
are members of the
Center for Astrophysics

The NASA Technical Officer for this grant is Dr. Louis J. Kaluzienski, Code SC-7, NASA Headquarters, Washington, D.C. 20546.

FUNDAMENTAL STUDIES IN X-RAY ASTROPHYSICS

Grant NAGW 246

Semiannual Progress Report No. 1

For the period 15 October 1981 through 14 April 1982

Principal Investigators

Dr. Donald Q. Lamb

Dr. Alan P. Lightman

Prepared for

National Aeronautics and Space Administration
Washington, D. C. 20546

April 1982

Smithsonian Institution
Astrophysical Observatory
Cambridge, Massachusetts 02138

The Smithsonian Astrophysical Observatory
and the Harvard College Observatory
are members of the
Center for Astrophysics

The NASA Technical Officer for this grant is Dr. Louis J. Kaluzienski, Code SC-7, NASA Headquarters, Washington, D.C. 20546.

FUNDAMENTAL STUDIES IN X-RAY ASTROPHYSICS

Grant NAGW 246

Semiannual Progress Report No. 1

For the period 15 October 1981 through 14 April 1982

Principal Investigators

Dr. Donald Q. Lamb

Dr. Alan P. Lightman

This report covers research by the Principal Investigators Don Q. Lamb and Alan P. Lightman, and by Visiting Scientist and Smithsonian Fellow Peter Mészáros who has been hired under the grant, during the period 15 October 1981 to 14 April 1982.

The research of Don Q. Lamb has concerned X-ray emission from degenerate dwarf stars, the physics of gamma-ray burst sources, and evolution of degenerate dwarf stars.

1. X-ray and UV Radiation from Accreting Nonmagnetic Degenerate Dwarfs

Lamb, in collaboration with N. D. Kylafis of Caltech and the Institute for Advanced Study, Princeton, has carried out an analytical model calculation of the circumstellar ionization structure of a spherically accreting degenerate dwarf. Unlike previous analytic treatments, they use self-consistent values of the parameters, and consider possible nuclear burning of the accreting matter. They find that the blackbody radiation emitted from the stellar surface ionizes hydrogen and helium out to distances much larger than a typical binary separation, and that the bremsstrahlung hard X-rays ionize heavy elements out to considerable distances. However, for low-mass stars or high accretion rates, absorption has a pronounced effect on the

observed X-ray spectrum. This work was recently submitted to The Astrophysical Journal.

2. Continuum and Line Spectra of Degenerate Dwarf X-ray Sources

Lamb summarizes recent observations of degenerate dwarf X-ray sources, and reviews theoretical work on their continuum spectra and lines. He discusses some of the important unresolved issues concerning these sources, and concludes with an outline of the kinds of X-ray observations that would best advance our understanding of them. This work is to be published in Proceedings of the Goddard Workshop on X-ray Astronomy, ed. S. Holt; and has been submitted to Space Science Reviews.

3. X-ray Emission from VV Puppis

Lamb, in collaboration with Joe Patterson, G. Fabbiano, and John Raymond (all of the Center for Astrophysics), Keith Horne (Caltech), and Nick White and Jean Swank (NASA-Goddard), has reported X-ray and ultraviolet observations of the accreting magnetic degenerate dwarf VV Puppis. These observations show it to be a spectacular source at soft X-ray energies (0.1-0.3 keV), but only weakly detected in hard X-rays and the ultraviolet. The orbital light curves in soft and hard X-rays are in excellent agreement with the mean optical light curve, indicating that essentially all the accretion luminosity data and the optical spectroscopy dictate a fairly well-constrained geometry for the system, but it is not understood why the soft X-rays so thoroughly dominate the energy budget of the system. This is a general problem in the AM Herculis stars, and possible solutions are discussed. This work is being submitted to The Astrophysical Journal.

4. Degenerate Dwarf Evolution

Lamb, in collaboration with Don Winget and Hugh Van Horn (University of Rochester), has carried out new evolutionary calculations of degenerate dwarf evolution. These calculations

include results for stratified envelopes composed of He/C and H/He/C. The results are generally in good agreement with the observational luminosity function recently derived by Liebert and Sion (1981). Comparison of the theoretical and observational luminosity function does indicate that the faint degenerate dwarfs now seen are descendants of the earliest-formed moderate mass stars in the galaxy, and has important implications for the rate of star formation in the galaxy at early times. This work is in preparation.

5. Gamma-ray Bursts

Lamb and Mészáros are working on the X-ray spectra and polarization properties of pair plasmas in strong magnetic fields, with application to the gamma-ray bursts. They find that the observed gamma-ray burst spectra are well-accounted for by high temperature cyclotron (gyrosynchrotron) emission, and that the circular and linear polarization properties of the spectrum are a unique diagnostic of the fraction of pairs in the plasma. They plan to extend their treatment to the cooling of hot pair plasmas, with the object of studying the temporal evolution of the continuum and the annihilation line, and comparing the results with observations.

The research of Alan P. Lightman concerned the structure of relativistic thermal plasmas and a general comparison of theories versus observations of the X-ray emission from quasars and active galaxies.

1. Pair Processes and Equilibria in Relativistic Thermal Plamsas

Lightman has investigated the equilibria available to relativistic thermal plasmas, taking into account the electron-positron creation and annihilation processes and photon production within the plasma. A major result is that for each value of $\tau_N \equiv RN\sigma_T$, there is a maximum temperature of an optically thin

plasma. (Here R and N are the size and proton number density, respectively, of the plasma and σ_T is the Thomson cross section.) This and associated results provide astrophysically relevant constraints on the sizes and temperatures of the emitting regions of quasars and active galaxies. Radiation spectra, which are directly observable, are also computed. This work was recently published in The Astrophysical Journal, 253, 842 (1982).

2. Cyclotron Photons in Relativistic Plasmas

The above project is now being extended by the inclusion of a magnetic field. Such a field produces cyclotron photons that may dominate the internally produced photons. The new photons will inverse Compton scatter up in energy and eventually participate in pair producing reactions. This work is still in progress.

3. Theory vs. Observations in X-rays from Quasars and Active Galaxies

We compile the observations of time variability and spectra from a large number of sources and test these results against various theoretical ideas for the conditions at the centers of AGN and QSOs and the radiation mechanisms. The observed time variabilities seem to require highly efficient $\epsilon \gtrsim 0.1$ accretion onto massive black holes, with emission regions near the Schwarzschild radius. The observed spectra, which are power law with energy index $\alpha \sim 0.7$, are consistent with nonthermal emission by relativistic electrons and possibly with thermal, Compton emission by semirelativistic electrons. It is important to observe spectral turnovers at high energies to further delineate theoretical models. This work is to be published in Proceedings of the Goddard Workshop on X-ray Astronomy, ed. S. Holt; and has been submitted to Space Science Reviews.

4. Statistical Analyses of X-ray Sources in Globular Clusters

Some outstanding puzzles regarding X-ray emitting globular clusters (XEGC) are (a) Why do globular clusters provide a favorable environment for forming discrete X-ray sources? (b) Why are XEGC

unusually near the galactic center? (c) Why do the observed clusters never contain more than a single discrete X-ray source? Adopting the model that X-ray sources in clusters consist of binary systems formed by two-body tidal interactions and using statistical analyses of the data, we find a plausible explanation for all these puzzles. We find a positive correlation between the two-body binary formation time, t_{B2}, and the distance from galactic center, R, for globular clusters in general. XEGC have significantly small values of R and t_{B2}. The values of t_{B2} and inferred lifetimes for X-ray sources yield rough quantitative agreement with the observed rate of occurrence of X-ray sources. This work was done in collaboration with Josh Grindlay and is in press of The Astrophysical Journal.

Peter Mészáros is working on accretion problems and plasma effects of e^+e^- pairs, with application to gamma-ray bursters and active galactic nuclei.

1. Plasma Effects of e^+e^- Pairs in a Neutron Star Magnetic Field

Mészáros, in collaboration with D. Lamb, is studying plasma effects of e^+e^- pairs in a neutron star magnetic field. When the pair density exceeds the nucleon density, they should strongly influence the dielectric properties of the medium, and produce observable effects in the polarization of X-rays. This would also modify the radiative cross sections (scattering, bremsstrahlung) to an extent that one can expect observable spectral effects to be correlated with the (possibly time dependent) pair density in gamma-ray bursters.

2. Time Dependent Behavior of a Light Pulse in a Scattering Medium

Time dependent behavior of a light pulse in a scattering medium is being studied in collaboration with G. Rybicki. The second time derivative of the time-dependent plane-parallel transfer equations was kept, and the Fourier transform was solved

by expansion in eigenfunctions, for the case of a finite slab, yielding an analytic solution. This is being tested at present to verify that it yields the correct physical behavior. This would be directly applicable to X-ray bursters, especially if in the future this is extended to include first order frequency changes in the scattering kernel.

3. Pair Formation Effects in Shocks Around Spherically Accreting Black Holes

Mészáros is studying pair formation effects in shocks around spherically accreting black holes with J. P. Ostriker (Princeton). At radii $\lesssim 10^3$ x Schwarzschild radius the post-shock electron temperature could be sufficient to create pairs, which then increase the opacity. It is suspected that for supercritical accretion rates this could give rise to a runaway pair density, which may stabilize at a particular shock radius, which depends on the pair density near the front and on the flow between the front and the Schwarzschild radius.

X-RAY AND UV RADIATION FROM ACCRETING NONMAGNETIC DEGENERATE DWARFS. III. PHOTOABSORPTION EFFECTS[1]

N.D. KYLAFIS

Department of Physics

University of Illinois at Urbana-Champaign

and

W.K. Kellogg Radiation Laboratory

California Institute of Technology

Pasadena, California 91125

and

D.Q. LAMB[2]

Department of Physics

University of Illinois at Urbana-Champaign

and

Harvard-Smithsonian Center for Astrophysics

---

1. Supported in part by the National Science Foundation [PHY78-04404, AST78-20123, and AST79-22012-A1], and the National Aeronautics and Space Administration [NSG7176 and NGR22-007-272].

2. John Simon Guggenheim Memorial Fellow.

ABSTRACT

We have carried out an analytical model calculation of the ionization structure of matter accreting onto a degenerate dwarf. Unlike previous analytic treatments of this problem, we use self-consistent values of the various parameters and include the possibility of nuclear burning of the accreting matter. We find that the blackbody radiation emitted from the stellar surface keeps hydrogen and helium ionized out to distances much larger than a typical binary separation. Except for low mass ($M \lesssim 0.5\ M_\odot$) stars or high accretion rates, the assumption of complete ionization of the elements heavier than helium is a good first approximation. For low mass stars or high accretion rates the validity of assuming complete ionization depends sensitively on the distribution of matter in the binary system.

I. INTRODUCTION

In a series of recent papers (Kylafis and Lamb 1981, hereafter Paper I; Weast *et al.*, 1981; Imamura *et al.*, 1981), the results of a comprehensive study of X-ray and UV emission from accreting nonmagnetic degenerate dwarfs were reported. One of the basic assumptions in this work was that the outgoing radiation is capable of keeping the infalling matter ionized without significant losses due to photoabsorption. In order to justify this assumption we have carried out a self-consistent analytical model calculation of the ionization and temperature structure of the accreting matter (Kylafis 1978; see also Hayakawa 1973; Fabian, Pringle, and Rees 1976; and Ross and Fabian 1980).

Among the first to consider the physical conditions of the gas surrounding a source of X-rays were Tarter, Tucker, and Salpeter (1969). They carried out numerical calculations of the ionization and temperature structure of a uniform density, optically thin spherical gas cloud with a point source of hard X-rays at its center, for a grid of radiation temperatures and hydrogen number densities. Optically thick environments with the same geometry were computed by Tarter and Salpeter (1969). A deficiency in both of the above calculations is that Compton heating of the gas was ignored. Tarter and McKee (1973) calculated numerically the various contributions to the average absorption cross section for a gas excited by power-law, bremsstrahlung, and blackbody sources of radiation. They used methods similar to Tarter, Tucker, and Salpeter (1969), but in addition they included Compton heating. Buff and McCray (1974) presented numerical calculations of the ionization and temperature structure of optically thin matter falling spherically symmetrically onto a neutron star or a black hole. Transfer of radiation through a spherically symmetric, optically thick gas cloud surrounding a point source of X-rays was also studied by Hatchett, Buff, and McCray (1976) in a way similar to that of Tarter and Salpeter (1969), but with Compton

heating and the Auger effect included. Their calculations, however, do not apply to cases where the optical depth of electron scattering is larger than one because they did not include the effects of Compton scattering on the X-ray spectrum. Such effects were included in subsequent calculations (Ross, Weaver, and McCray 1978; Langer, Ross, and McCray 1978; and Ross 1979).

Hayakawa (1973) carried out analytical model calculations of the ionization structure of matter accreting onto compact stars, but due to unavailable calculations he adopted inconsistent values of the X-ray luminosity, the bremsstrahlung temperature, and the stellar mass in his attempt to explain the spectrum of Sco X-1. Ross and Fabian (1980) were the first to compute numerically the effects of photoabsorption on the spectrum produced by spherical accretion onto a degenerate dwarf when the infalling gas is optically thick to Compton scattering. They described the results obtained for accretion onto a 1 $M_\odot$ degenerate dwarf and discussed briefly the implications for lower mass stars. A more complete survey for all stellar masses is now underway and will be presented elsewhere (Ross, Fabian, Kylafis, and Lamb 1981).

In this paper we present an analytical model calculation of the ionization and temperature structure of the matter accreting onto a degenerate dwarf, as well as the effects of photoabsorption on the emitted X-ray spectrum, using a method similar to that of Hayakawa (1973), but taking values for the different parameters consistent with our earlier calculations (Paper I; Weast *et al.* 1981). This work does not have the accuracy of the numerical calculations of Ross and Fabian (1980), but it has the advantage of being analytical.

The calculations reported here assume: (1) steady, spherically symmetric accretion, (2) weak or no magnetic field, and (3) that elements heavier than hydrogen have only two stages of ionization: hydrogenic and fully ionized. The first two assumptions were justified in Paper I. The third one is reasonable, because the

photoionization cross sections are dominated by the K-shell. This assumption, however, will cause the absorption edges to appear at higher energies than expected for neutral elements (Brown and Gould 1970; Fireman 1974).

In § II we estimate the physical conditions of the accreting matter, the ionization due to bremsstrahlung and blackbody radiation, and the effect of photoabsorption on the emitted X-ray spectrum. In § III we discuss our results and draw several conclusions.

II. CALCULATIONS

a) Physical Conditions

A qualitative picture of X-ray emission by accreting degenerate dwarfs was presented in Paper I. One of the conclusions there was that the outgoing spectrum consists of three components: the bremsstrahlung from the emission region, the blackbody radiation from the stellar surface, and the secondary radiation emitted from the heated infalling matter. In what follows we neglect the secondary radiation and make the following simplifying assumptions: 1) We approximate the bremsstrahlung component with an exponential spectrum

$$L(E) = \frac{L_x}{kT_x} e^{-E/kT_x} , \tag{1}$$

where L_x is the total luminosity of this component and T_x is its characteristic temperature, and 2) we assume that the blackbody component is described by a Planckian distribution of temperature T_{bb} given by equation (A11) in the Appendix, i.e., we neglect Comptonization effects because they are small. In contrast, Compton scattering effects on the bremsstrahlung component are very important and we take them into account by using the so-called scattering time approximation (Paper I). In this approximation, the final energy of a photon traversing an optical depth to electron scattering τ_{es} will be less than

$$E_0 = m_e \frac{c^2}{\tau_{es}^2} , \tag{2}$$

independent of its initial energy (Illarionov and Sunyaev 1972); that is, all photons with initial energy greater than E_0 will be degraded to about $E = E_0$. If we identify the energy E_0 with kT_x, and use equation (A24) we find from equation (2) the optical depth

τ_{es} up to which no significant degradation of the X-ray spectrum occurs. We get

$$\tau_{es} = 4.1 \left(\frac{M}{M_\odot}\right)^{-1/2} \left(\frac{R}{5 \times 10^6 \text{ cm}}\right)^{1/2} , \tag{3}$$

which corresponds to an accretion rate $\dot{M} \approx 5 \times 10^{-2} \dot{M}_E$, independent of stellar mass. Thus, we take the bremsstrahlung component to be described by equation (1) with the spectral temperature T_x given by

$$kT_x = \begin{cases} kT_0 = 30 \left(\frac{M}{M_\odot}\right) \left(\frac{R}{5 \times 10^6 \text{ cm}}\right)^{-1} \text{ keV} & \text{for } \dot{M} \lesssim 5 \times 10^{-2} \dot{M}_E \\ \\ \frac{\tau m_e c^2}{\tau_{es}^2} = 7.6 \times 10^{-3} \left(\frac{M}{M_\odot}\right) \left(\frac{R}{5 \times 10^6 \text{ cm}}\right)^{-1} \left(\frac{\dot{M}}{\dot{M}_E}\right)^{-2} \text{ keV} & \text{for } \dot{M} > 5 \times 10^{-2} \dot{M}_E \end{cases} \tag{4}$$

The luminosity L_x is given, in the same approximation, by

$$L_x = f_x \frac{GM\dot{M}}{R} , \tag{5}$$

where

$$f_x = \begin{cases} (1 - f_b) & \text{for } \dot{M} \lesssim 5 \times 10^{-2} \dot{M}_E \\ \\ (1 - f_b)\{1 - [e^{-x} - xE_1(x)]\} & \text{for } \dot{M} > 5 \times 10^{-2} \dot{M}_E , \end{cases} \tag{6}$$

if nuclear burning of the accreting matter does not occur (see Appendix A) and significantly less than that if nuclear burning occurs at the accretion rate (Weast *et al.* 1981). Here $x = m_e c^2 / (\tau_{es}\, kT_0)$ and $E_1(x)$ is an exponential integral tabulated by Abramowitz and Stegun (1965).

We can estimate the physical conditions of the accreting matter by considering the relevant physical processes and comparing the corresponding timescales. The most important heating mechanisms are compression, Compton scattering, free-free absorption, and photoabsorption, while the dominant cooling mechanism is bremsstrahlung (Paper I). At low accretion rates, a comparison of timescales shows compression to be the dominant heating mechanism with a timescale equal to the free-fall one. The accreting matter in this case is completely ionized and the temperature profile is that given in Paper I. At high accretion rates, the major contributions to heating come from Compton scattering, free-free absorption, and photoabsorption with timescales t_{Ch}, t_{ffa}, and t_p respectively (see Appendix). A comparison of these timescales gives

$$\frac{t_{Ch}}{t_{ffa}} = 1.7\left(\frac{fx}{0.5}\right)^{-1}\left(\frac{T}{T_x}\right)^{1/2}\left(\frac{T}{T_{bb}}\right)^{-5/2}\left(\frac{r}{5\times 10^6\ \mathrm{cm}}\right)^{-1/2}$$

$$\left(\frac{R}{5\times 10^6\ \mathrm{cm}}\right)^{7/2}\left(\frac{M}{M_\odot}\right)^{-2}\ , \qquad (7)$$

$$\frac{t_{Ch}}{t_p} = 6.3\times 10^4\left(\frac{M}{M_\odot}\right)^{-2}\left(\frac{R}{5\times 10^6\ \mathrm{cm}}\right)^{2}\sum_Z \chi_Z\, a(Z)\left\{E_3\left(\frac{I_Z}{kT_x}\right) - E_4\left(\frac{I_Z}{kT_x}\right)\tau\right\}\ , \qquad (8)$$

where $E_3(y)$ and $E_4(y)$ are exponential integrals tabulated by Abramowitz and Stegun (1965), χ_Z is the fraction of neutral atoms with atomic number Z, and $a(Z)$ the abundance of element Z relative to hydrogen. Since $T << T_x$, we see from equation (7) that Compton heating dominates free-free absorption, except for high accretion rates or when the accreting matter undergoes nuclear burning. In both cases, $f_x << 0.5$.

Heating due to photoabsorption comes primarily from the most abundant of the heavy elements. For these elements we use the abundances $a(Z)$ relative to

hydrogen given by Brown and Gould (1970) and Fireman (1974): C (4.0×10^{-4}), N (1.1×10^{-4}), O (8.9×10^{-4}), Ne (1.0×10^{-4}), Mg (2.5×10^{-5}), Si (3.2×10^{-5}), S (2.2×10^{-5}), Ar (7.8×10^{-6}), and Fe (4.0×10^{-5}). With these abundances and equation (8) we are led to the conclusion that for high mass stars Compton heating dominates over heating by photoabsorption. Thus, the temperature profile of the accreting matter is determined by balancing Compton heating and bremsstrahlung cooling for low and moderate accretion rates and by balancing free-free absorption and bremsstrahlung for high accretion rates or when nuclear burning occurs. We get then respectively

$$T(r) = \begin{cases} 6.6 \times 10^7 \left(\frac{X}{2}\right)\left(\frac{f_z}{0.5}\right)^2\left(\frac{M}{M_\odot}\right)^5\left(\frac{R}{5 \times 10^8 \text{ cm}}\right)^{-4}\left(\frac{r}{5 \times 10^8 \text{ cm}}\right)^{-1} \text{K} & \text{for } \dot{M} \lesssim 5 \times 10^{-2}\, \dot{M}_E \\ 4.2 \times 10^2 \left(\frac{X}{2}\right)\left(\frac{f_z}{0.5}\right)^2\left(\frac{M}{M_\odot}\right)^5\left(\frac{R}{5 \times 10^8 \text{ cm}}\right)^{-4}\left(\frac{r}{5 \times 10^8 \text{ cm}}\right)^{-1}\left(\frac{\dot{M}}{\dot{M}_E}\right)^{-4} \text{K} & \text{for } \dot{M} > 5 \times 10^{-2}\, \dot{M}_E \end{cases} \tag{9a}$$

and

$$T(r) = 7.2 \times 10^5 \left(\frac{X}{2}\right)^{2/5}\left(\frac{f}{0.5}\right)^{1/4}\left(\frac{M}{M_\odot}\right)^{5/4}\left(\frac{R}{5 \times 10^8 \text{ cm}}\right)^{3/10} \left(\frac{r}{5 \times 10^8 \text{ cm}}\right)^{-4/5}\left(\frac{\dot{M}}{\dot{M}_E}\right)^{1/4} \text{K} \,. \tag{9b}$$

For low mass stars or high accretion rates, photoabsorption may alter the picture significantly. Detailed numerical calculations of the ionization and temperature structure of matter accreting onto degenerate dwarfs of any mass are now underway and will be reported elsewhere (Ross *et al.* 1981; see also Ross and Fabian 1980).

In the next two subsections we determine the ionization structure of the infal-

ling matter by balancing locally the rate of photoionization with the rate of recombination. This local balance is justified because the timescales for photoionization (A24) and recombination (A27) are much smaller than the free fall timescale (A3). Collisional ionization and recombination, as well as dielectronic recombination, are not important because of the low temperature of the accreting gas (Tucker and Gould 1966).

b) Blackbody Spectrum

By balancing the rate of photoionization (A22) by the blackbody component with the rate of recombination (A25) and assuming that photoabsorption by the accreting matter does not alter the blackbody spectrum we get

$$\frac{N_Z^Z}{N_Z^{Z-1}} = \frac{l_Z}{r} \quad . \tag{10}$$

where N_Z^Z and N_Z^{Z-1} are the number densities of ionized and neutral atoms, respectively, with atomic number Z and l_Z is defined as the radius at which the element with atomic number Z is half ionized and half neutral. In deriving equation (10) it was assumed that $\sigma^{(0)}(I_Z/kT)$ (see eq. [A26]) is a constant. Substituting for the different quantities we get

where T_{bb} is given by equation (A11) and the temperature profile (9a) has been used. Figure 1 shows l_Z as a function of $\dot{M}$ for hydrogen, helium, and carbon for a 1.2 $M_\odot$ degenerate dwarf. These curves were calculated using $f = f_b = 0.5$, f_z consistent with equation (6), $\chi = 2$, and $\sigma^{(0)}(I_Z/kT) = 1$. One sees that hydrogen and helium are indeed ionized out to distances much larger than a typical binary separation. Elements heavier than carbon are essentially unaffected for the parameters used in this case.

c) Bremsstrahlung Spectrum

As in the previous subsection, a balancing of the rate of photoionization by the bremsstrahlung component with the rate of recombination results in an equation of the form (10) with

$$l_Z = 2.0 \times 10^{10}\left(\frac{X}{2}\right)\left(\frac{fx}{0.5}\right)\left(\frac{M}{M_\odot}\right)^3\left(\frac{R}{5 \times 10^8\ \mathrm{cm}}\right)^{-2} E_4\left(\frac{I_Z}{kT_z}\right) \frac{1}{Z^4}\, \sigma^{(0)}\left(\frac{I_Z}{kT}\right)\ \mathrm{cm} \quad (12)$$

for all accretion rates. In deriving equation (12) we used equation (9a) and assumed again that photoabsorption by the infalling matter does not alter the bremsstrahlung spectrum. Although l_Z does not depend explicitly on $\dot{M}$, the accretion rate comes in implicitly via f_z and T_z. Figure 2 shows the variation of l_Z with $\dot{M}$ for the most abundant elements heavier than helium and a 1.2 $M_\odot$ degenerate dwarf. Again $f = f_b$ was taken equal to 0.5, f_z consistent with eq. (6), $\chi = 2$, and $\sigma^{(0)}(I_Z/kT) = 1$. Hydrogen and helium are not shown because the photoionizing capability of the bremsstrahlung spectrum on these elements is much smaller than that of the blackbody spectrum.

From Figure 2 one sees that the heavy elements are strongly ionized. It is nevertheless important to ask the following question. Suppose that a photon of energy E reaches l_Z without being absorbed. At this point the photon begins encountering mainly neutral atoms of atomic number Z. How far will it go beyond l_Z before being absorbed? In other words, we want to calculate the mean free path to absorption

$l_a(E,Z)$ at the radius $r = l_Z$. The dimensionless parameter $\gamma_Z(E) \equiv l_Z/l_a(E,Z)$ (Tarter and Salpeter 1969) then gives a qualitative picture of the ionization structure of the element Z near $r = l_Z$. If $\gamma_Z << 1$, the transition from mostly ionized to mostly neutral atoms Z within l_Z is negligible. If $\gamma_Z >> 1$, on the other hand, the above transition is sharp and one has a characteristic Stromgren sphere situation for the element Z. In this case there is significant absorption within l_Z and the Stromgren sphere will form near the radius at which the optical depth to absorption due to element Z becomes equal to one. Since

$$\frac{1}{l_a(E,Z)} = \sigma(E,Z)\, N_Z^{-1} = \frac{6.3 \times 10^{-18}}{Z^2}\left(\frac{I_Z}{E}\right)^3 a(Z) N_H \ , \qquad (13)$$

one gets for γ_Z

$$\gamma_Z(E) = \frac{7.71 \times 10^{12}}{Z^2}\left(\frac{I_Z}{E}\right)^3 a(Z)\, \frac{1}{l_Z^{1/2}}\left(\frac{R}{5 \times 10^{9}\ \mathrm{cm}}\right)\left(\frac{M}{M_\odot}\right)^{-1/2}\left(\frac{\dot{M}}{\dot{M}_E}\right) \ . \qquad (14)$$

The largest value of $\gamma_Z(E)$ occurs at $E = I_Z$, and it is this value that is plotted in Figure 3 as a function of $\dot{M}$ for a 1.2 $M_\odot$ degenerate dwarf and for the most abundant heavy elements. Since the individual curves for silicon, magnesium and sulfur lie very close to one another, all three of them have been represented by one curve. The same is true for nitrogen and neon. It is evident from Figure 3 that for accretion rates up to $10^{-3}\ \dot{M}_E$ none of the heavy elements forms a Stromgren sphere. As the accretion rate is increased, first oxygen and then carbon form Stromgren spheres, while the rest of the heavy elements are still not contributing significantly to photoabsorption of the radiation.

Knowing the ratio of ionized to neutral atoms Z from eq. (12), one can write for the number density of neutral atoms Z as a function of r

$$N_Z^{-1} = \frac{a(Z)N_H}{(1 + \frac{l_Z}{r})} \quad . \tag{15}$$

Then, the optical depth to photoabsorption $\tau_a(E,Z)$ due to element Z from R to infinity is given by

$$\tau_a(E,Z) = 2\gamma_Z(E)l\{\frac{\pi}{2} - \tan^{-1}(\frac{R}{l_Z})^{1/2}\} \quad . \tag{16}$$

The attenuation of the radiation is described by $\tau^* = (3\tau_a\tau_{es})^{1/2}$ rather than by τ_a (Bahcall 1966). For $\tau^* >> 1$ the attenuation goes roughly as $\tau^* e^{-\tau^*}$, while for $\tau^* << 1$ it goes as $e^{-\tau^*}$. Figure 4 gives τ_Z^* at the ionization potential of each element as a function of $\dot{M}$ for a 1.2 $M_\odot$ star. Again, Si, Mg, and S have been represented by one curve because the individual curves lie very close to each other; similarly N and Ne have been represented by one curve. A series of spectra for a 1.2 $M_\odot$ degenerate dwarf and accretion rates $\dot{M} = 10^{-3}$, 4×10^{-3}, 10^{-2}, and $4 \times 10^{-2}\ \dot{M}_E$ is shown in Figure 5. The effect of the blackbody spectrum on carbon is not taken into account in this figure. One sees that for accretion rates above $10^{-2}\ \dot{M}_E$ carbon and oxygen absorption edges begin to cut significantly into the spectrum. Yet, most of the hard X-ray luminosity escapes because Compton degradation is negligible for accretion rates up to about $5 \times 10^{-2}\ \dot{M}_E$. For higher accretion rate, photoabsorption of the lower part of the spectrum and Compton degradation of the upper part result in a rapid decrease of the hard X-ray luminosity.

III. DISCUSSION

Although a number of assumptions have been made in the above model calculation, the results shed considerable light onto the problem of photoabsorption by the accreting matter. The fact that the stellar blackbody radiation ionizes the infalling hydrogen and helium out to distances larger than a typical binary separation has two important consequences. First, as far as Compton scattering is concerned, all of the infalling matter is ionized because the elements heavier than helium constitute only a small fraction of it. Therefore, the Compton scattering effects discussed in Paper I are still valid independent of any absorption effects. Second, the radiation pressure on the accreting matter due to photoabsorption is much less than what it would be if hydrogen and helium were neutral and therefore electron scattering is the dominant source of radiation pressure. As a result, the limiting luminosity is not significantly reduced from the Eddington value.

The secondary radiation emitted from the accreting matter has been neglected in this calculation, but it could modify the calculated ionization structure. Although it is not expected to have any effect on iron, it could enhance the ionization of carbon and oxygen, and therefore reduce photoabsorption. An increase in the ionization of carbon can also be caused by the blackbody radiation as we can see from Figure 1. Compton scattering tends to smear out any absorption edges that are present (Ross, Weaver, and McCray 1978). However, this effect has not been taken into account here.

In summary, our results lead one to the conclusion that the assumption of complete ionization is a good first approximation for high mass ($M \gtrsim 1\ M_\odot$) stars, but may not be adequate for low mass ($M \lesssim 0.5\ M_\odot$) stars. It should be pointed out, however, that unlike scattering, photoabsorption occurs far from the star. Thus, the importance of photoabsorption is a strong function of the distribution of matter in the binary system. It is possible, therefore, in some degenerate dwarf X-ray sources to

have small photoabsorption, yet degradation due to Compton scattering could be large.

APPENDIX A

The velocity, density, inflow timescale, and kinetic temperature of matter falling freely and spherically symmetrically onto a degenerate dwarf of mass M and radius R are given as functions of radius r and accretion rate $\dot{M}$ by

$$v_{ff} = \left(\frac{2GM}{r}\right)^{1/2} = 7.3 \times 10^{8} \left(\frac{M}{M_{\odot}}\right)^{1/2} \left(\frac{r}{5 \times 10^{9}\ \mathrm{cm}}\right) \mathrm{cm\ s^{-1}} , \qquad \text{(A1)}$$

$$\rho_{ff} = \frac{\dot{M}}{4\pi r^2 v_{ff}} = 2.4 \times 10^{-7} \left(\frac{r}{5 \times 10^{9}\ \mathrm{cm}}\right)^{-3/2} \left(\frac{R}{5 \times 10^{9}\ \mathrm{cm}}\right) \left(\frac{M}{M_{\odot}}\right)^{-1/2}$$

$$\left(\frac{\dot{M}}{\dot{M}_E}\right) \mathrm{g\ cm^{-3}} , \qquad \text{(A2)}$$

$$t_{ff} = \frac{r}{v_{ff}(r)} = 6.8 \times 10^{-1} \left(\frac{r}{5 \times 10^{8}\ \mathrm{cm}}\right)^{3/2} \left(\frac{M}{M_{\odot}}\right)^{-1/2} \mathrm{s} , \qquad \text{(A3)}$$

$$T_{ff} = \left(\frac{\mu}{N_0 k}\right)\left(\frac{GM}{r}\right) = 2.0 \times 10^{9} \left(\frac{M}{M_{\odot}}\right)\left(\frac{r}{5 \times 10^{8}\ \mathrm{cm}}\right)^{-1} \mathrm{K} , \qquad \text{(A4)}$$

where N_0 is Avogadro's number, μ is the mean molecular weight per particle, G is the gravitational constant, and a composition $X = 0.7$, $Y = 0.3$ has been assumed. The non-relativistic electron-ion bremsstrahlung rate of energy emission per unit volume (Allen 1973) is

$$\Lambda_{NR}^{i} = \frac{32}{3}\left(\frac{2\pi}{3}\right)^{1/2} \frac{e^6 Z^2}{h m_e c^2} \left(\frac{kT}{m_e c^2}\right)^{1/2} g\, n_e\, n_i , \qquad \text{(A5)}$$

where n_e and n_i are the number densities of electrons and ions respectively, T is their temperature, Z is the ionic charge, and g is the Gaunt factor. Using the density profile

(A2) we can find the bremsstrahlung cooling timescale. It is

$$t_{br} = \frac{\frac{3}{2} n_e kT}{\Lambda \hat{N}\hat{R}^{-1}} = 9.1 \times 10^{-3} \left(\frac{r}{5 \times 10^8 \text{ cm}}\right)^{3/2} \left(\frac{T}{10^8 \text{ K}}\right)^{1/2} \left(\frac{M}{M_\odot}\right)^{1/2}$$

$$\left(\frac{R}{5 \times 10^8 \text{ cm}}\right)^{-1} \left(\frac{\dot{M}}{\dot{M}_E}\right)^{-1} \text{ s} \ . \qquad \text{(A6)}$$

For a bremsstrahlung source of photons of luminosity L_x and temperature $kT_x << m_e c^2$ and a Maxwellian distribution of electrons with temperature $T << T_x$, the nonrelativistic rate per unit volume of energy lost by the photons to the electrons is given by (Levich and Sunyaev 1970)

$$\Gamma_{NR} = U_x \, c \, n_e \, \sigma_T \frac{kT_x}{m_e c^2} \ , \qquad \text{(A7)}$$

where the luminosity $L_x = f_x CM\dot{M}/R$ and the energy density U_x are related via

$$cU_x = \chi \frac{L_x}{4\pi r^2} \ , \qquad \text{(A8)}$$

where χ determines the isotropy of the radiation field. The Compton heating timescale is then given by

$$t_{Ch} = \frac{\frac{3}{2} n_e kT}{\Gamma_{NR}} = 3.9 \times 10^{-2} \left(\frac{\chi}{2}\right)^{-1} \left(\frac{f_x}{0.5}\right)^{-1} \left(\frac{r}{5 \times 10^8 \text{ cm}}\right)^{2} \left(\frac{M}{M_\odot}\right)^{-1}$$

$$\left(\frac{\dot{M}}{\dot{M}_E}\right)^{-1} \left(\frac{T}{T_x}\right) \text{ s} \ . \qquad \text{(A9)}$$

where the fraction f_x varies in the range $0 \lesssim f_x \lesssim 0.5$ (Paper I).

Consider blackbody radiation with luminosity

$$L_{bb} = f_b \frac{GM\dot{M}}{R} + q\,X\,\dot{M} = f\,\frac{GM\dot{M}}{R}\ , \qquad \text{(A10)}$$

produced by accretion onto a degenerate dwarf. Here f_b is the fraction of the accretion luminosity emitted as blackbody radiation and we have included the possibility that the accreting matter is burning at the accretion rate. The value of q for the PPI chain is 6.3×10^{18} ergs s^{-1}. If nuclear burning does not occur, $q = 0$ and the parameter $f = f_b$ ranges from ~ 0.5 to $\lesssim 1.0$ depending on the accretion rate (Paper I). However, if nuclear burning occurs, $4 \lesssim f = f_b + q\,X\,R/(GM) \lesssim 240$ (Weast 1981). The temperature of such blackbody radiation is given by

$$T_{bb} = \left(\frac{L_{bb}}{\sigma 4\pi R^2}\right)^{1/4} = 8.0 \times 10^5 \left(\frac{f}{0.5}\right)^{1/4}\left(\frac{M}{M_\odot}\right)^{1/4}$$

$$\left(\frac{R}{5 \times 10^8\ \mathrm{cm}}\right)^{-1/2}\left(\frac{\dot{M}}{\dot{M}_E}\right)^{1/4} \mathrm{K}\ , \qquad \text{(A11)}$$

where σ is the Stefan-Boltzmann constant. When this radiation passes through accreting matter of temperature T, free-free absorption results in heating of the matter with a rate

$$\Gamma_{ffa} = \frac{4\pi^3}{9}\frac{N_0 e^6}{h m_e c^2}\,X\,\frac{R^2}{r^2}\,\rho n_e \left(\frac{\frac{2\pi}{3}kT_{bb}}{m_e c^2}\right)^{1/2}\left(\frac{T_{bb}}{T}\right)^2 \qquad \text{(A12)}$$

and a corresponding timescale

$$t_{ff} = 2.3 \times 10^{-8} \left(\frac{X}{2}\right)^{-1} \left(\frac{T}{T_{bb}}\right)^{5/2} \left(\frac{T}{T_z}\right)^{1/2} \left(\frac{r}{5 \times 10^6 \text{ cm}}\right)^{7/2} \left(\frac{R}{5 \times 10^6 \text{ cm}}\right)^{-7/2}$$

$$\left(\frac{M}{M_\odot}\right)\left(\frac{\dot{M}}{\dot{M}_E}\right)^{-1} \text{ s} \ . \qquad \text{(A13)}$$

Note that in equations (A12) and (A13) we assume $T \gtrsim T_{bb}$, we used the semiempirical formula (Paper I)

$$kT_z \approx 30 \left(\frac{M}{M_\odot}\right)\left(\frac{R}{5 \times 10^6 \text{ cm}}\right)^{-1} \text{ keV} \ . \qquad \text{(A14)}$$

and we assumed that the energy density U_{bb} and the flux $L_{bb}/4\pi r^2$ are related in a way similar to that of equation (A8).

Let N_Z^{Z-1} be the number density of the hydrogenic element with atomic number Z, $I_Z = 13.6\ Z^2$ eV its ionization potential, and $U(E,r)$ the spectral energy density of the radiation field. Then the heating rate per unit volume Γ_Z^p due to photoabsorption by the element Z is given by

$$\Gamma_Z^p = N_Z^{Z-1} \int_{I_Z}^{\infty} \frac{cU(E,r)}{E} \sigma(E,Z)\,(E - I_Z)\,dE \ . \qquad \text{(A15)}$$

where the hydrogenic photoionization cross section $\sigma(E,Z)$ is given by Bethe and Salpeter (1975)

$$\sigma(E,Z) = \frac{6.3 \times 10^{-18}}{Z^2} \left(\frac{I_Z}{E}\right)^3 \text{ cm}^2 \ ; \ E \geq I_Z \ . \qquad \text{(A16)}$$

We take the spectral energy density $U(E,r)$ for the ionizing X-rays to be

$$cU(E,r) = \frac{\chi}{4\pi r^2}\,\frac{L_x}{kT_x}\,e^{-E/kT_x} \quad . \tag{A17}$$

and the photoabsorption rate per unit volume due to element Z then becomes

$$\Gamma_Z^Z = N_Z^{Z-1}\frac{\chi}{4\pi r^2}\,L_x\frac{I_Z}{kT_x}\,\frac{6.3\times10^{-18}}{Z^2}\,l\{E_3(\frac{I_Z}{kT_x}) - E_4(\frac{I_Z}{kT_x})\tau\} \quad . \tag{A18}$$

where $E_3(x)$ and $E_4(x)$ are exponential integrals tabulated by Abramowitz and Stegun (1965). If we denote the total number density of atoms with atomic number Z by N_Z and the fraction of neutrals by χ_Z, we can write

$$N_Z^{Z-1} = \chi_Z\, a(Z)\, N_H \quad , \tag{A19}$$

where $a(Z)$ is the abundance of the element with atomic number Z relative to hydrogen and N_H is the total number density of hydrogen. Since hydrogen and helium are the most abundant elements in the accreting matter, and since they are completely ionized out to very large distances from the stellar surface (see § II, b), we take

$$n_e = N_H + 2N_{He} = N_H(1 + 2\times 8.3\times10^{-2}) = 1.17\,N_H \quad . \tag{A20}$$

where we have adopted the abundance of helium relative to hydrogen given by Brown and Gould (1970): He (8.3×10^{-2}). Then the timescale t_p for heating due to photoabsorption is

$$t_p = \frac{\frac{3}{2} n_e kT}{\sum_Z \Gamma_Z^B} = 6.2 \times 10^{-7}$$

$$\times \frac{(\frac{X}{2})^{-1}(\frac{f_x}{0.5})^{-1}(\frac{\tau}{5 \times 10^{10}\ \mathrm{cm}})^2(\frac{M}{M_\odot})(\frac{R}{5 \times 10^{10}\ \mathrm{cm}})^{-2}(\frac{T}{T_x})(\frac{\dot{M}}{\dot{M}_E})^{-1}}{\sum_Z x_Z\, a(Z)\, l\{E_3(\frac{I_Z}{kT_x}) - E_4(\frac{I_Z}{kT_x})\tau\}} \quad . \quad \text{(A21)}$$

where expression (A14) has been used.

The rate of photoionization per unit volume is written as

$$R_p = N_Z^{Z-1}\, \zeta_Z \quad . \quad \text{(A22)}$$

where

$$\zeta_Z = \int_{I_Z}^{\infty} \sigma(E,Z)\, \frac{cU(E,\tau)}{E}\, dE \quad \text{(A23)}$$

is the photoionization rate coefficient and its inverse is defined as the photoionization timescale t_Z^B. For a spectral energy density $U(E,\tau)$ of the form (A17) we get

$$t_Z^B = 1.6 \times 10^{-10}\, \frac{Z^2}{E_4(\frac{I_Z}{kT_x})} (\frac{X}{2})^{-1}(\frac{f_x}{0.5})^{-1}(\frac{\tau}{5 \times 10^{10}\ \mathrm{cm}})^2$$

$$(\frac{R}{5 \times 10^{10}\ \mathrm{cm}})^{-1}(\frac{\dot{M}}{\dot{M}_E})^{-1}\ \mathrm{s} \quad \text{(A24)}$$

where f_x is the fraction of the accretional luminosity that constitutes the outgoing ionizing hard X-ray radiation.

The rate of recombination per unit volume is given by

$$R_r = n_e N_Z^Y \alpha(Z,T) \ . \qquad (A25)$$

where $\alpha(Z,T)$ is the recombination coefficient, N_Z^Y is the number density of fully ionized atoms with atomic number Z, and T is the temperature of the gas. For radiative recombinations to all states of any ion, Seaton (1959) derived the following simple expression for $\alpha(Z,T)$

$$\alpha(Z,T) \approx 1 \times 10^{-11} \frac{Z^2}{T^{1/2}} \sigma^{(0)}\left(\frac{I_Z}{kT}\right) \text{ cm}^3 \text{ s}^{-1} \ . \qquad (A26)$$

where $\sigma^{(0)}(I_Z/kT)$ is a slowly varying function of order unity tabulated by Seaton (1959). Thus, the recombination timescale is given by

$$t_r = \frac{N_Z^Y}{R_r} = \frac{6.6 \times 10^{-3}}{Z^2 \sigma^{(0)}\left(\frac{I_Z}{kT}\right)} \left(\frac{r}{5 \times 10^9 \text{ cm}}\right)\left(\frac{R}{5 \times 10^9 \text{ cm}}\right)^{-3}$$

$$\left(\frac{M}{M_\odot}\right)^3 \left(\frac{\dot{M}}{\dot{M}_E}\right)^{-1} \text{ s} \ . \qquad (A27)$$

REFERENCES

Abramowitz, M., and Stegun, I.A. 1965, *Handbook of Mathematical Functions* (New York: Dover, 5th printing), p. 228.

Allen, C.W. 1973, *Astrophysical Quantities* (3rd ed; London: Athlone Press).

Bahcall, J.N. 1966, *Ap. J.*, **145**, 684.

Bethe, H.A., and Salpeter, E.E. 1957, *Quantum Mechanics of One- and Two-electron Systems* (New York: Academic Press).

Brown, R.L., and Gould, R.J. 1970, *Phys. Rev. D.*, **1**, 2252.

Buff, J., and McCray, R. 1974, *Ap. J.*, **189**, 147

Fabian, A.C., Pringle, J.E., and Rees, M.J. 1976, *M.N.R.A.S.*, **175**, 43.

Fireman, E.L. 1974, *Ap. J.*, **187**, 57.

Hatchett, S., Buff, J., and McCray, R. 1976, *Ap. J.*, **206**, 847.

Hayakawa, S. 1973, *Prog. Theoret. Phys.*, **50**, 459.

Illarionov, A.F., and Sunyaev, R.A. 1972, *Astr. Zh.*, **49**, 58 (English translation in *Soviet Astr. - A.J.*, **16**, 45, 1972).

Imamura, J.N., Durisen, R.H., Lamb, D.Q., and Weast, G.J. 1981, to be submitted to *Ap. J.*.

Kylafis, N.D. 1978, Ph.D. Thesis, University of Illinois.

Kylafis, N.D., and Lamb, D.Q. 1981, *Ap. J.*, in print (Paper I).

Langer, S.H., Ross, R.R., and McCray, R. 1976, *Ap. J.*, **222**, 959.

Levich, E.V., and Sunyaev, R.A. 1970, *Astron. Zh.*, **48**, 461 (English translation *Soviet Astron. - A.J.*, **15**, 363, 1971).

Ross, R.R. 1979, *Ap. J.*, **233**, 334.

Ross, R.R., and Fabian, A.C. 1980, *M.N.R.A.S.*, **193**, 1P.

Ross, R.R., Fabian, A.C., Kylafis, N.D., and Lamb, D.Q. 1981, in preparation.

Ross, R.R., Weaver, R., and McCray, R. 1978, *Ap. J.*, **219**, 292.

Seaton, M.J. 1959, *M.N.R.A.S.*, **119**, 81.

Tarter, C.B., and McKee, C.F. 1973, *Ap. J. (Letters)*, **186**, L63.

Tarter, C.B., and Salpeter, E.E. 1969, *Ap. J.*, **156**, 953.

Tarter, C.B., Tucker, W.H., and Salpeter, E.E. 1969, *Ap. J.*, **156**, 943.

Tucker, W.H., and Gould, R.J. 1966, *Ap. J.*, **144**, 244.

Weast, G.J. 1981, Ph.D. Thesis, University of Illinois.

Weast, G.J., Durisen, R.H., Imamura, J.N., Kylafis, N.D., and Lamb, D.Q. 1981, to be submitted to *Ap. J.*

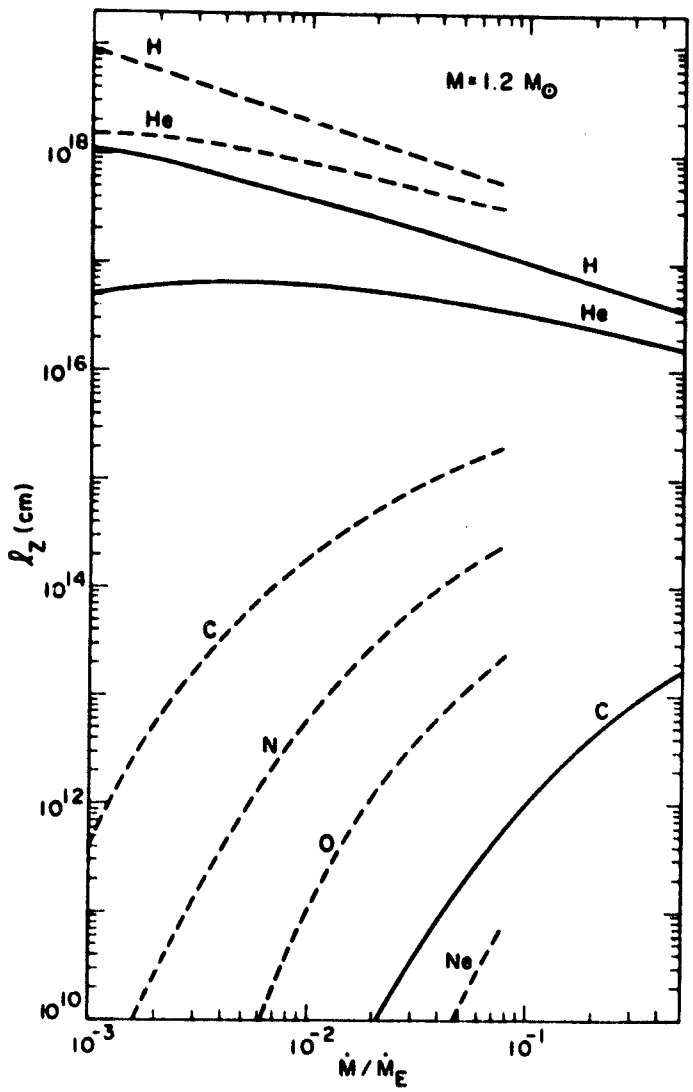
M = 1.2 M⊙
H
He
H
He
C
N
O
C
Ne
10^{18}
10^{16}
10^{14}
10^{12}
10^{10}
l_z (cm)
10^{-3}
10^{-2}
10^{-1}
$\dot{M}/\dot{M}_E$

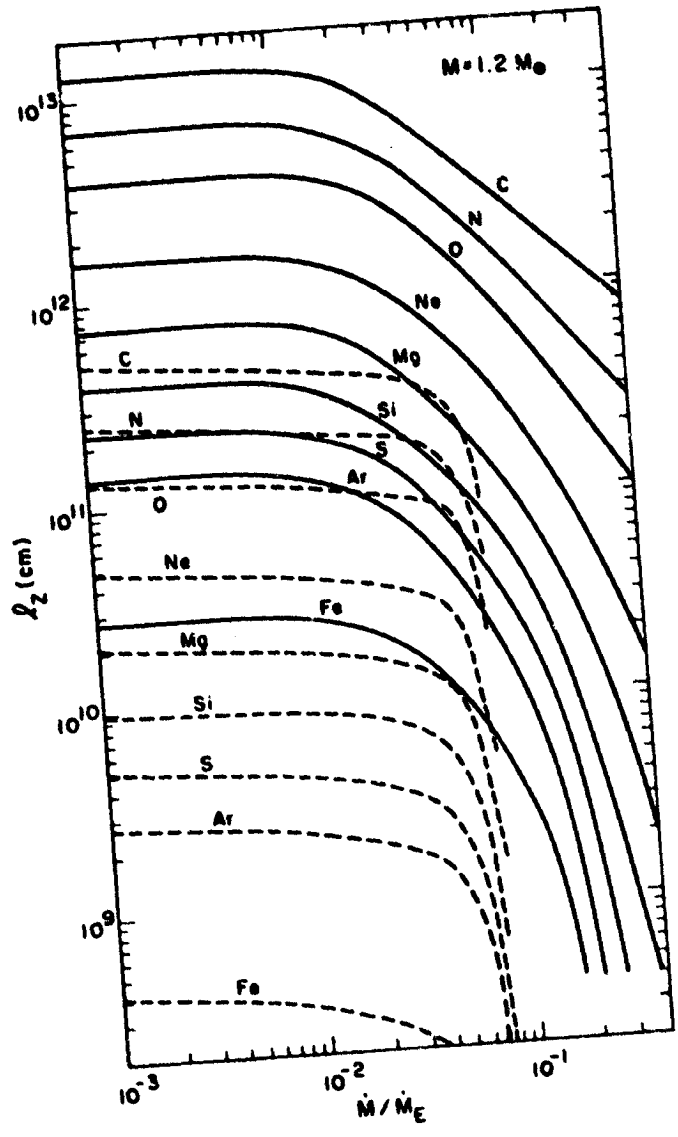
M=1.2 M⊙
C
N
O
Ne
Mg
Si
S
Ar
Fe
10^{13}
10^{12}
10^{11}
10^{10}
10^{9}
ℓ_z (cm)
10^{-3}
10^{-2}
10^{-1}
$\dot{M}/\dot{M}_E$

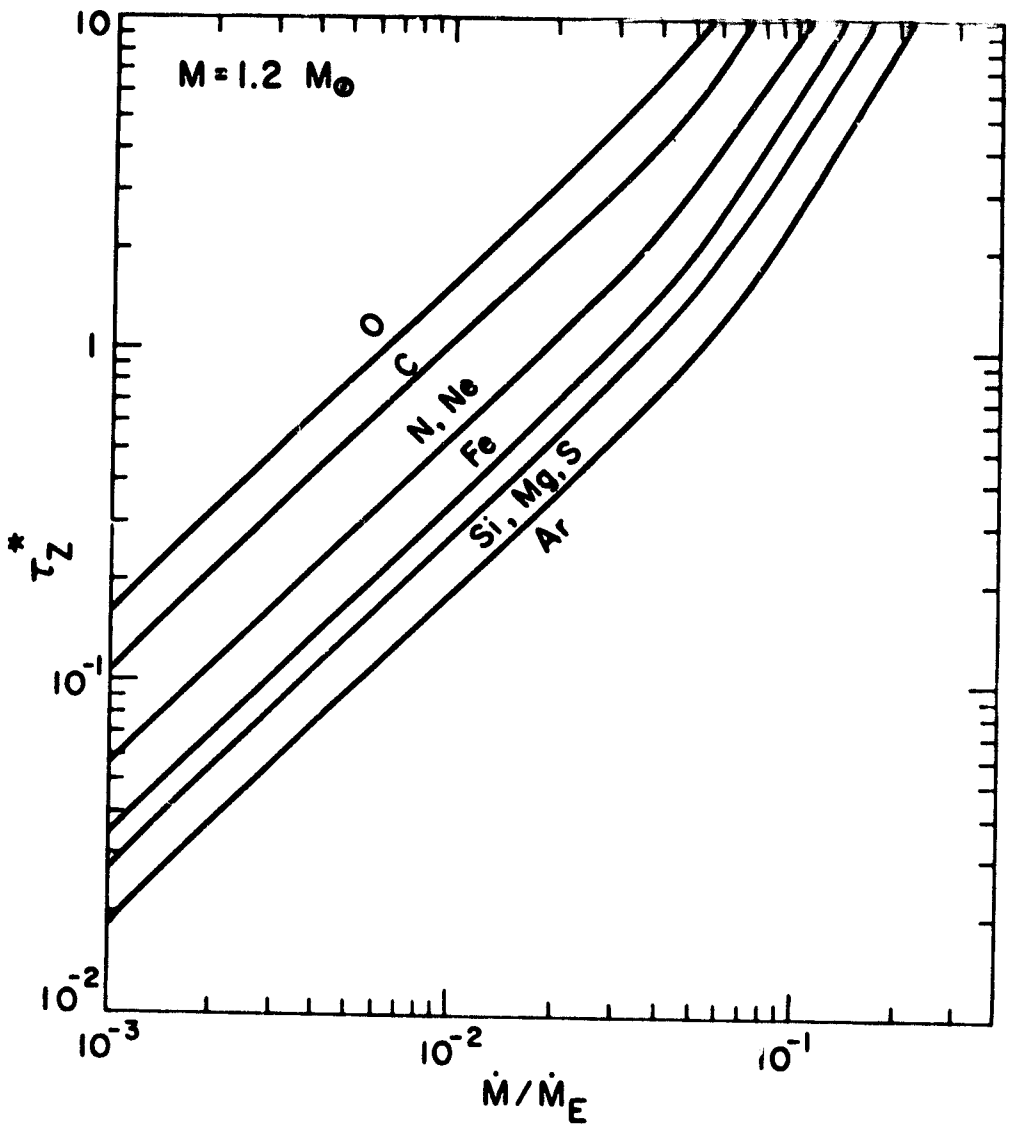
M = 1.2 M⊙
O
C
N, Ne
Fe
Si, Mg, S
Ar
10
1
10^-1
10^-2
10^-3
10^-2
10^-1
τ*Z
Ṁ/Ṁ_E

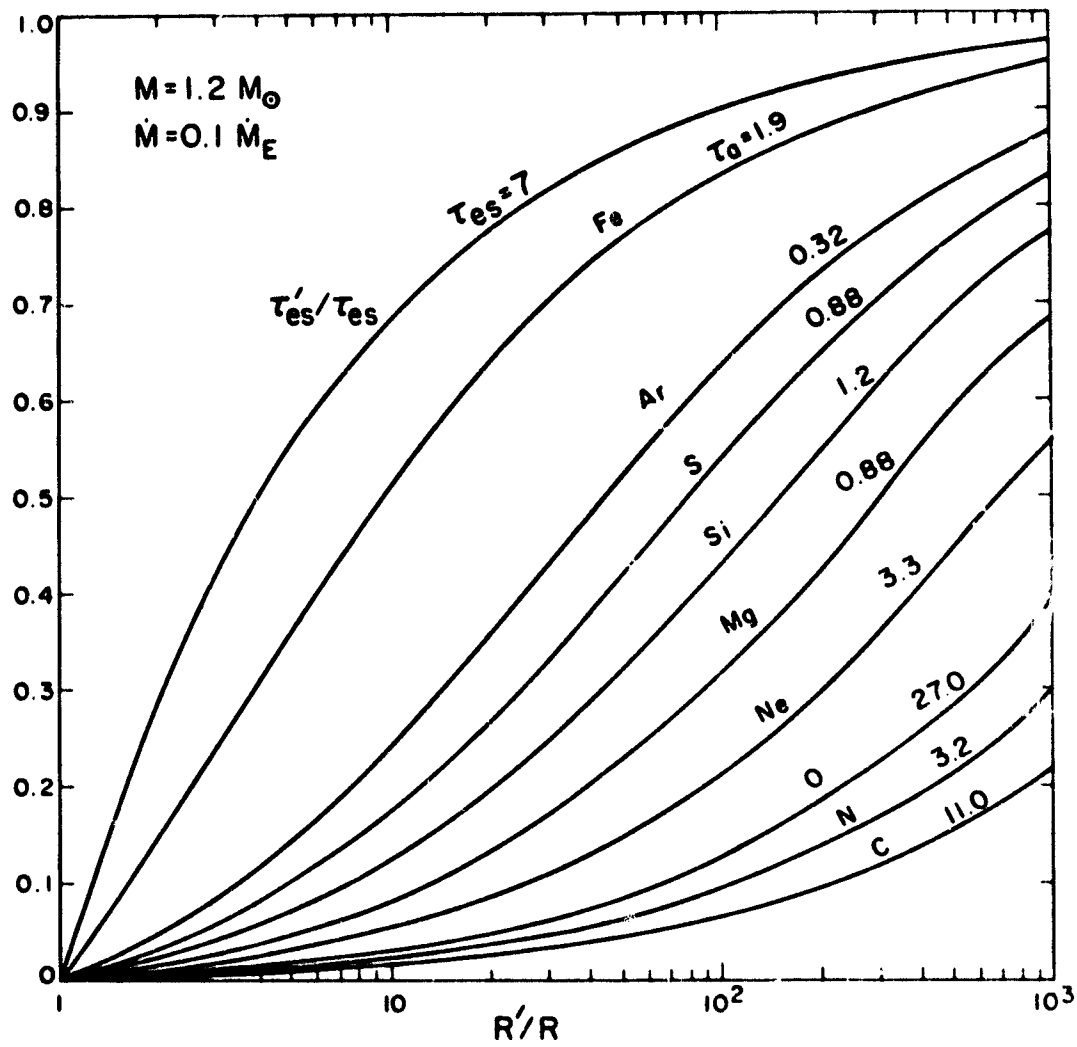
M = 1.2 M⊙
Ṁ = 0.1 Ṁ_E
τ_es = 7
τ_a = 1.9
Fe
0.32
Ar
0.88
S
1.2
Si
0.88
Mg
3.3
Ne
27.0
O
3.2
N
11.0
C
τ'_es/τ_es
1.0
0.9
0.8
0.7
0.6
0.5
0.4
0.3
0.2
0.1
0
1
10
10^2
10^3
R'/R

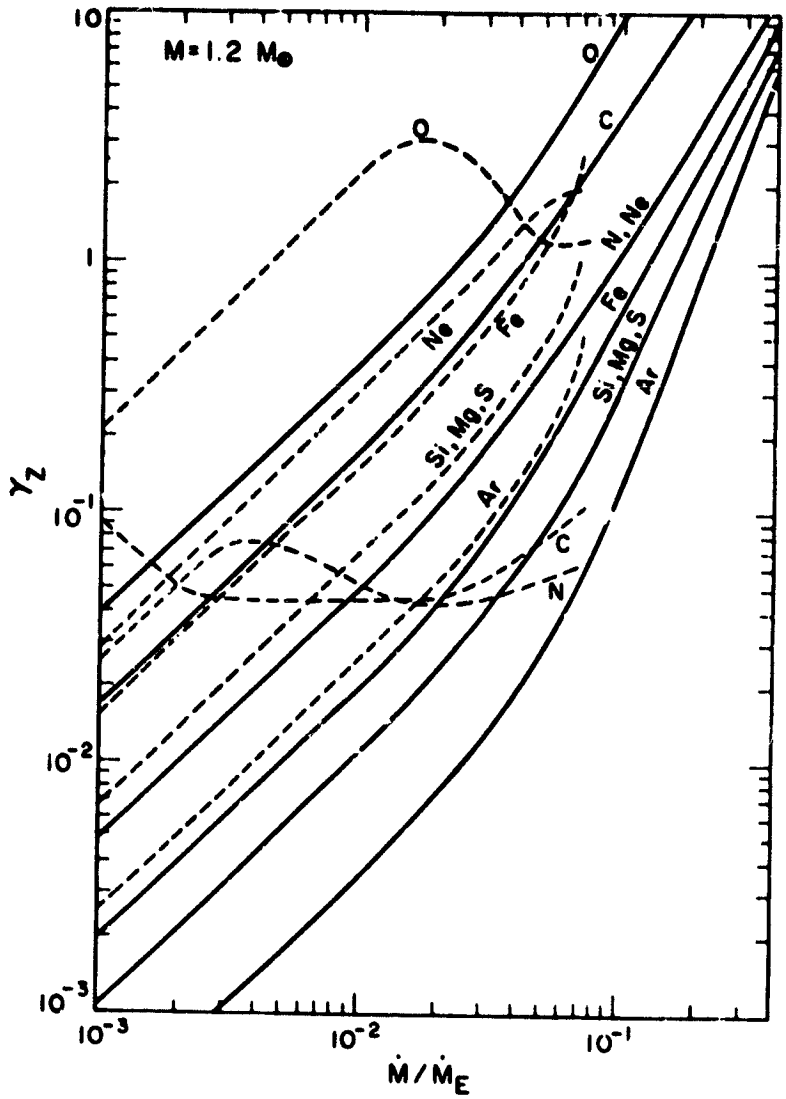
M=1.2 M⊙
O
C
Q
N, Ne
Ne
Fe
Si, Mg, S
Ar
Fe
Si, Mg, S
Ar
C
N
10
1
10⁻¹
10⁻²
10⁻³
Y_Z
10⁻³
10⁻²
10⁻¹
Ṁ / Ṁ_E

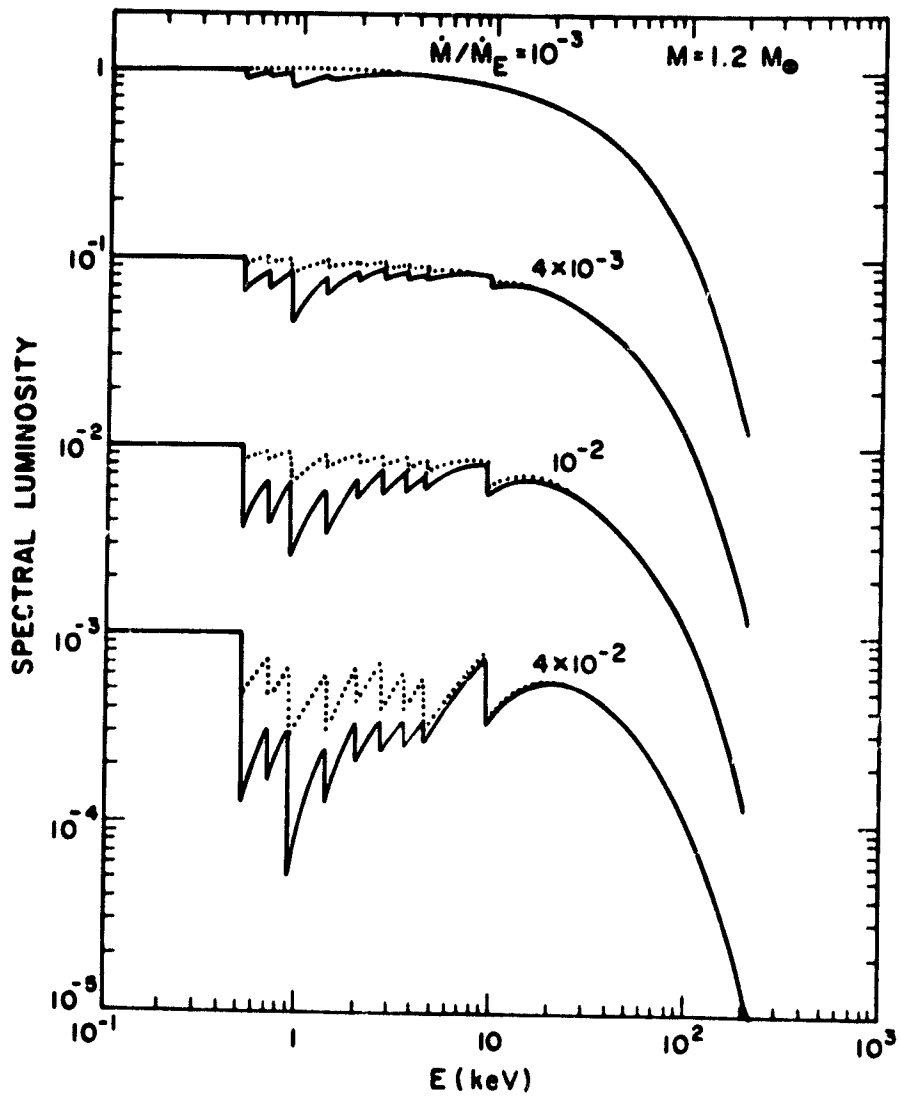
$\dot{M}/\dot{M}_E = 10^{-3}$
$M = 1.2\ M_\odot$
4×10^{-3}
10^{-2}
4×10^{-2}
SPECTRAL LUMINOSITY
E (keV)
1
10^{-1}
10^{-2}
10^{-3}
10^{-4}
10^{-5}
10^{-1}
1
10
10^{2}
10^{3}

CONTINUUM AND LINE SPECTRA OF DEGENERATE DWARF X-RAY SOURCES*

D. Q. Lamb
Harvard-Smithsonian
Center for Astrophysics

ABSTRACT

We summarize recent observations of degenerate dwarf X-ray sources, and review theoretical work on their continuum spectra and lines. We discuss some of the important unresolved issues concerning these sources, and conclude with an outline of the kinds of X-ray observations that would best advance our understanding of them.

I. INTRODUCTION

a) Historical Remarks

The first degenerate dwarf X-ray source was discovered in 1974 when Rappaport et al. (1974) detected an unexpected soft X-ray source during a brief rocket flight and deduced that the source was SS Cyg in outburst.

Two years later Berg and Duthie (1976) suggested that the cataclysmic variable AM Her was the optical counterpart of the hard X-ray source 4U1814+50. This identification was confirmed by Hearn et al. (1976), who detected AM Her in soft X rays. Soon after the optical identification, Szkody and Brownlee (1977) and Cowley and Crampton (1977) found that AM Her has a binary period of 3.1 hours. More remarkably, Tapia (1977a) discovered that the optical light from AM Her is nearly 10% circularly and linearly polarized and that the degenerate dwarf is strongly magnetic. The periods of the circular and linear polarization curves, the radial velocity curves, and the optical, soft and hard X-ray light curves are identical. Thus the rotation period of the accreting magnetic degenerate dwarf is phase-locked to the binary orbital period of 3.1 hours. Within less than a year, two other similar sources, AN UMa and VV Pup, were identified from their optical emission line spectrum and confirmed by detection of linear and circular polarization (Krzeminski and Serkowski 1977, Tapia 1977b).

Soft and hard X-rays were soon also detected from the well-known cataclysmic variables U Gem (Mason et al. 1978; Swank et al. 1978), EX Hya (Watson, Sherrington, and Jameson 1978; Cordova and Riegler 1979), and GK Per (King, Ricketts, and Warwick 1979), in addition to SS Cyg (Heise et al. 1978; Mason, Cordova, and Swank 1979).

Subsequent examination of nearby cataclysmic variables turned up many more X-ray sources. A few of these were discovered by Ariel 5 and HEAO-1, but most detections required the high sensitivity of the focusing instrument on Einstein. Other cataclysmic variables have been found by looking for the optical counterparts of faint

*This research was supported in part by NASA grant NAGW 246.

galactic X-ray sources, and this method promises to become increasingly important in the future. More than 53 of these accreting degenerate dwarf X-ray sources are now known (Cordova and Mason 1982).

Soft X-rays have also been detected from several hot (T_{eff} > 30,000 - 60,000 K) isolated degenerate dwarfs, including Sirius B (Martin et al. 1982 and references therein) and HZ 43 (Hearn et al. 1976).

b) Potential

The study of degenerate dwarf X-ray sources can provide many returns. For example, these sources afford a laboratory in which to explore the physics of hot, dense plasmas in strong magnetic fields (the parameter regime is, in fact, similar to that of interest in plasma fusion reactors). We can also learn from them a great deal about the masses, internal structure, and magnetic fields of degenerate dwarfs themselves. Potentially, the pulsing sources can provide as much information as has been obtained from the pulsing neutron star X-ray sources. Noise measurements can be used to probe the accretion process, reflection and reprocessing effects give clues to the geometry of the disk and the binary system, and time delay curves yield the parameters of the binary system and thereby lend insight into its formation and evolution.

However, because most degenerate dwarf X-ray sources were found only recently, we know very little about their X-ray properties. Only three (AM Her, SS Cyg, and U Gem) have been studied in any detail. The situation is similar in this respect to that of the stellar X-ray sources also found by Einstein (Linsky 1982). Exploration of the X-ray emission from both has only begun, and future X-ray astronomy missions must provide the data with which to understand it.

In this review, we concentrate on the soft and hard X-ray spectra produced by accreting degenerate dwarfs. We first summarize the observations in §II. We then discuss the theory of formation of the continuum spectrum in §III, and of emission and absorption lines in §IV. In §V, we mention some of the important unresolved issues. Finally, in §VI we outline the kinds of X-ray observations that would best advance our understanding of these sources. For reviews of the optical properties of cataclysmic variables, see Robinson (1976) and Warner (1976); for reviews of the X-ray observations, see Garmire (1979) and Cordova and Mason (1982). Lamb (1979) and Kylafis et al. (1980) contain earlier reviews of theoretical work.

II. OBSERVATIONAL PROPERTIES

a) Luminosities and Space Densities

Probably all cataclysmic variables are X-ray sources. The ones detected so far have X-ray luminosities $L \sim 10^{31} - 10^{33}$ ergs s^{-1}. None of the bright ($L \sim 10^{36}$-10^{38} ergs s^{-1}) galactic X-ray sources have been identified with degenerate dwarfs. Thus the known accreting degenerate dwarf X-ray sources are $\sim 10^{5}$ times fainter than, e.g., the pulsing neutron stars (Lamb 1982) but $\sim 10^{3}$ times brighter than ordinary stars (Linsky 1982).

The nearest cataclysmic variable X-ray sources lie at distances d of only 75 - 100 pc (Cordova and Mason 1982). This implies a space density $n \sim 3 \times 10^{-7}$ $(d/100\ pc)^{-3}$ pc^{-3}. Assuming a uniform distribution of sources throughout the galaxy and a galactic

volume V $\sim$ 1 x 10^{12} pc^3, the above space density implies that the total number of sources in the galaxy is N $\sim$ 3 x 10^5 (d/ 100 pc)$^{-3}$. Thus the total number of degenerate dwarf X-ray sources in the galaxy may exceed a million. This compares with a total number of bright (L $\sim$ 10^{36}- 10^{38} ergs s^{-1}) neutron star sources of $\sim$ 100.

b) X-Ray Spectra and Temporal Behavior

Among accreting degenerate dwarf X-ray sources, there are two recognized classes involving magnetic degenerate dwarfs: the AM Her stars and the DQ Her stars (Lamb 1979, Patterson and Price 1981). The remaining systems show no clear-cut manifestation of a magnetic field. However, if the past is a guide, some of these sources will be reclassified as AM Her or DQ Her stars on the basis of future observations. We may even speculate that magnetic fields are endemic in degenerate dwarfs. If so, most, perhaps all, of the other systems also contain magnetic degenerate dwarfs. However, the field strengths may be less. Below we discuss the X-ray spectra and temporal behavior of the AM Her stars, the DQ Her stars, and the other cataclysmic variables.

i) AM Her stars

Table 1 lists the seven AM Her stars that are now known and summarizes some of their properties. These stars show strong (> 10%) circular and linear polarization of their infrared and visible light, and are believed to be accreting magnetic degenerate dwarfs (Chanmugam and Wagner 1977, 1978; Stockman et al. 1977). The polarization (Tapia 1977a) of the visible light from AM Her, the prototype of this class, is shown in Figure 1. The X-ray spectra of these stars typically have two distinct components: an apparent blackbody component with T_{bb} < 100 ev and a bremsstrahlung component with T_{br} > 10 kev. The inferred blackbody luminosity is greater than the bremsstrahlung luminosity, often by a factor of 10 or more (cf. Tuohy et al. 1978, 1981; Szkody et al. 1981; Patterson et al. 1982). Figure 2 shows the soft and hard X-ray spectrum of AM Her recently constructed from HEAO-1 observations by Rothschild et al. (1981). The bremsstrahlung spectra of these sources also show strong iron line emission at $\sim$ 7 keV, as is evident in Figure 2. In these systems, the periods of the polarized light, the optical and X-ray light, and the orbital velocity curves are all the same. Thus the rotation period of the degenerate dwarf is synchronized with the orbital period of the binary system, probably due to interaction of the magnetic field of the degenerate dwarf with the companion star (Joss, Katz, and Rappaport 1979). Figure 3 shows the resulting 3.1 hour "pulse profile" of AM Her in soft X-rays (Tuohy et al. 1978).

The source EF Eri (2A0311-227) is the second most well-studied in X-rays of the AM Her stars. Figures 4 and 5 show its 1.3 hour "pulse profile" in soft X-rays (Patterson et al. 1981) and its bremsstrahlung hard X-ray spectrum (White 1981). Note again the strong iron emission line at $\sim$ 7 keV.

ii) DQ Her stars

Table 2 lists the seven systems we have classified as DQ Her stars and summarizes some of their properties. DQ Her, the prototype of this class, is believed to be an accreting magnetic degenerate dwarf (Bath, Evans, and Pringle 1974; Lamb 1974). However, it shows little, if any, polarization of its infrared and visible light (Swedlund, Kemp, and Wolstencroft 1974). This system underwent a nova outburst in 1934 and shows coherent small amplitude optical pulsations at 71 seconds, which are believed to

TABLE 1

AM HER STARS

STAR	P_b (Hours)	d (pc)[a]	L_s (10^{30} ergs s^{-1})[b]	T_{bb} (eV)	L_h (10^{30} ergs s^{-1})[b]	T_{br} (keV)	REFERENCES
EF Eri (=2A0311-227)	1.35	[100]	24	≤80	170	18.1±3.0	8, 15, 18
VV Pup	1.67	144	160	20^{+60}_{-10}	7.0	>10	2, 7, 14
E1405-451	1.69	[100]	9.7	...	...	...	6
H0139-68	1.82	[100]	72	≤300	...	...	1, 17
PG1550+191	1.89	[100]	...	...	...	...	10
AN UMa	1.91	[100]	0.86 33	≤40	...	...	3, 5, 12
AM Her	3.09	75±10	45-480 21	28-40	260 480	30.9±4.5	4, 9, 11, 13, 16, 19

[a] Distances in brackets are assumed.

[b] Luminosities assume a distance of 100 pc, except for AM Her and VV Pup.

(1) Agrawal et al. (1981)
(2) Bailey (1981)
(3) Hearn and Marshall (1979)
(4) Hearn and Richardson (1977)
(5) Krzeminski and Serkowski (1977)
(6) Mason et al. (1982)
(7) Patterson et al. (1982)
(8) Patterson et al. (1981)
(9) Rothschild et al. (1981)
(10) Stockman et al. (1981)
(11) Swank et al. (1977)
(12) Szkody et al. (1981)
(13) Tapia (1977a)
(14) Tapia (1977b)
(15) Tapia (1979)
(16) Tuohy et al. (1981)
(17) Visvanathan et al. (1982)
(18) White (1981)
(19) Young and Schneider (1979)

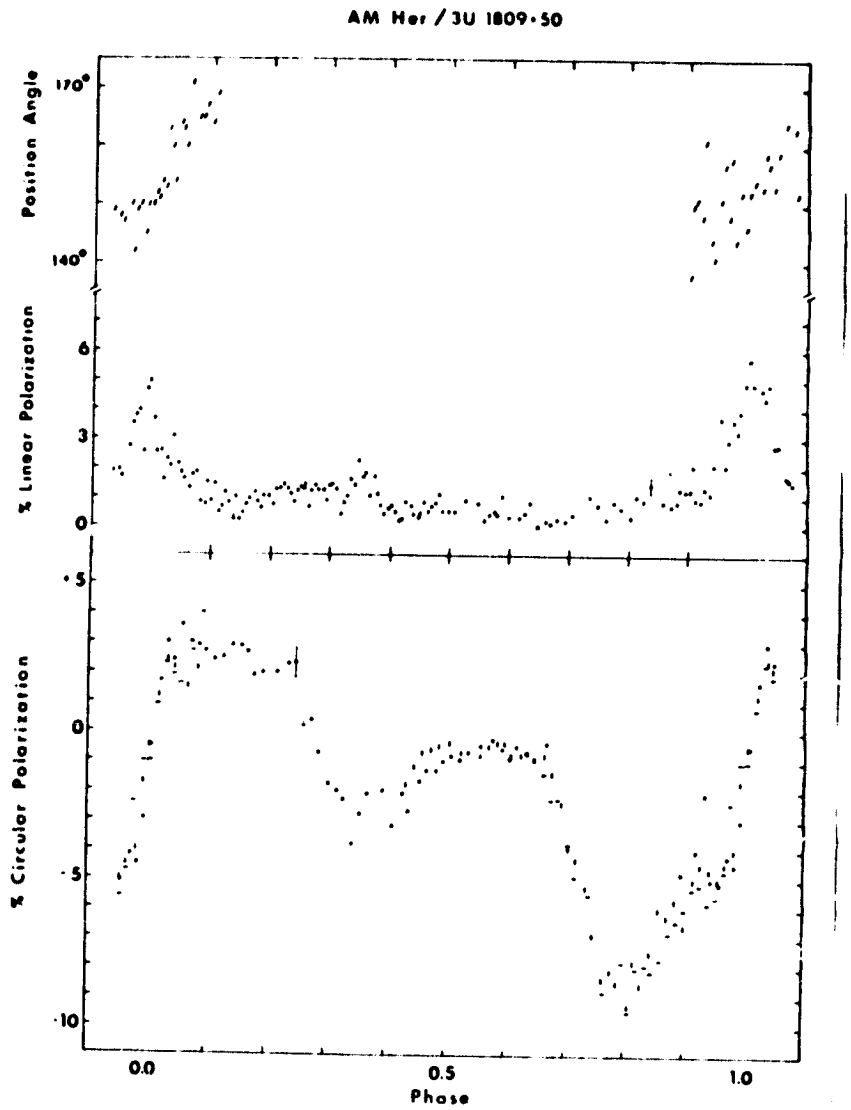

Fig. 1--Circular and linear polarization of the optical light from AM Her as a function of the phase of the 3.1 hour rotational period of the degenerate dwarf (from Tapia 1977).

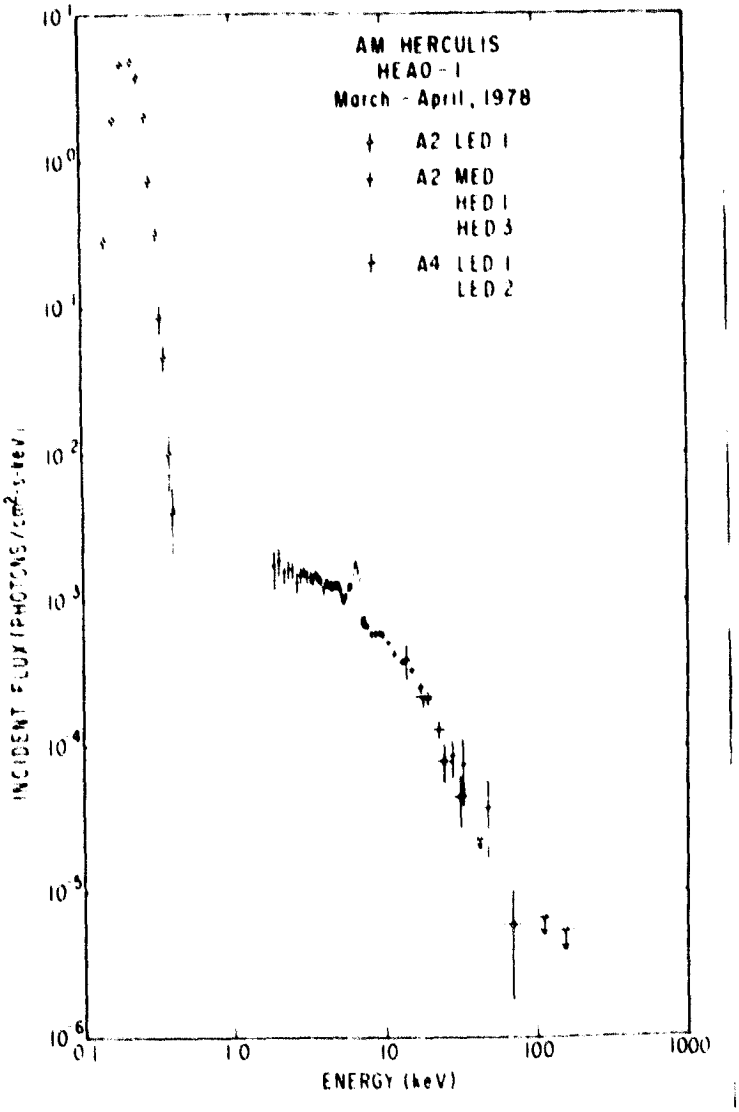

Fig. 2--Hard and soft X-ray spectrum of AM Her (from Rothschild et al. 1981). The two distinct components with T ≈ 30 keV and T < 40 eV are clearly visible.

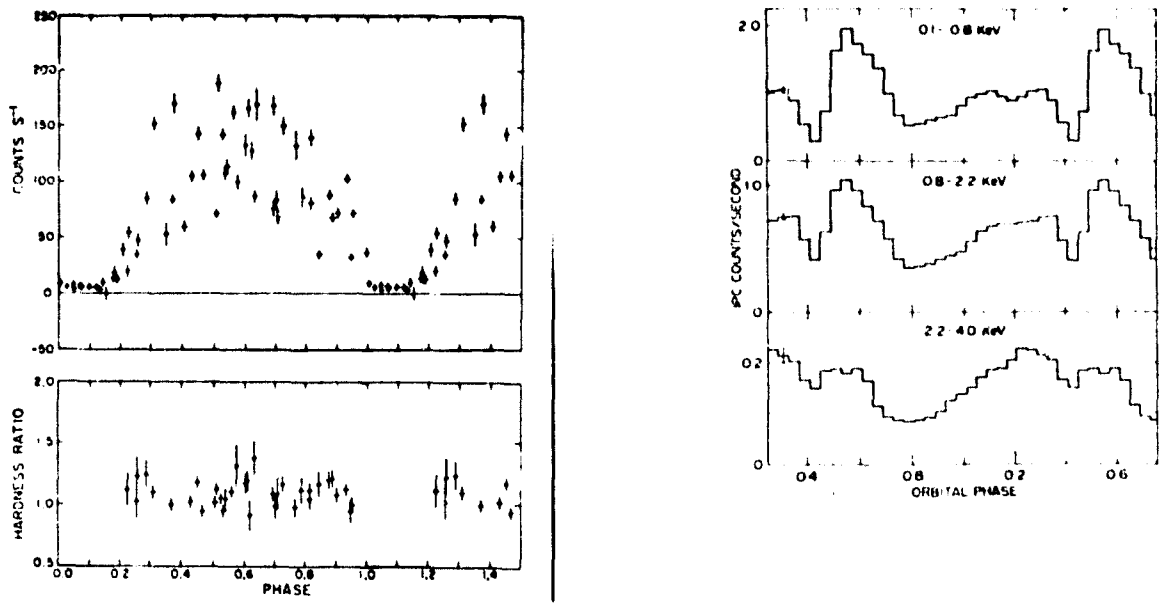

Fig. 3--Soft X-ray pulse profile and hardness ratio of AM Her as a function of the phase of the 3.1 hour rotational period of the degenerate dwarf (from Tuohy et al. 1978).

Fig. 4--X-ray pulse profile of EF Eri (2A0311-227) observed by Einstein as a function of orbital phase (or, equivalently, phase of the rotational period of the degenerate dwarf) (from Patterson et al. 1981).

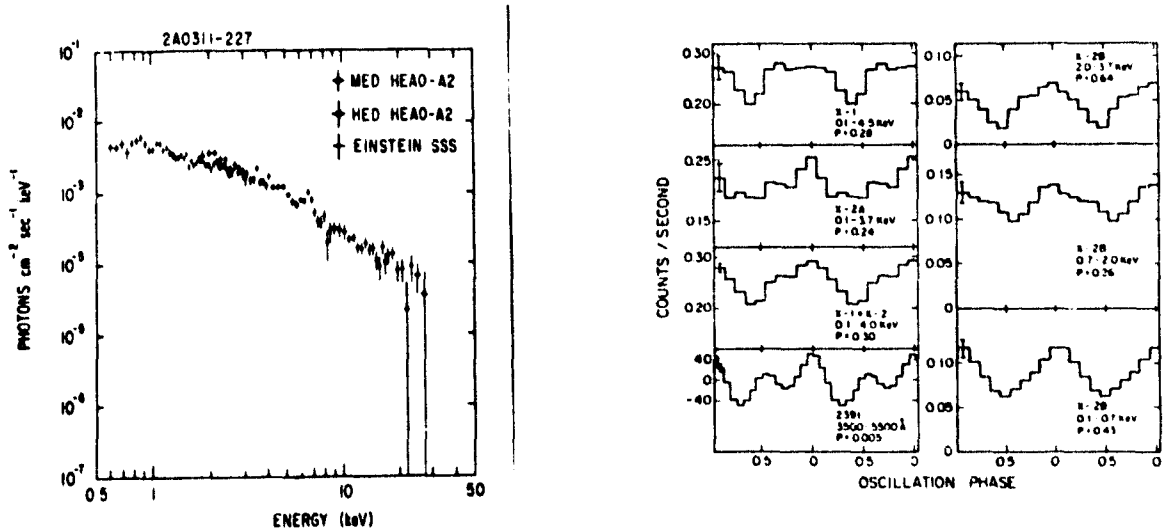

Fig. 5--Hard X-ray spectrum of EF Eri (2A0311-227) (from White et al. 1981). Note the iron emission line at ≈ 7 keV.

Fig. 6--Comparison of the pulse profile in soft X-rays and in optical light of AE Aqr through the 33 second rotation period of the degenerate dwarf (from Patterson et al. 1980).

TABLE 2

DQ HEP STARS

STAR	P_b (Hours)	d (pc)[a]	P (s)	$\lvert\dot{P}\rvert^{-1}$	L_s (10^{30} ergs s^{-1})[b]	T_{bb} (eV)	L_h (10^{30} ergs s^{-1})[b]	T_{br} (keV)	REFERENCES
DQ Her	4.65	420	71.0653	1.2×10^{12}	< 2.4	...	...	...	2, 11
V533 Her	≈ 7	1000–1500	63.63307	$> 3 \times 10^{12}$	< 20–40	...	...	...	2, 5, 7
AE Aqr	9.88	84	33.076737	2×10^{13}	5.4	...	...	...	1, 6, 7, 9
EX Hya (?)	1.64	100	4021.62	2.2×10^{10}	14	570	60 100	≈ 5 ≈ 4.5	3, 4, 15
H2252-035	3.59	[100]	805.21	$> 5 \times 10^{9}$	...	...	80	> 20	8, 10, 16, 17
H2215-086	4.03	[100]	1254.5	$> 3 \times 10^{8}$	5	...	12 30	≥ 10 ≥ 10	12
V1223 Sgr	...	[100]	794.380	$> 5 \times 10^{9}$	...	...	100	≥ 10	13, 14

[a] Distances in brackets are assumed.

[b] Luminosities assume a distance of 100 pc if distance is unknown.

(1) Bailey (1981)
(2) Cordova, Mason, and Nelson (1981)
(3) Cordova and Riegler (1979)
(4) Gilliland (1982)
(5) Patterson (1979a)
(6) Patterson (1979b)
(7) Patterson (1982a)
(8) Patterson (1982b)
(9) Patterson et al. (1980)
(10) Patterson and Price (1981)
(11) Patterson, Robinson, and Nather (1978)
(12) Patterson and Steiner (1982)
(13) Steiner (1981)
(14) Steiner et al. (1981)
(15) Swank (1980)
(16) Warner, O'Donoghue, and Fairall (1981)
(17) White and Marshall (1981)

represent the rotation period of the degenerate dwarf (Patterson, Robinson, and Nather 1978, and references therein). Two other members of this class are V533 Her, which underwent a nova outburst in 1963 and shows coherent small amplitude optical pulsations at 63 seconds (Patterson 1979a), and AE Aqr, which shows similar pulsations at 33 seconds (Patterson 1979b). Embarrassingly, neither DQ Her nor V533 Her have been detected in X rays (see Table 2). In the case of DQ Her, it has been suggested that the X rays are blocked by the disk because we are nearly in the orbital plane of the system, while in the case of V533 it can be argued that the system is too far away, and therefore too faint, to have been detected. Thankfully (for theorists), X rays have now been detected from AE Aqr and are pulsed with the 33 second optical period (Patterson et al. 1980). Figure 6 compares the optical and soft X-ray pulse profiles of AE Aqr.

Recently, several faint galactic X-ray sources have been identified with systems that are optically similar to cataclysmic variables. They exhibit large amplitude optical and X-ray pulsations with periods $\gtrsim$ 1000 seconds that are believed to represent the rotation period of the accreting star (Patterson and Price 1981; Warner, O'Donoghue, and Fairall 1981; White and Marshall 1981). There is controversy as to whether these X-ray sources are actually degenerate dwarfs or are neutron stars (cf. Patterson and Price 1981, White and Marshall 1981). We believe, based on their optical appearance and their X-ray to optical luminosity ratio, that they are degenerate dwarfs. They have also been called "interlopers" between the previously known DQ Her stars, with short rotation periods of 33 - 71 seconds, and the AM Her stars, with rotation synchronous with their orbital periods of 1.2 - 2.1 hours (Patterson and Price 1981). However, we believe that they should be regarded as members of the DQ Her class, in analogy with the short and long period pulsing neutron star X-ray sources, and therefore we include them in Table 2.

The source H2252-035 was the first of these systems to be optically identified (Griffiths et al. 1980). Figure 7 shows its optical light curve (Patterson and Price 1981). Clearly visible are the optical pulsations with a period of 859 seconds, which are thought to be produced by repossessing of the 805 second X-ray pulse. Figures 8 and 9 show the pulse profile and the spectrum of the hard X-rays (White and Marshall 1981). The hard X-ray spectrum exhibits iron line emission at $\sim$ 7 keV.

Recently, a 67 minute (4022 second) periodicity has been identified in the well-studied cataclysmic variable X-ray source EX Hya (Vogt, Krzeminski, and Sterken 1980; Gilliland 1982). This period is also evident in soft X-rays but not in hard (Swank and White 1981), as shown in Figure 10. The coherence of the period over many years suggests that it may also be due to rotation of a magnetic degenerate dwarf. We have therefore included EX Hya in Table 2, but with a question mark to indicate its uncertain status.

iii) Other cataclysmic variables

Table 3 lists 10 sources selected from the remaining 44 cataclysmic variable X-ray sources currently known (Cordova and Mason 1982). Among these are the prototypical dwarf novae, SS Cyg and U Gem, which undergo outbursts every $\sim$ 100 days. During quiescence, both exhibit a hard X-ray spectrum with $T_{br} \sim 10 - 20$ keV (Mason, Cordova, and Swank 1979; Swank 1979). During outburst, the hard X-ray luminosity first increases and then decreases, the spectral temperature of the hard X-rays decreases, and an intense blackbody component with temperature $T_{bb} < 100$ eV appears in soft X-rays (cf. Mason, Cordova, and Swank 1979). Figure 11 compares the hard X-ray spectrum of SS Cyg in quiescence and in outburst with the spectrum of AM Her.

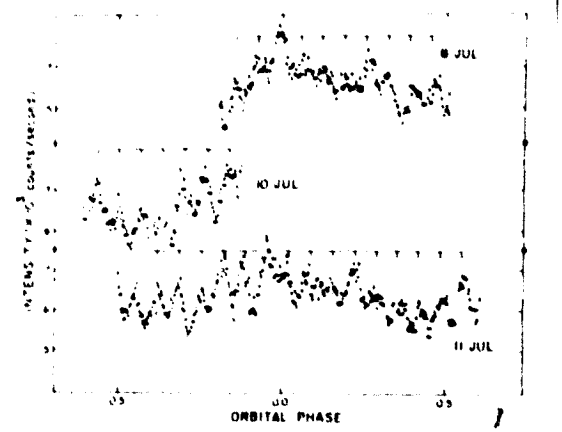

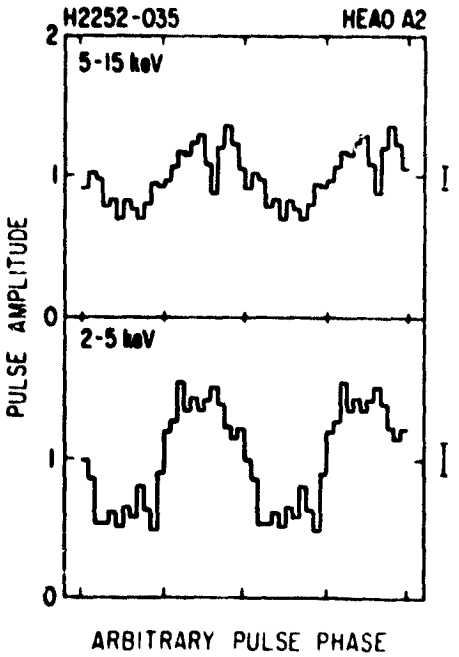

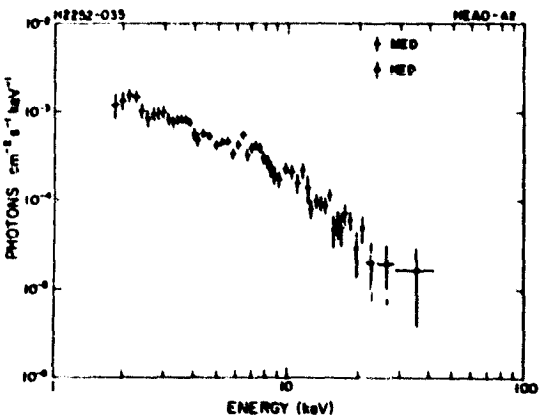

Fig. 7--Fast photometry of the optical light from H2252-035 (from Patterson and Price 1981). The 859 second pulsations, corresponding to reprocessed light from a stationary point in the binary system, are clearly visible.

Fig. 8--Hard X-ray pulse profile of H2252-035 through the 805 second rotation period of the degenerate dwarf (from White and Marshall 1981).

Fig. 9--Hard X-ray spectrum of H2252-035 (from White and Marshall 1981). The iron emission line at ≈ 7 keV is again clearly visible.

TABLE 3

SELECTED OTHER CATACLYSMIC VARIABLES (AFTER CÓRDOVA AND MASON 1982)

STAR[a]	P_b (Hours)	d (pc)[b]	P (s)[c]	L (10^{30} ergs s^{-1})[d]	T_{br} (keV)[e]	REFERENCES
WZ Sge	1.36	[100]	27.87, 28.97 (c)	6.0 (o)	[10]	14, 20
VW Hyi	1.78	[100]	24-32 (q) 88, 413 (q)	3.2 (q)	[10]	3, 7, 13
Z Cha	1.79	125±20	27.7 (c)	1.2 (o) 2.5 (q)	[10] [10]	1, 23
V603 Aql	3.33	430	...	160	[10]	2
U Gem	4.25	76±30	20-30 73-146	20 (o) 2 (q)	≈ 5 [10]	3, 5, 6, 19
UX UMa	4.72	214	28.5-30.0 (c)	2.0	[10]	1, 12
SS Cyg	6.60	125±25	8.5-10.9 (c, q) 32-36 (q)	100 (o) 410 (q)	≈ 8.5 ≈ 20	1, 4, 5, 8, 9, 11, 15, 17, 19, 21
Z Cam	6.96	[100]	16.0-18.8 (c)	1.9 (s)	[10]	18, 22
RU Peg	8.90	[100]	11.6-11.8 (c) ~ 51 (q)	23 (q)	[10]	2, 3, 16, 19
GK Per	16.43	480	~ 380 (q)	5200 (o) 130-220 (q)	[10] [10]	10, 15

[a] All stars are dwarf novae except GK Per (classical nova) and UX UMa (nova-like).
[b] Distances in brackets are assumed.
[c] Symbols "c" and "q" in parentheses denote "coherent" and "quasi-periodic", respectively.
[d] Luminosities assume a distance of 100 pc if distance is unknown; the symbols "o", "q", and "s" in parentheses denote "outburst", "quiescence", and "standstill", respectively.
[e] Temperatures in brackets are assumed.

(1) Becker (1981)
(2) Becker and Marshall (1981)
(3) Cordova, Mason, and Nelson (1981)
(4) Cordova et al. (1980)
(5) Cordova et al. (1981)
(6) Fabbiano et al. (1981)
(7) Haefner, Schoembs, and Vogt (1979)
(8) Hillebrand, Spiller, and Stiening (1981)
(9) Horne and Gomer (1980)
(10) King, Ricketts, and Warwick (1979)
(11) Mason, Cordova, and Swank (1979)
(12) Nather and Robinson (1974)
(13) Patterson (1979)
(14) Patterson (1980)
(15) Patterson (1981)
(16) Patterson, Robinson, and Nather (1977)
(17) Patterson, Robinson, and Kiplinger (1978)
(18) Robinson (1973)
(19) Robinson and Nather (1979)
(20) Robinson, Nather, and Patterson (1978)
(21) Swank (1979)
(22) Swank (1980)
(23) Warner (1974)

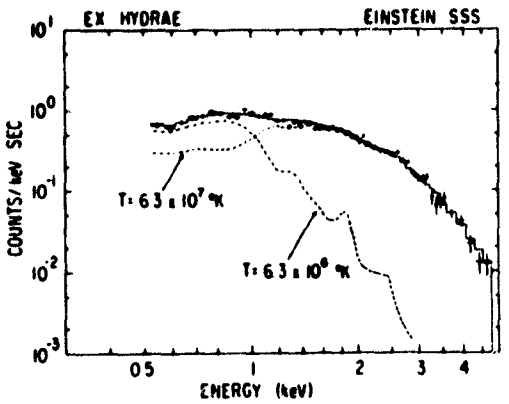

Fig. 10--Soft X-ray spectrum of EX Hydra measured by Einstein and showing the necessity of invoking at least two components (from Swank and White 1981).

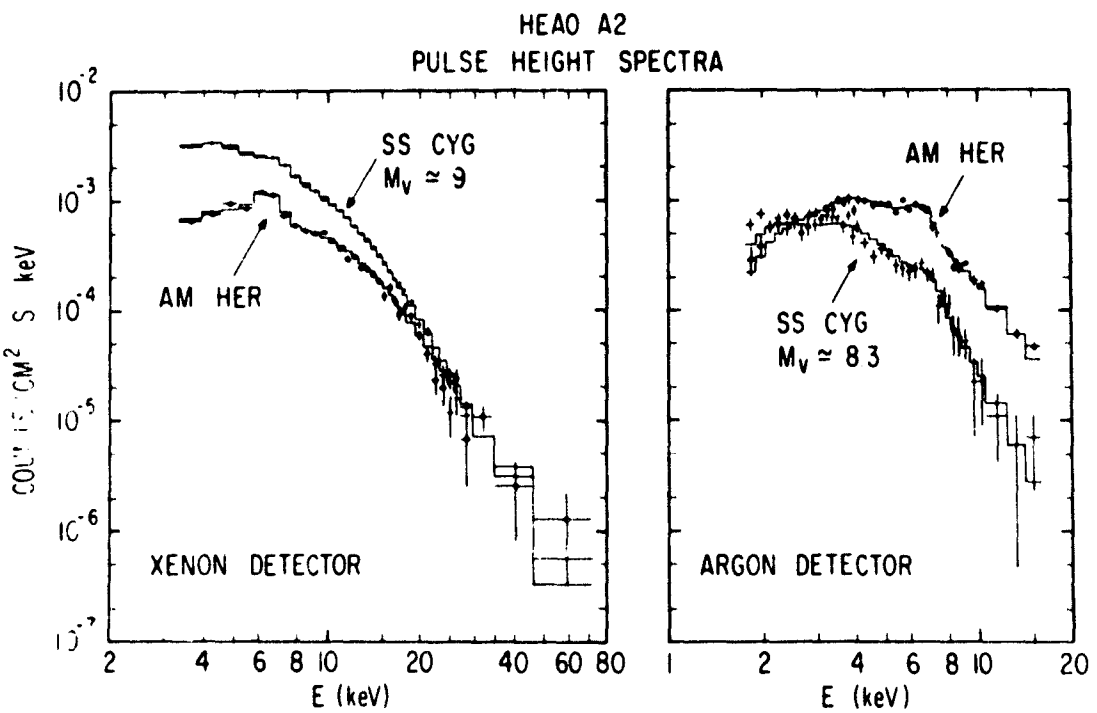

Fig. 11--Hard X-ray spectra of SS Cyg during quiescence (left panel) and during outburst (right panel) compared with the spectrum of AM Her (from Swank 1979). The presence of iron line emission at ≈ 7 keV in all spectra and the absence of low energy absorption in the spectrum of SS Cyg in outburst are evident.

The temporal behavior of the hard and soft X-ray luminosities of U Gem during an outburst is shown in Figure 12, while Figure 13 shows the way in which the hard X-ray spectrum of SS Cyg varies during an outburst.

Most of the remaining cataclysmic variables show only a hard X-ray component. It is not known whether the failure to detect a soft component during quiescence, or even during outburst in some sources, is due to its absence or due to the fact that it may have so low a spectral temperature that it is unobservable in soft X-rays.

Essentially all of the cataclysmic variables listed in Table 3 exhibit small amplitude quasi-periodic or coherent optical pulsations, usually during the onset of an outburst (Robinson 1976). Of special interest are the $\sim$ 8 - 10 second quasi-periodic pulsations in SS Cyg. They are strongly present in soft X-rays during outburst, yet their coherence persists for only 3-5 pulse periods (Cordova et al. 1980, 1981).

iv) Isolated stars

Sirius B, the first degenerate dwarf discovered, was detected as a very soft X-ray source by Mewe et al. (1975). Subsequently, very soft X rays were also detected from the hot degenerate dwarf HZ 43 (Hearn et al. 1976). Both of these degenerate dwarfs are members of binaries, but the binary separations are so large that the companions are not believed to play any role in the X-ray emission. Feige 24, another hot degenerate dwarf, has been detected in the extreme UV (Margon et al. 1976); however, it was not detected by the HEAO-1 soft X-ray survey and, unfortunately, Einstein ceased operating before observations of it were carried out. Table 4 lists these three sources and summarizes some of their properties.

The emission fron Sirius B, HZ 43, and Feige 24 at optical, UV, and X-ray wavelengths can be understood as photospheric emission from a hydrogen-rich [$n_{He}/n_H \sim 10^{-5}$] atmosphere with $T_{eff} \sim$ 30,000 - 60,000 K (Shipman 1976, Margon et al. 1976, Wesselius and Koester 1978, Martin et al. 1982). An upper limit in the extreme UV (200 - 800 A) for Sirius B (Cash, Bowyer, and Lampton 1978) appeared to conflict with photospheric models for the X-ray emission and to lend support to coronal models. However, UV observations yielded no evidence for a corona (Bohm-Vitense, Dettmann, and Kapranidis 1979) and Martin et al. (1982) have recently demonstrated that soft X-ray data from HEAO-1, together with the optical, UV, and extreme UV data, are consistent with photospheric emission at $\sim$ 28,000 K, as shown in Figure 14. For more detailed, but earlier, reviews of extreme UV and soft X-ray emission from isolated degenerate dwarfs, see Garmire (1979) and Bowyer (1979).

III. CONTINUUM SPECTRA

a) Qualitative Picture

In the remainder of this review, we shall focus on X-ray emission by accreting degenerate dwarfs.

i) Disk inflow near the star

Many of the cataclysmic variable X-ray sources show clear optical and UV evidence of accretion disks. If the disk extends all the way in to the stellar surface, viscous dissipation in the disk will release approximately half of the available

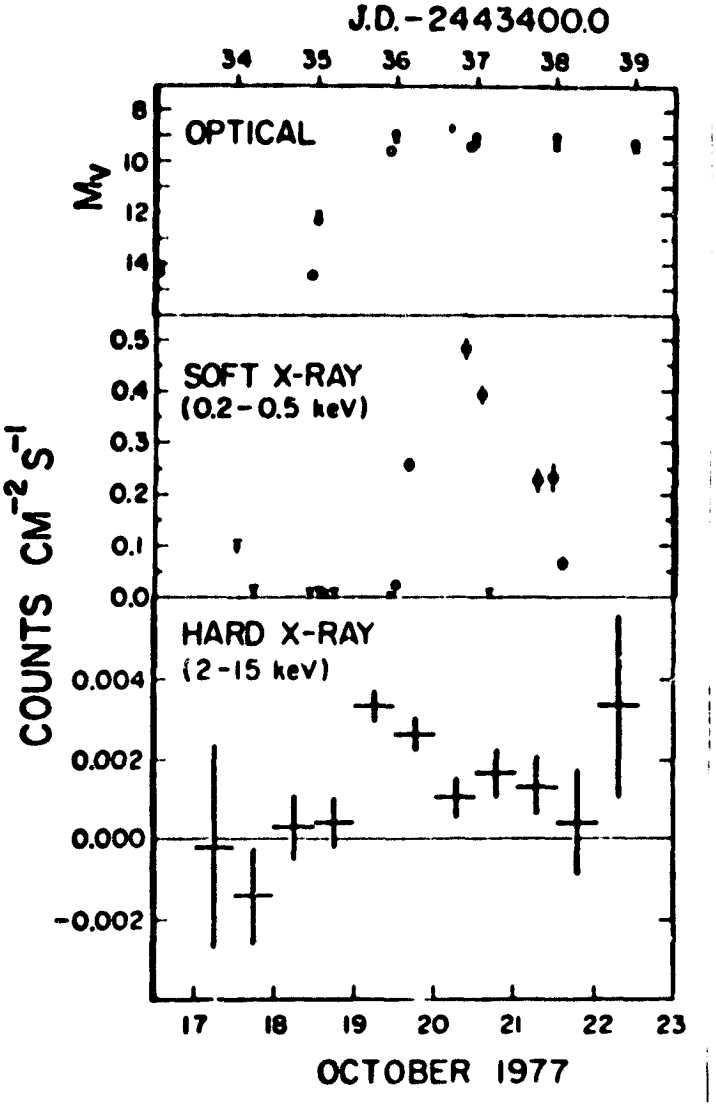

Fig. 12--Optical, soft X-ray, and hard X-ray light curves of U Gem through an outburst (from Mason, Cordova, and Swank 1979).

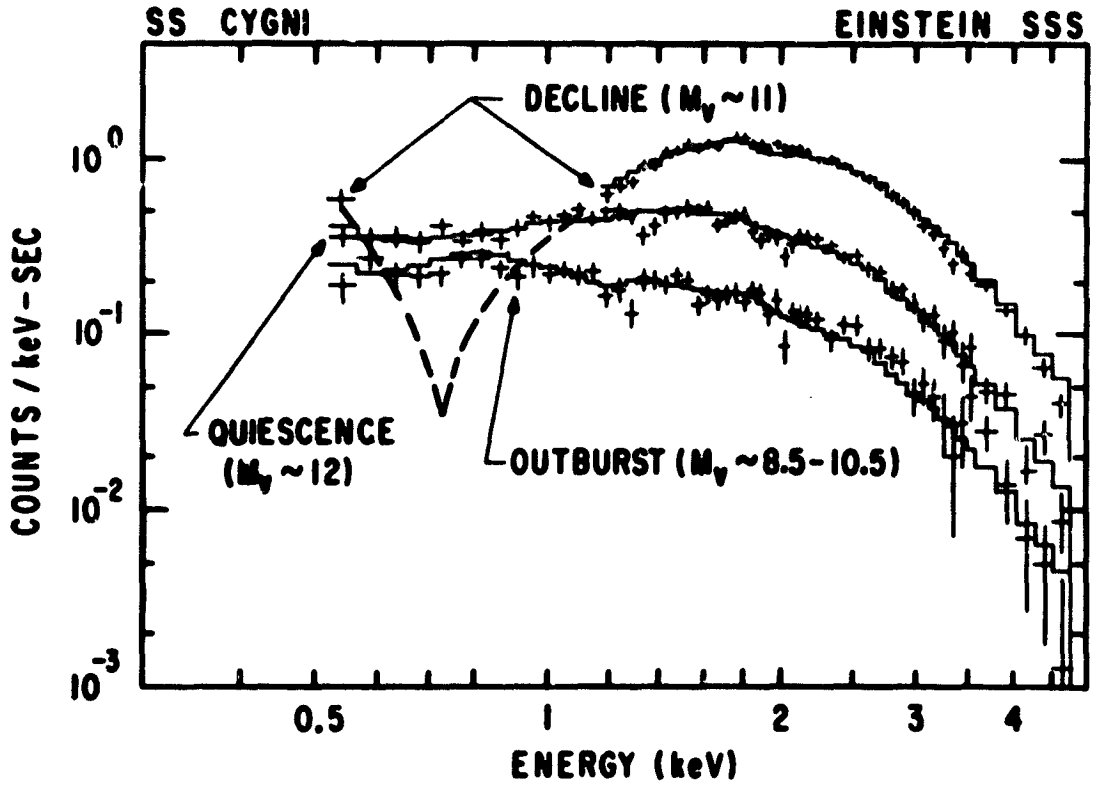

Fig. 13--Soft X-ray spectrum of SS Cyg showing the variation in the spectrum from outburst through decline to quiescence (from Swank and White 1981).

TABLE 4

ISOLATED STARS

STAR	d (pc)	L (10^{30} ergs s^{-1})	T_{eff} (k)	REFERENCES
Sirius B	2.7	0.06	≈ 28,000	4, 5, 6
HZ 43	65	40	≈ 60,000	2, 7
Feige 24	90	< 3	≈ 60,000	1, 3

(1) Bowyer (1979)

(2) Hearn et al. (1976)

(3) Margon et al. (1976)

(4) Martin et al. (1982)

(5) Mewe et al. (1975)

(6) Shipman (1976)

(7) Wesselius and Koester (1978)

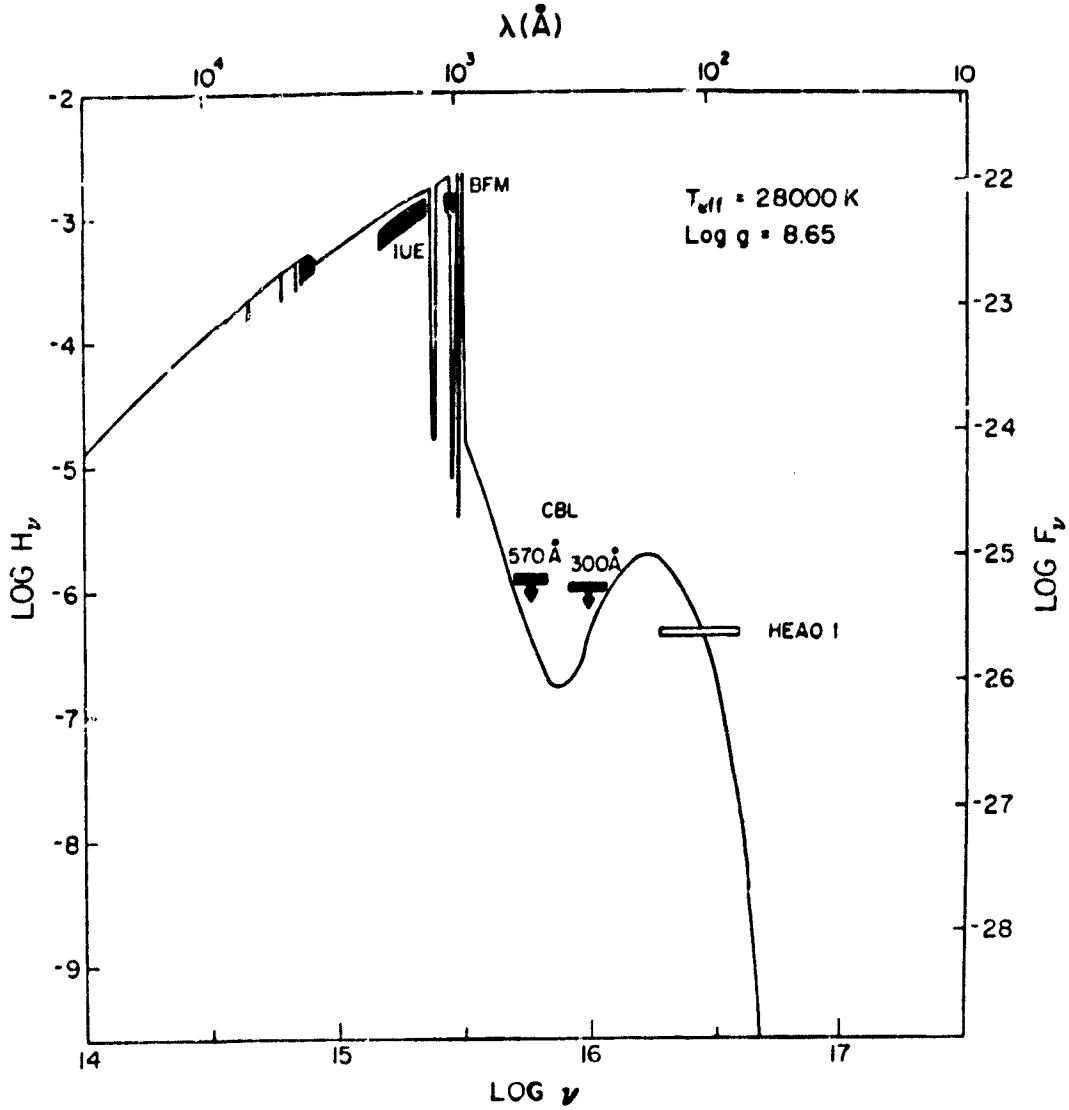

Fig. 14--Comparison of the flux from a 28,000 K hydrogen-rich model atmosphere with measurements and upper limits at UV, extreme UV, and soft X-ray wavelengths (from Martin et al. 1982).

gravitational energy, which will appear as blackbody radiation from the disk surfaces. The other half of the available gravitational energy will be released in a boundary layer at the inner edge of the disk where it encounters the surface of the star, unless the star is rotating near breakup. This luminosity is

$$L_{bdry} = \frac{1}{2}\frac{GM\dot{M}}{R} = 4 \times 10^{32} (M/M_\odot) (R/10^9 \text{ cm})^{-1} (\dot{M}/10^{-10} M_\odot \text{ yr}^{-1}) \text{ ergs s}^{-1}, \quad (1)$$

where M and R are the mass and radius of the star, and $\dot{M}$ is the mass accretion rate. At moderate or high accretion rates, the boundary layer is capable of producing soft X-rays by blackbody emission (Pringle 1977). After it was found that most cataclysmic variables emit hard, but not soft, X rays during quiescence, Pringle and Savonije (1979) proposed that the boundary layer might produce hard X-ray emission by optically thin bremsstrahlung if shocks occurred there. The maximum possible shock temperature is

$$T_s = \frac{3}{8} T_{ff} = 2 \times 10^8 (M/M_\odot (R/10^9 \text{ cm})^{-1} \text{ K}, \quad (2)$$

and thus the shocks must be strong ones. This is difficult to achieve in the strongly sheared flow of the inner disk whose geometry would tend to favor production of a large number of cooler, oblique shocks (in principle, the disk can join onto the star without the occurrence of any shocks). To attain the required strong shocks, Pringle and Savonije (1979) suggest a two-stage process in which gas that is initially mildly shocked in the boundary layer expands into the path of, and collides with, gas still circulating in the inner disk. Tylenda (1981), however, argues that turbulent viscosity will be a more efficient mechanism than shocks for dissipating energy in the boundary layer and that this mechanism can account for the observed high temperatures without resorting to complicated flow geometries.

Knowledge of whether the boundary layer can produce hard X-rays and, if so, how, is important for understanding the cataclysmic variable X-ray sources. But as yet, the ideas that have been proposed have not been worked out in any detail.

For up-to-date discussions of disks, see the review by Pringle (1981) and the paper by Tylenda (1981).

ii) Radial inflow near the star

If the degenerate dwarf has a magnetic field,

$$B \gtrsim 2 \times 10^3 (10^{-10} M_\odot \text{ yr}^{-1})^{1/2} (R/10^9 \text{ cm})^{-5/4} (M/M_\odot)^{1/4} \text{ gauss}, \quad (3)$$

the field will disrupt the disk and lead to approximately radial inflow near the star. This picture certainly applies to the AM Her and DQ Her stars, and may apply to other cataclysmic variables if magnetic fields are endemic in degenerate dwarfs as speculated earlier. Radial inflow may also occur if mass transfer takes place via a stellar wind rather than via Roche lobe overflow. Most theoretical work has assumed radial inflow because it is far more tractable; in the remainder of this review, we will concentrate on radial inflow.

A qualitative picture of X-ray emission by radially accreting degenerate dwarfs is shown in Figure 15. As accreting matter flows toward the star, a strong standoff shock forms far enough above the star for the hot, post-shock matter to cool and come to rest at the stellar surface (Hoshi 1973; Aizu 1973; Fabian, Pringle, and Rees 1976). The

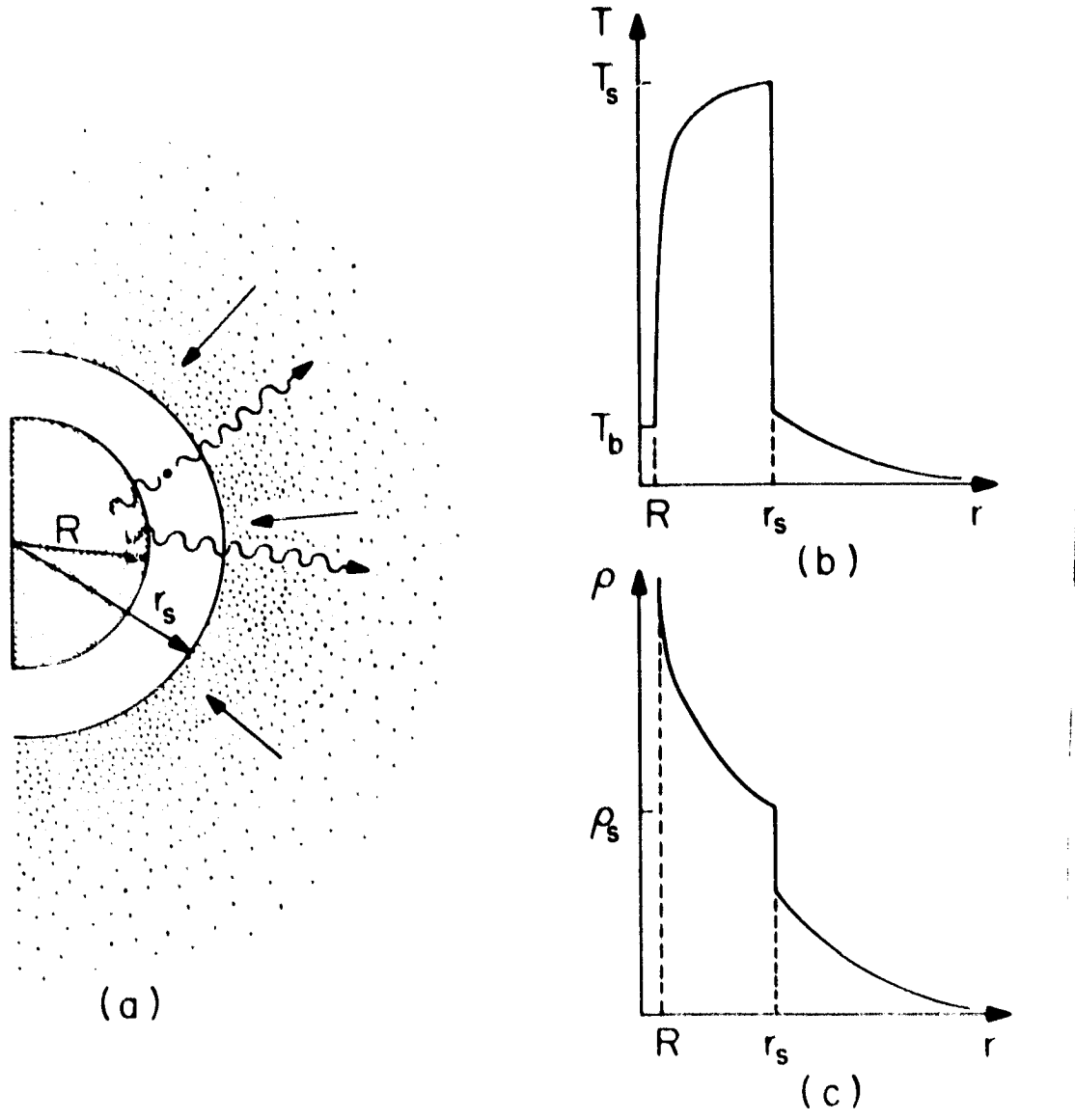

Fig. 15--Qualitative picture of X-ray emission from an accreting degenerate dwarf. a) Configuration of the star, the emission region, and the infalling matter. R is the stellar radius and r_s is the shock radius. The straight arrows indicate infalling matter, the wiggly arrows photons. b) Temperature profile of the infalling matter. T_s is the post-shock temperature and T_b is the stellar blackbody temperature. c) Density profile of the infalling matter; ρ_s is the post-shock density.

standoff distance

$$d \equiv r_s - R = 1/4\, v_{ff}(r_s)\, t_{cool}(r_s), \tag{4}$$

where r_s is the shock radius, R is the stellar radius, v_{ff} is the free-fall velocity, and t_{cool} is the time scale for cooling, due to bremsstrahlung and, if a magnetic field is present, cyclotron emission. Roughly half of the bremsstrahlung flux is emitted outward and forms a hard X-ray component. Roughly half of the cyclotron flux is emitted outward and forms a blackbody-limited component in the UV. The other halves of the bremsstrahlung and cyclotron fluxes are emitted inward and are reflected or absorbed by the stellar surface. The resulting blackbody flux forms a UV or soft X-ray component with

$$L_{bb} = L_{cyc} + L_{br}, \tag{5}$$

where L_{bb}, L_{cyc}, and L_{br} are the luminosities in the blackbody, cyclotron, and bremsstrahlung components. The total luminosity $L = GM\dot{M}/R$, or twice that given by equation (1).

If we allow for the possible presence of a magnetic field, the accreting matter may be channeled onto the magnetic poles and accretion may occur over only a fraction f of the stellar surface. The effective accretion rate of the accreting sector is $\dot{M}/f$, and the corresponding luminosity is L/f. X and UV radiation from magnetic degenerate dwarfs is thus a function of stellar mass M, magnetic field strength B, and effective luminosity L/f. The dependence on stellar mass is significant but is less than on the other two variables. If we specify the mass of the star, the parameter regimes encountered are conveniently displayed on a (B,L/f)-plane, as shown in Figure 16 for a 1 $M_\odot$. The upper left of the plane corresponds to low magnetic field strengths and high effective luminosities (and thus high densities in the emission region). In this portion of the plane, bremsstrahlung cooling dominates cyclotron cooling in the hot, post-shock emission region, and the character of the X-ray emission is essentially the same as that of a nonmagnetic degenerate dwarf. As one increases B or lowers L/f, moving toward the lower right in Figure 16, cyclotron cooling becomes more important until eventually it dominates (Masters et al. 1977). The solid line shows the location at which this occurs, as determined from detailed numerical calculations equating t_{cyc} and t_{br}, the cyclotron and bremsstrahlung cooling time scales. This line is approximately given by

$$B = 6 \times 10^6 \, (Lf^{-1}/10^{36} \text{ ergs s}^{-1})^{2/5} \text{ gauss}. \tag{6}$$

To the lower right of this solid line, the magnetic field qualitatively alters the character of the X-ray emission.

b) Magnetic Stars

Fabian, Pringle, and Rees (1976), Masters et al. (1977), and King and Lasota (1979) have discussed the qualitative features of X-ray emission by magnetic degenerate dwarfs. Lamb and Masters (1979; see also Masters 1978) carried out detailed numerical calculations of high harmonic cyclotron emission from a hot plasma, and from them developed a self-consistent, quantitative model of the X-ray and UV emission. Wada et al. (1981) have carried out a few calculations for the regime im which bremsstrahlung,

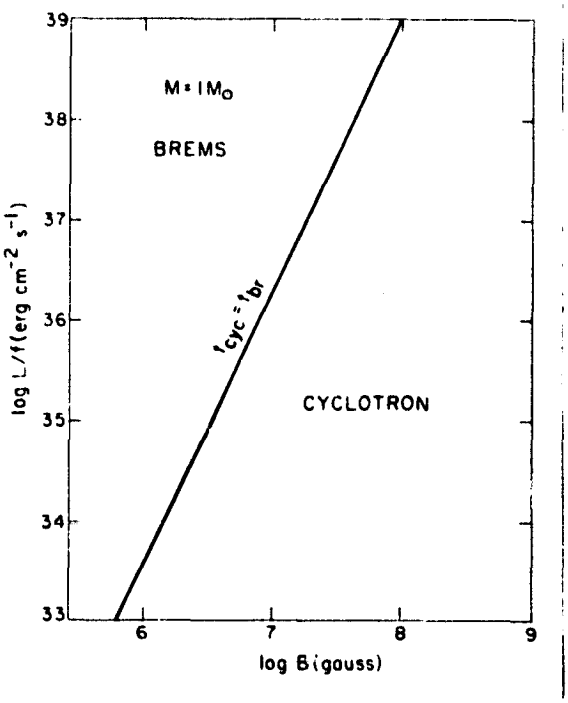

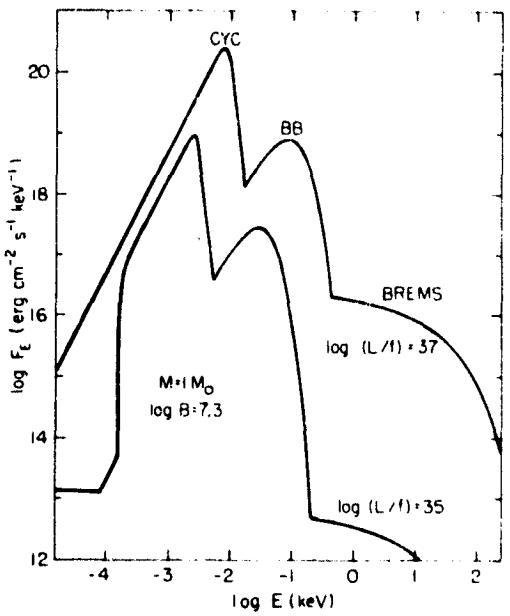

Fig. 16--Bremsstrahlung and cyclotron emission regimes in the (L/f,B)-plane for a 1 $M_\odot$ star (after Lamb and Masters 1979).

Fig. 17--X-ray and UV spectra produced by accretion onto a 1 $M_\odot$ star at two different accretion rates. The spectrum with $L/f = 10^{37}$ ergs s^{-1} is in the bremsstrahlung dominated regime, while the spectrum with $L/f = 10^{35}$ ergs s^{-1} is in the cyclotron dominated regime (from Lamb and Masters 1979).

not cyclotron emission, dominates (see Figure 16).

i) Spectra

The X and UV spectrum produced by accretion onto magnetic degenerate dwarfs generally has four components: 1) a blackbody-limited UV cyclotron component produced by the hot emission region, 2) a hard X-ray bremsstrahlung component also produced by the hot emission region, 3) a hard UV or soft X-ray blackbody component produced by cyclotron and bremsstrahlung photons that are absorbed by the stellar surface and re-emitted, and 4) secondary radiation from infalling matter above the shock or, possibly, from the stellar surface around the emission region. The first three components are clearly visible in Figure 17, which shows spectra produced by the hot, post-shock emission region alone. Since the secondary radiation is not included, the spectra do not accurately represent the observed spectrum below $\sim$5 eV. Figure 17 shows the X and UV spectra produced by accretion at two different rates, corresponding to $L/f = 10^{35}$ and 10^{37} erg s^{-1}, onto a 1.0 $M_\odot$ star having a magnetic field of 2×10^7 gauss.

The spectra illustrated in Figure 17 show two important features. First, strongly magnetic degenerate dwarfs should be intense UV sources with only a few percent of the total accretion luminosity ordinarily appearing as optical or soft and hard X-rays, and therefore easily accessible. Second, the position and relative strength of the spectral components change with variations in the accretion rate. For example, the change in accretion rate shown in Figure 17 moves the blackbody component from the UV into the soft X-ray region, and the luminosity of the bremsstrahlung hard X-ray component increases by nearly 4 orders of magnitude while the total accretion luminosity increases only by 2.

ii) Correlation between spectral temperature and luminosity

Variations in the shape and the strength of the spectral components are a function of both mass accretion rate and magnetic field strength. They can be conveniently displayed by plotting contours on a (B,L/f)-plane. Sets of such contours are shown in Figures 18 and 19 for a 1.0 $M_\odot$ star. Bremsstrahlung and cyclotron emission dominate in the same regions as in Figure 16. In Figure 18, contours of constant shock standoff distance $d = \delta R/R$ are shown as thick solid lines. The thin solid lines in the bremsstrahlung-dominated region show contours of constant $q = L_{cyc}/L_{br}$, while those in the cyclotron-dominated region show contours of constant T_e, the temperature of the bremsstrahlung hard X-ray component. In Figure 19, contours of constant E^*, the peak of the blackbody-limited cyclotron component, are shown as thick solid lines while contours of constant T_{bb}, the temperature of the blackbody component, are shown as dashed lines. The thin solid lines have their same meaning as in Figure 18. To the upper right of the curve labelled "soft excess" in Figure 19, the blackbody luminosity in soft X-rays exceeds the bremsstrahlung luminosity in hard X-rays.

Near and above $L/f = L_E = 1.4 \times 10^{38}$ erg s^{-1}, radiation pressure can be important and modify the results, but because photons can easily scatter out of the accretion column if $f \ll 1$, the Eddington luminosity does not represent the stringent upper limit to the luminosity that it does in the case of nonmagnetic degenerate dwarfs. Below and to the left of the curve $E^* = 2$ eV in Figure 19, the assumption $d < R$ breaks down, as can be seen from Figure 18.

If the geometry of the hot, post-shock emission region is such that most of the flux escapes through the face rather than through the edges of the emission region (i.e., $d \ll \sqrt{(2f)}R$), then Compton degradation of the bremsstrahlung hard X-ray component will occur if L/f exceeds $\sim 10^{37}$ erg s^{-1}. Such degradation is identical to that encountered

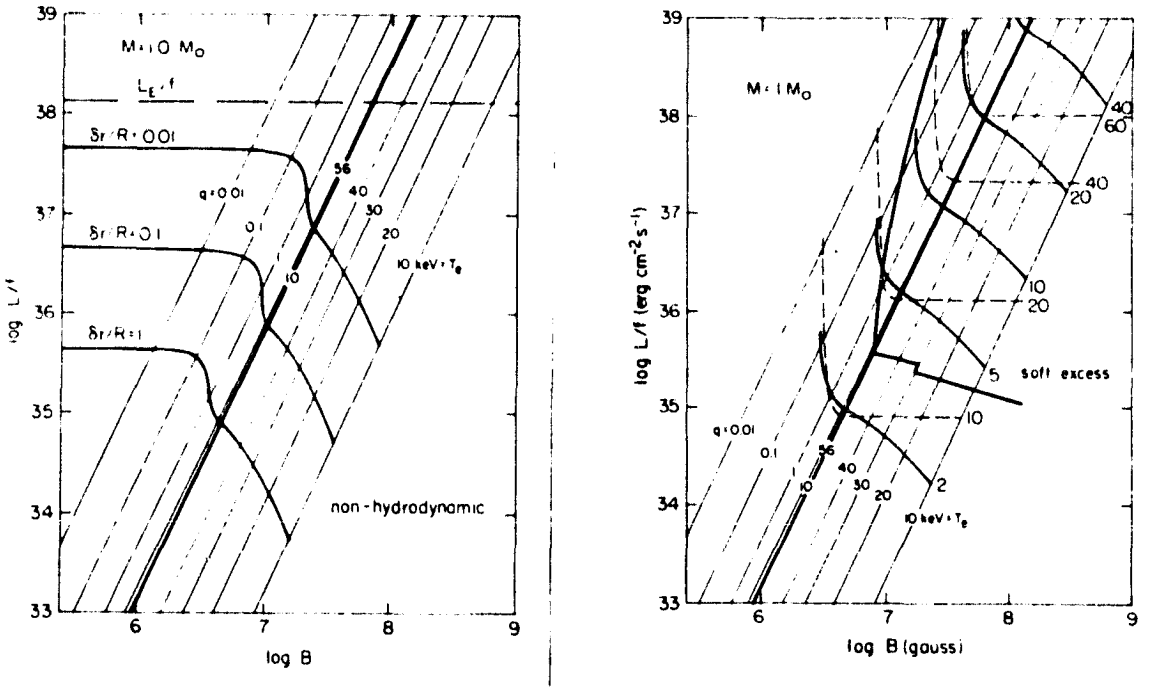

Fig. 18--Contours in the (L/f,B)-plane for a 1 $M_\odot$ star. For an explanation of the various lines, see the text.

Fig. 19--More contours in the (L/f,B)-plane for a 1 $M_\odot$ star (from Lamb and Masters 1979). For an explanation of the various lines, see the text.

in nonmagnetic degenerate dwarfs, and will be discussed below.

Figure 19 illustrates a third important feature of X-ray emission from magnetic degenerate dwarfs: observations of the qualitativr features of the X and UV spectrum can determine fairly accurately the physical conditions in the emission region, including the value of the magnetic field.

c) Nonmagnetic Stars

Studies of X-ray emission from accreting nonmagnetic degenerate dwarfs include those by Hoshi (1973), Aizu (1973), Hayakawa (1973), DeGregoria (1974), Hayakawa and Hoshi (1976), Fabian, Pringle, and Rees (1976), Katz (1977), and Kylafis and Lamb (1979, 1982a,b). These calculations are applicable, even if a magnetic field is present, as long as the accretion flow is approximately radial and bremsstrahlung cooling dominates cyclotron cooling in the X-ray emission region (recall Figure 16). Thus they are relevant to the AM Her stars, such as AM Her itself, which has a magnetic field $B \sim 2 \times 10^7$ gauss (Lamb and Masters 1979; Schmidt, Stockman, and Margon 1981; Latham, Liebert, and Steiner 1981), and VV Pup, which has a magnetic field $B \sim 3 \times 10^7$ gauss (Visvanathan and Wickramasinghe 1979; Stockman, Liebert, and Bond 1979), as well as to the DQ Her stars.

i) Spectra

The X and UV spectrum produced by accretion onto nonmagnetic degenerate dwarfs generally has three components: 1) a hard X-ray bremsstrahlung component produced by the hot, post-shock emission region, 2) a soft X-ray blackbody component produced by bremsstrahlung photons that are absorbed by the stellar surface and re-emitted, and 3) secondary radiation produced by Compton heating of infalling matter above the shock.

These components are clearly visible in Figure 20, which shows six spectra that span the entire range of accretion rates. Figure 21 shows for comparison three similar spectra when nuclear burning occurs at the accretion rate (see below). At low accretion rates, $\tau_{es} < 1$ and the observed hard X-ray spectrum is essentially the same as that produced in the emission region. As the accretion rate is increased, τ_{es} exceeds unity and Compton scattering begins to degrade the spectrum (Illarionov and Sunyaev 1972). The blackbody component then contains a contribution from bremsstrahlung photons which are backscattered by the accreting matter and absorbed by the stellar surface. The secondary radiation, which arises from accreting matter heated by the Compton scattering of the bremsstrahlung photons, is important only when degradation of the bremsstrahlung is substantial. As the accretion rate is increased further, this degradation becomes more severe. Finally, due to the combined effects of degradation and weakening of the shock by radiation pressure, the bremsstrahlung component disappears altogether. The star then ceases to be a hard (i.e., $T_{obs} > 2$ keV) X-ray source.

Figure 20 illustrates two important features of X-ray emission from nonmagnetic degenerate dwarfs. First, an intense blackbody soft X-ray component is always present. Second, at high accretion rates Compton degradation leads to low spectral temperatures even for high mass stars.

ii) Correlation between spectral temperature and luminosity

The resulting correlation between T_{obs} and L_h is shown in Figure 22 for stars of mass $M = 0.2\text{-}1.2\ M_\odot$. Note that the accretion rate increases as one moves from upper left to lower right along the curves. For sources found in the lower right of the figure,

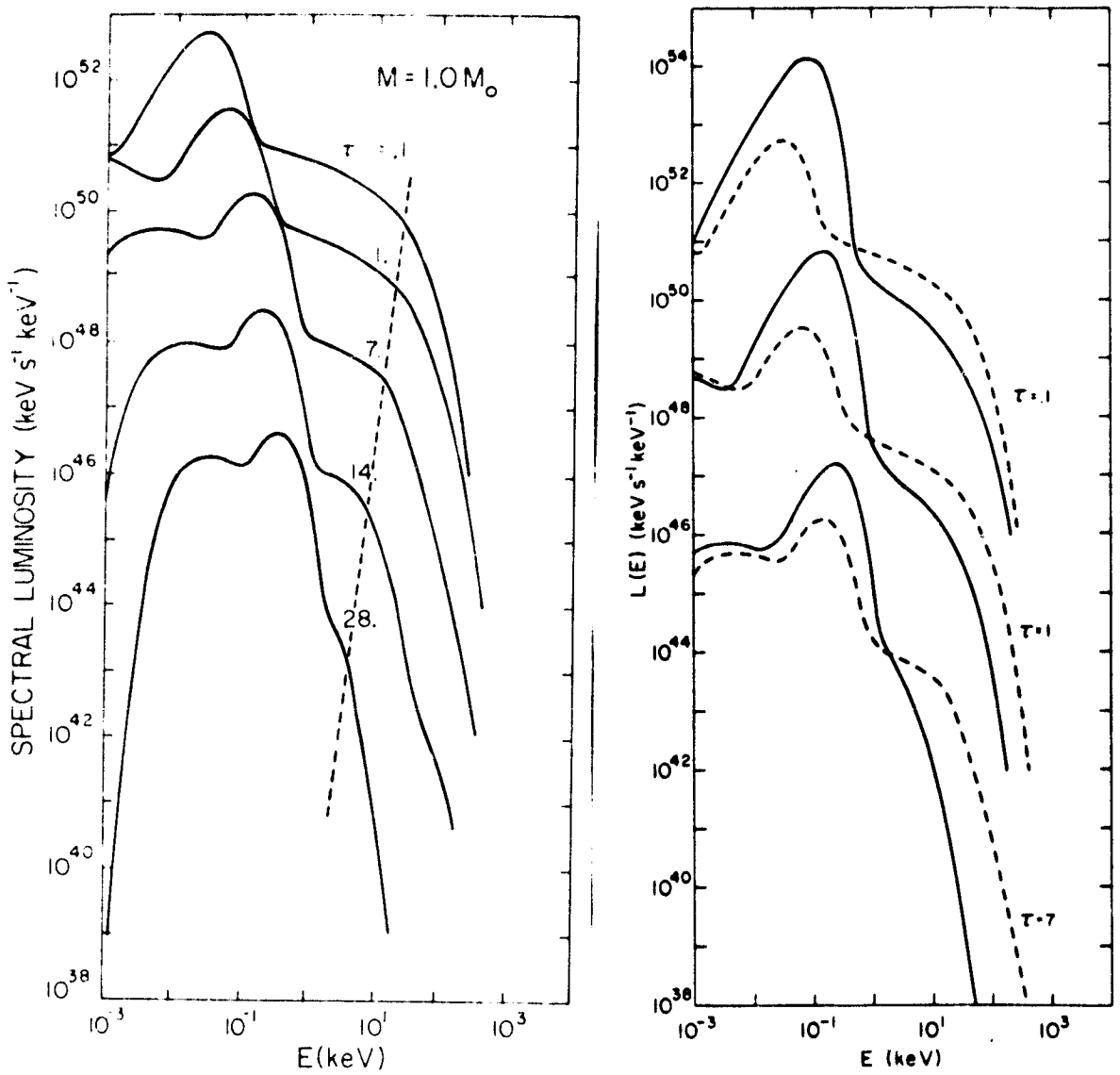

Fig. 20--X and UV spectra produced by accretion onto a 1 $M_\odot$ star for six different accretion rates (from Kylafis and Lamb 1982a). The dashed line shows the changing cutoff due to Compton degradation.

Fig. 21--Comparison of X and UV spectra produced by accretion onto a 1 $M_\odot$ star with nuclear burning at the accretion rate (solid curves) and without nuclear burning (dashed curves) (from Weast et al. 1982).

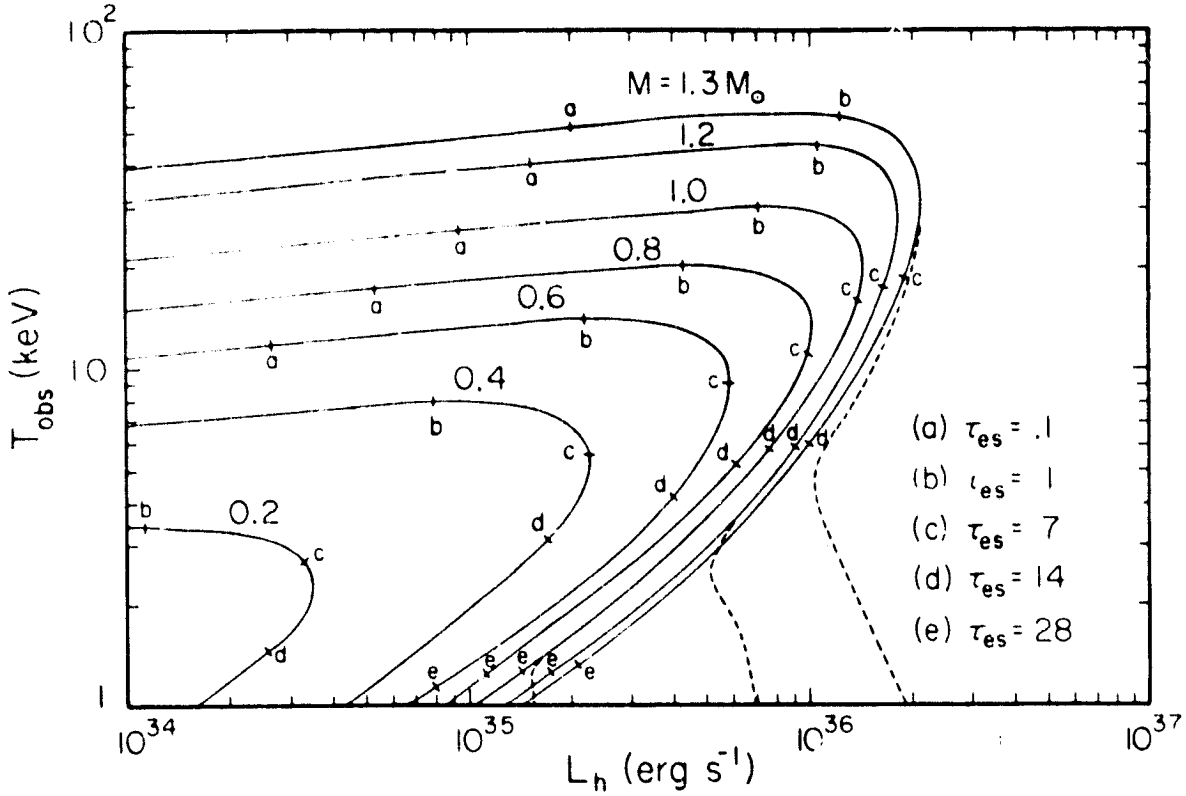

Fig. 22--Correlation between T_{obs} and L_h for stars with masses 0.2 - 1.2 $M_\odot$ (from Kylafis and Lamb 1982a). The dashed lines give the same correlation when the contribution of the blackbody component is included in L_h.

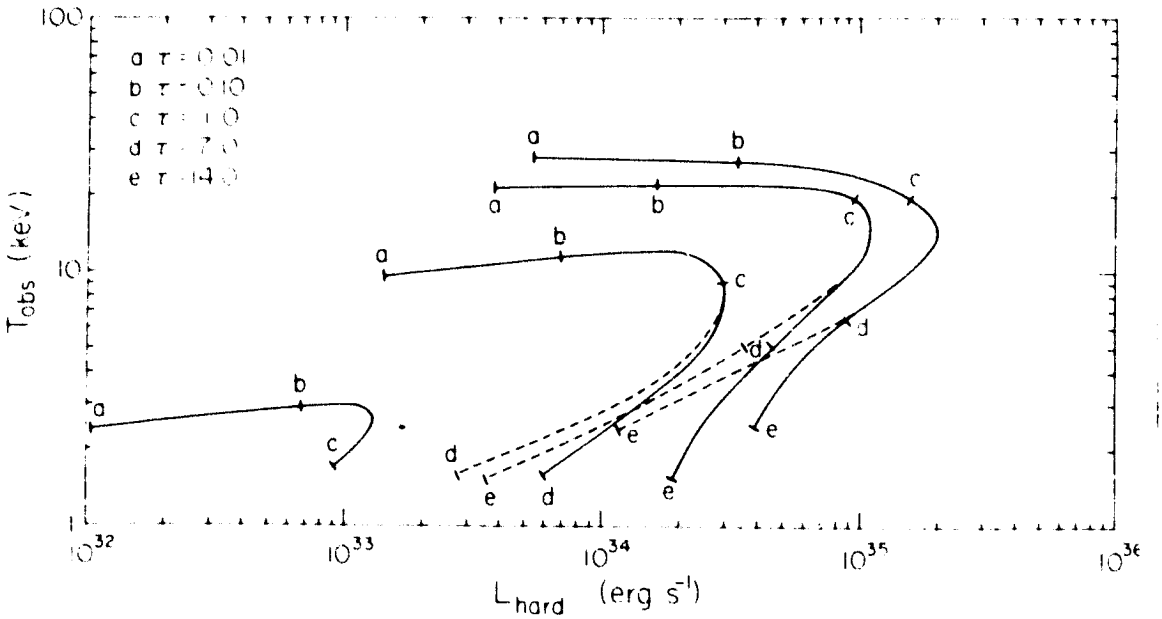

Fig. 23--Correlation between T_{obs} and L_h for stars with masses 0.2 - 1.2 $M_\odot$ (from Weast et al. 1982). The dashed lines give the same correlation when the contribution of the blackbody component is omitted.

an increase in T_{obs} and L_h therefore corresponds to a decrease in the accretion rate: t_{obs} and L_h increase since the smaller accretion rate lessens Compton degradation of the hard X-ray spectrum.

Figure 22 illustrates the dramatic variation in the spectral temperature at high accretion rates and the pronounced correlation between X-ray spectral temperature and luminosity.

d) Effects of Nuclear Burning

The energy liberated by nuclear burning of matter accreting onto degenerate dwarfs can be more than an order of magnitude greater than that available from the release of gravitational energy. If burning occurs quiescently, the resulting energy is transported to the stellar surface and produces an intense blackbody soft X-ray flux. Steady nuclear burning has therefore recently received a great deal of attention as a possible explanation of the intense blackbody soft X-ray components inferred in the AM Her stars (Raymond et al. 1979, Patterson et al. 1982) and in other cataclysmic variables, such as SS Cyg and U Gem, during outburst (Fabbiano et al. 1981).

i) Conditions for steady nuclear burning

Unfortunately, the conditions under which steady nuclear burning can occur are poorly understood. Detailed spherically symmetric calculations by Paczynski and Zytokow (1978), Sion, Acierno, and Turnshek (1978), and Sion, Acierno, and Tomczyk (1979) show that if the degenerate dwarf is initially cold and the accretion rate is not too high, the accreting matter becomes highly degenerate before it ignites. Electron conduction then rapidly transports energy away into the core, and it must be heated before ingition can occur. If the degenerate dwarf is hot, or if the accretion rate is high, the hydrogen in the accreting matter soon ignites due to compressional heating. In either case, eventually a violent nuclear outburst ensues. Such outbursts are believed to account for novae (cf. Starrfield, Sparks, and Truran 1974).

The outbursts are separated by quiescent periods, in which nuclear burning occurs steadily at only a small fraction of the accretion rate. The quiescent periods are shorter for higher accretion rates and can last from $\sim$ 20 years or less (Sion et al. 1979) to $> 10^7$ years (Paczynski and Zytkow 1978). For a narrow range of higher accretion rates, steady nuclear burning is possible at the rate of accretion (e. g. $1.0 - 2.7 \times 10^{-7}$ $M_\odot\ yr^{-1}$ for a 0.8 $M_\odot$ star; Paczynski and Zytkow 1978). Still higher accretion rates lead to envelope expansion and the formation of a red giant with a degenerate core.

Depletion of CNO nuclei in the accreting matter and the burning region by diffusion can lead to burning via the p-p chain rather than via the more temperature sensitive CNO-cycle (Starrfield, Truran, and Sparks 1981), and stabilize the burning at higher accretion rates. However, theoretical investigations show that such rapid depletion is unlikely (Fujimoto and Truran 1981; Papaloizou, Pringle, and MacDonald 1982).

Effects due to non-spherical geometries also warrant investigation. For example, in the AM Her and DQ Her stars a strong magnetic field channels the accreting matter onto the magnetic poles. If the matter is confined and burns over only a small fraction of the stellar surface, the burning might be stabilized by the rapid transport of energy horizontally.

ii) Effects on X-ray emission

The effects of nuclear burning on X-ray emission by nonmagnetic degenerate dwarfs have been investigated in detail by Imamura et al. (1979, 1982) and Weast et al. (1979, 1982). The accreting matter does not burn in the hot X-ray emission region, but may do so deeper in the envelope of the star. The energy thus liberated is transported to the stellar surface and enhances the blackbody flux in soft X-rays. This flux of soft X-ray photons cools the X-ray emission region by inverse Compton scattering. As a result, the hard X-ray luminosity is often an order of magnitude less than it would be in the absence of nuclear burning, the hard X-ray spectrum is softer, and the soft X-ray luminosity can be 100 times the hard X-ray luminosity. Figure 21 compares the X-ray spectra of a 1 $M_\odot$ star in which nuclear burning occurs at the accretion rate to the spectra in the absence of burning. The three spectra shown span the entire range of accretion rates. Figure 23 shows the correlation between T_{obs} and L_h when nuclear burning occurs at the accretion rate for stars of mass 0.2 - 1.2 $M_\odot$. These curves should be compared with those in Figure 22, which assumes no nuclear burning.

The effects of nuclear burning on X-ray emission by magnetic degenerate dwarfs are not expected to be as dramatic. As long as cooling by cyclotron emission dominates cooling by inverse Compton scattering of the blackbody photons, the cyclotron UV and bremsstrahlung hard X-ray luminosities will be little changed. The spectral temperatures of these components will also be little affected. The blackbody soft X-ray luminosity will, however, be much larger.

IV. LINE SPECTRA

a) Ionization Structure

The circumstellar ionization structure of degenerate dwarf X-ray sources has been calculated analytically by Hayakawa (1973) and more recently by Kylafis and Lamb (1982b). These calculations assume spherical symmetry, and assume that the optical depth to absorption is small. The degenerate dwarf X-ray sources detected so far have low luminosities and low accretion rates. Therefore, the analytical calculations are valid, provided that the accretion flow is approximately radial.

The calculations by Kylafis and Lamb (1982b) show that the blackbody soft X-ray flux ionizes H, He, and C out to distances large compared with a typical binary separation. Furthermore, for high mass stars and low accretion rates, the bremsstrahlung hard X-ray flux ionizes heavy elements out to considerable distances. These features are illustrated in Figures 24 and 25, which show l_Z, the radius at which the element with charge Z is half ionized and half neutral, as a function of mass accretion rate for a 1.2 $M_\odot$ star. Figure 24 shows the effect of the blackbody soft X-ray flux, while Figure 25 shows the effect of the bremsstrahlung hard X-ray flux. In both figures, the solid lines correspond to no nuclear burning and the dashed lines to nuclear burning at the accretion rate.

The absorption optical depth τ^*_Z at the ionization edges of heavy elements remains small until the accretion rate exceeds about 3×10^{-3} $\dot{M}_E$ but thereafter increases rapidly, as shown in Figure 26. Compton scattering and the resulting degradation of the hard X-ray spectrum occurs primarily close to the star, while most of the absorption occurs relatively far from the star, as illustrated in Figure 27. Thus the amount of Compton degradation is less sensitive, and the amount of absorption more sensitive, to the distribution of accreting matter.

b) Absorption Features

Figure 28 shows the emergent hard X-ray spectrum from a 1.2 $M_\odot$ star for four different accretion rates as calculated analytically by Kylafis and Lamb (1982b), taking absorption into account. Ross and Fabian (1981) have carried out detailed numerical calculations of the emergent spectrum from a 1.0 $M_\odot$ star for three different accretion rates. The latter calculations treat the atomic physics carefully and are valid even for large absorption optical depths. The results are shown in Figures 29-31. Note both the absorption K-edges due to O VIII (0.87 keV), Si XIV (2.7 keV), and Fe XXI-XXVI (8.2 - 9.3 keV), and the emission lines, broadened by Compton scattering, due to the Kα lines of O VIII (0.65 keV), Si XIV (2.0 keV), and Fe XXV (6.7 keV).

c) Emission Lines

The temperatures in the X-ray emission regions of degenerate dwarf X-ray sources are high enough (> 10 keV) to produce thermal emission lines, including those of Fe at $\sim$ 7 keV, with significant equivalent widths. Emission lines can also be produced by fluorescence in the accreting matter above the X-ray emission region, as seen in Figures 29-31. Fluorescent emission lines may also be produced by X-rays striking the stellar surface surrounding the emission region, the disk, and even the companion star.

The emission lines may be broadened by 1) thermal Doppler broadening, 2) Compton scattering, and 3) Doppler broadening due to bulk streaming velocities. Thermal Doppler broadening produces a relative line width,

$$\Delta\nu/\nu \sim (2kT/m_e c^2)^{1/2}. \tag{7}$$

The resulting width is $\sim$ 0.5 keV for the $\sim$ 7 keV Fe lines if they are formed in an X-ray emission region with temperature $T_e \sim$ 10 keV. Compton scattering produces a relative line width

$$\Delta\nu/\nu \sim \tau^2 \frac{h\nu}{m_e c^2} \sim 0.1\,\tau^2\,(h\nu/7\ \text{keV}). \tag{8}$$

Thus the $\sim$ 7 keV Fe emission lines will be relatively broad even if the electron scattering optical depth through accreting matter is only modest. Doppler broadening due to bulk motion produces a relative line width

$$\Delta\nu/\nu \sim v/c \sim 2 \times 10^{-2} \frac{v}{v_{ff}(R)}, \tag{9}$$

where in the last step we have scaled from the freefall velocity at the surface of a 1 $M_\odot$ star. Doppler broadening due to bulk motion is therefore generally less than thermal Doppler broadening and Compton scattering. These results imply that the X-ray emission lines produced by degenerate dwarfs are relatively broad. However, as noted above, emission lines can be produced by recombination and fluorescence in accreting matter far from the star. In this case, the temperatures may be low, and the electron scattering optical depth small. If so, narrow emission lines can be produced.

V. ISSUES

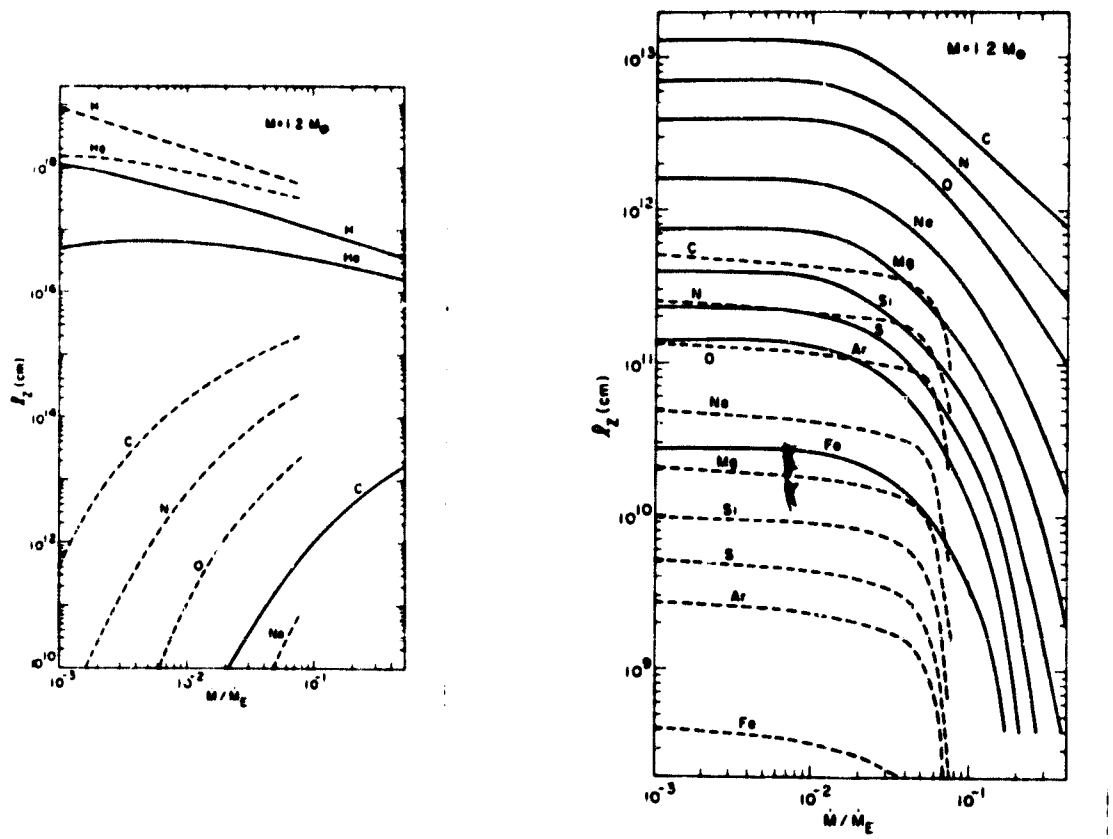

Fig. 24--Circumstellar ionization structure as a function of accretion rate produced by the blackbody soft X-ray flux of a 1.2 $M_\odot$ star (from Kylafis and Lamb 1982b). The quantity l_Z, the radius at which the element with charge Z is half ionized, is shown assuming no nuclear burning (solid lines) and nuclear burning at the accretion rate (dashed lines).

Fig. 25--Circumstellar ionization structure as a function of accretion rate produced by the bremsstrahlung hard X-ray flux of a 1.2 $M_\odot$ star (from Kylafis and Lamb 1982b). The curves have the same meaning as in Fig. 24.

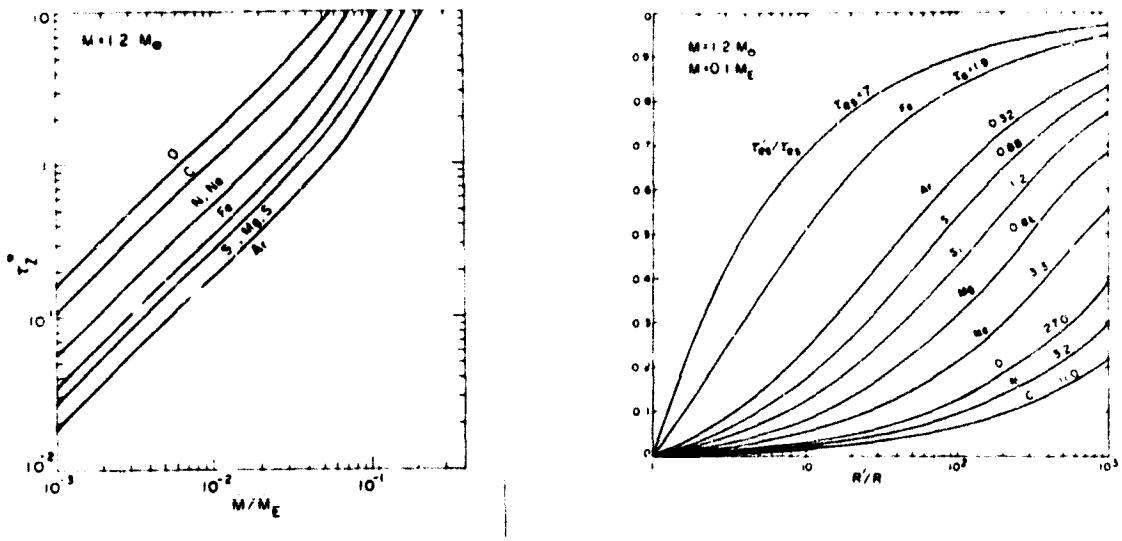

Fig. 26--Optical depth τ_Z^* at the absorption edge of a given element as a function of accretion rate for a 1.2 $M_\odot$ star without nuclear burning (from Kylafis and Lamb 1982b).

Fig. 27--Fractional electron scattering and absorption optical depths reached at a given radius for a 1 $M_\odot$ star accreting at a rate 0.1 $\dot{M}_E$ (from Kylafis and Lamb 1982b). Note that the electron scattering optical depth increases rapidly near the star, while the absorption optical depths remain small until larger radii.

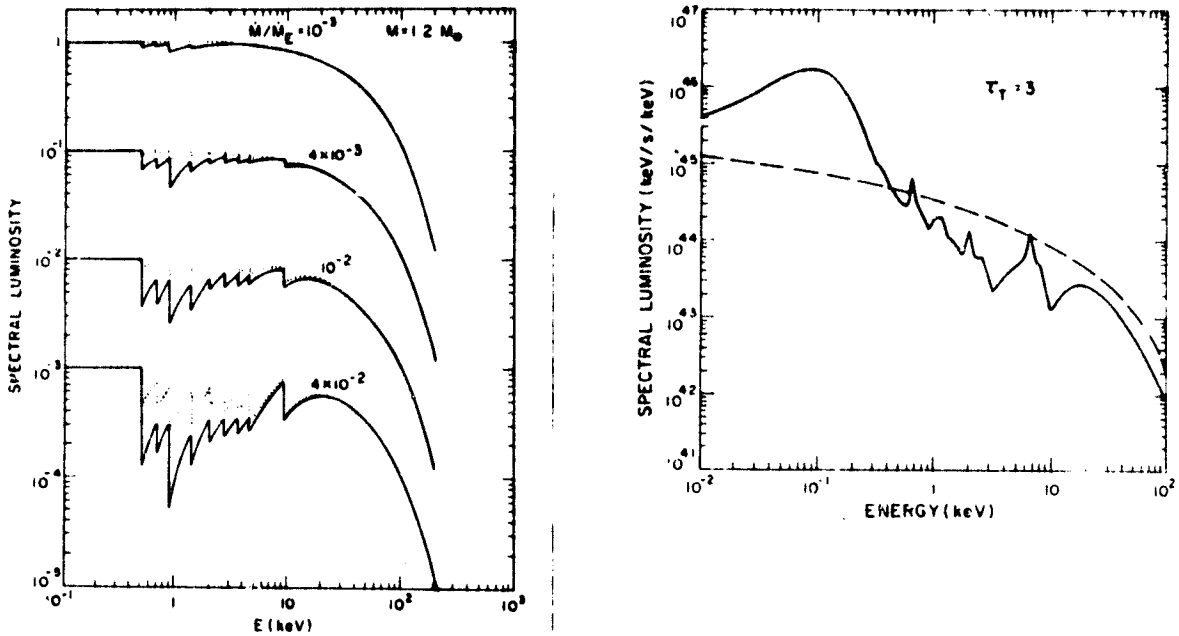

Fig. 28--Bremsstrahlung hard X-ray spectra produced by accretion onto a 1.2 $M_\odot$ star at 4 different accretion rates, taking into account the effects of absorption analytically (from Kylafis and Lamb 1982b).

Fig. 29--X and UV spectrum produced by a 1 $M_\odot$ star at an accretion rate 0.045 $\dot{M}_E$ (τ = 3) taking into account the effects of photoabsorption through detailed numerical calculations (from Ross and Fabian 1980).

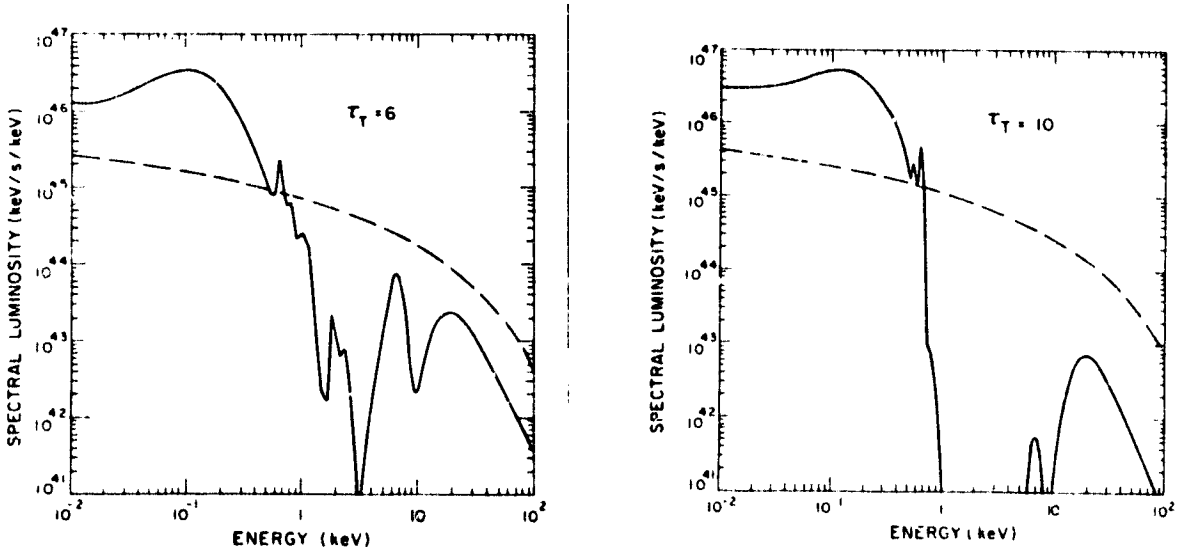

Fig. 30--Same as Fig. 29 for an accretion rate 0.090 $\dot{M}_E$ (τ = 6) (from Ross and Fabian 1980).

Fig. 31--Same as Fig. 29 for an accretion rate 0.15 $\dot{M}_E$ (τ = 10) (from Ross and Fabian 1980).

Among the important unresolved issues concerning degenerate dwarf X-ray sources are the following.

a) Magnetic Fields

Do only a few degenerate dwarfs have magnetic fields, and are the AM Her and DQ Her stars the only cataclysmic variables with magnetic fields? Or are magnetic fields endemic in degenerate dwarfs, and therefore in cataclysmic variables? If so, what are the field strengths? Are they large enough to affect the disk and the accretion flow near the stellar surface?

b) Origin of Hard X Rays

What is the origin of the hard X-rays emitted by cataclysmic variables? Are they produced by optically thin emission in the boundary layer between the disk and the star? If so, are the required high temperatures achieved by strong shocks, turbulence, or some other mechanism? Alternatively, are magnetic fields present in these sources sufficient to disrupt the disk near the star, producing quasi-radial inflow and a strong shock?

c) Origin of Soft X Rays

What is the origin of the intense blackbody soft X-ray emission inferred in the AM Her stars? How can it be so large compared to the optical and hard X-ray emission? Is its origin the same as the soft X-ray emission seen in SS Cyg and U Gem at outburst, or is it different?

d) Nuclear Burning

Under what conditions is steady nuclear burning possible? If it is generally not possible, as many calculations suggest, why are outbursts not more evident? Can steady burning occur more easily in non-spherical situations, as in the AM Her stars? If so, could it account for the intense blackbody soft X-ray emission in these stars? Could it account for the blackbody soft X-ray emission seen in cataclysmic variables like SS Cyg and U Gem?

e) Long Period Pulsing Sources

What is the nature of the long period pulsing sources? Are they actually degenerate dwarfs, or are they neutron stars? Why are they rotating so slowly; that is, why have they not been spun up more by their accretion torque? Does their rotation rate increase and then decrease with time, like the previously known pulsing neutron star X-ray sources with long periods?

f) Cyclotron-Dominated Sources

Although the AM Her stars are strongly magnetic, bremsstralung, not cyclotron emission, is the dominant cooling mechanism in the X-ray emission region (because the

accretion flow is channeled onto such a small fraction f $\sim 10^{-3}$ of the stellar surface that the density in the emission region is very high). Where are the sources in which cyclotron cooling dominates? Will they be found by a UV or extreme UV survey?

g) High Luminosity Sources

To date no high luminosity (L $\sim 10^{36}$ - 10^{38} ergs s^{-1}) X-ray source has been unequivocally identified with a degenerate dwarf, and the future does not look promising. Are there no high luminosity degenerate dwarf X-ray sources? If not, why not?

From these brief remarks, it should be evident that we have only begun to explore the nature of degenerate X-ray sources. We must rely on future X-ray astronomy missions to provide the data needed to understand them. In the following section, we outline the kind of instruments that would best advance our knowledge.

VI. OBSERVATIONAL NEEDS

a) High Throughput

Because degenerate dwarf X-ray sources are faint, the most important attribute of any instrument designed to study them effectively is high throughput. This requirement implies that the instrument should have a large area and a low background rate. A low background rate implies, almost inevitably, the necessity of a focusing instrument. A focusing instrument is also desirable from the standpoint of source confusion, which could be a problem at lower energies.

b) Pointing Capability and Flexibility

A central characteristic of degenerate dwarf X-ray sources, like other compact X-ray sources, is their time variability. They show quasi-periodicities on time scales ranging from several seconds to a thousand seconds, pulsing due to rotation periods ranging from 33 to as much as 4000 seconds, flaring behavior, variability correlated with the binary period, and, of course, the outbursts from which the cataclysmic variables derive their name. Pointing capability is essential for any instrument which is to study them successfully, and flexibility (so that one can move onto the source when it goes into outburst, for example) is desirable.

c) Hard and Soft X-Ray Spectral Sensitivity

As we have seen, many, and perhaps all, degenerate dwarf X-ray sources have two distinct components, one with $T_{br} > 10$ keV and another with $T_{bb} < 100$ eV. As a result, a soft X-ray capability is important and should extend down to at least 0.1 - 0.25 keV. Conversely, a number of sources have hard X-ray spectra with temperatures as high as 30 keV (e.g., AM Her). Therefore a hard X-ray capability extending up to at least $\sim$ 35

keV, and possibly beyond, would be highly desirable.

d) Broad-Band Spectral Measurements

Correlations between the shapes and intensities of both the hard and soft X-ray components have been seen, for example, as a source declines from outburst. Although many of these correlations are not yet understood, theoretical work indicates that they are potentially a powerful source of information about the physical conditions in the X-ray emission region, such as temperature, density, magnetic field strength, and mass accretion rate. Therefore broad band spectral measurements have been, and will continue to be, very useful.

e) Moderate Spectral Resolution

Further studies of the iron emission lines in these sources may yield information about the X-ray emission region, the accretion flow, and the geometry of the binary system. Other emission lines, if present, could provide similar information. All of them may be broadened, either thermally or by Compton scattering. Studies of such emission lines require instruments with moderate ($\Delta\lambda/\lambda \sim 10 - 50$) spectral resolution.

Table 5 summarizes the observational needs we have discussed above.

TABLE 5

FUTURE OBSERVATIONAL NEEDS

SOURCE FEATURE	INSTRUMENTAL REQUIREMENT
Faint	• Large area • Low background • Small field of view
Variable	• Pointing essential • Flexibility desirable
Distinct soft X-ray and hard X-ray components	• Soft X-ray capability important • Hard X-ray capability, extending up to ~40 keV desirable
Continuum spectral shape correlated with luminosity	• Low spectral resolution
Iron emission line seen, broad absorption lines expected	• Moderate spectral resolution

REFERENCES

Agrawal, P. C., Rao, A. R., Riegler, G. R., Pickles, A. J., and Visvanathan, N. 1981, IAU Circ. No. 3649.

Aizu, K. 1973, Prog. Theor. Phys., 49, 1184.

Bailey, J. 1981, M.N.R.A.S., 197, 31.

Bath, G. T., Evans, W. D., and Pringle, J. E. 1974, M.N.R.A.S., 166, 113.

Becker, R. H. 1981, Ap. J., in press.

Becker, R. H., and Marshall, F. E. 1981, Ap. J. (Letters), 244, L93.

Berg, R., and Duthie, J. 1977, Ap. J., 211, 859.

Bohm-Vitense, E., Dettmann, T., and Kapranidis, S. 1979, Ap. J. (Letters), 232, L189.

Bowyer, S. 1979, in IAU Colloquium 53, White Dwarfs and Variable Degenerate Stars, ed. H. M. Van Horn and V. Weidemann (Rochester, N.Y.: University of Rochester), p. 65.

Cash, W, Bowyer, S. and Lampton, M. 1978, Ap. J. (Letters), 221, L87.

Chanmugam, G., and Wagner, R. L. 1977, Ap. J. (Letters), 213, L13.

Chanmugam, G., and Wagner, R. L. 1978, Ap. J., 222, 641.

Cordova, F. A., and Mason, K. O. 1982, in Accretion Driven Stellar X-Ray Sources, ed. W. H. G. Lewin and E. P. J. van den Heuvel (Cambridge, England: Cambridge University Press), in press.

Cordova, F. A., and Riegler, G. R. 1979, M.N.R.A.S., 188, 103.

Cordova, F. A., Chester, T. J., Mason, K. O., Kahn, S. M., Garmire, G. P., and Middleditch, J. 1981, submitted to Ap. J.

Cordova, F. A., Chester, T. J., Tuohy, I. R., and Garmire, G. P. 1980, Ap. J., 235, 163.

Cordova, F. A., Mason, K. O., and Nelson, J. E. 1981, Ap. J., 245, 609.

Cowley, A., and Crampton, D. 1977, Ap. J. (Letters), 212, L121.

DeGregoria, A. J. 1974, Ap. J., 189, 555.

Fabian, A. C., Pringle, J. E., and Rees, M. J. 1976, M.N.R.A.S., 173, 43.

Fabbiano, G., Hartmann, L., Raymond, J., Steiner, J., Branduardi-Raymont, G., and Matilsky, T. 1981, Ap. J., 243, 911.

Fujimoto, M. Y., and Truran, J. W. 1981, Ap. J., in press.

Garmire, G. 1979, in Compact Galactic X-Ray Sources, ed. F. K. Lamb and D. Pines (Urbana, Illinois: University of Illinois), p.62.

Gilliland, R. L. 1982, Ap. J., in press.

Griffiths, R., Lamb, D. Q., Ward, M. M., Wilson, A., Charles, P. A., Thorstensen, J., McHardy, I. M., and Lawrence, A. 1980, M.N.R.A.S., 193, 25P.

Haefner, R., Schoembs, R.,and Vogt, N. 1979, Astr. Ap., 77, 7.

Hayakawa, S. 1973, Prog. Theor. Phys., 50, 459.

Hayakawa, S., and Hoshi, R. 1976, Prog. Theor. Phys., 55, 1320.

Hearn, D. R., and Marshall, F. J. 1979, Ap. J. (Letters), 232, L21.

Hearn, D. R., and Richardson, J. A. 1977, Ap. J., 213, L115.

Hearn, D. R., Richardson, J. A., and Clark, G. W. 1976, Ap. J. (Letters), 210, L23.

Hearn, D., Richardson, J. A., Bradt, H. V. D., Clark, G. W., Lewin, W. H. G., Mayer, F., McClintock, J. E., Primini, F. A., and Rappaport, S. A. 1976, A. J. (Letters), 203, L21.

Heise, J., Mewe, R., Brinkman, A. C., Groenschild, E. H. B. M., den Boggende, A. J. F., Schrijver, J., and Grindlay, J. E. 1978, Astron. Ap., 63, L1.

Hildebrand, R. H., Spiller, E. J., and Stiening, R. F. 1981, Ap. J., 243, 223.

Horne, K., and Gomer, R. 1980, Ap. J., 237, 845.

Hoshi, R. 1973, Prog. Theor. Phys., 49, 776.
Illarionov, A. F., and Sunyaev, R. A. 1972, Astr. Zh., 49, 58 (English transl. in Soviet Astr.-AJ, 16, 45, 1972).
Imamura, J. N., Durisen, R. H., Lamb, D. Q., and Weast, G. J. 1979, in IAU Colloquium 53, White Dwarfs and Variable Degenerate Stars, ed. H. M. Van Horn and V. Weidemann (Rochester, N.Y.: University of Rochester), p. 406.
Imamura, J. N., Durisen, R. H., Lamb, D. Q., and Weast, G. J. 1982, submitted to Ap. J.
Joss, P. C., Katz, J. I., and Rappaport, S. 1979, Ap. J., 230, 176.
Katz, J. I. 1977, Ap. J., 215, 265.
King, A. R., Ricketts, M. J., and Warwick, R. S. 1979, M.N.R.A.S., 187, 77P.
King, A. R., and Lasota, J. P. 1979, M.N.R.A.S., 188, 653.
Krzeminski, W., and Serkowski, K. 1977, Ap. J. (Letters), 216, L45.
Kylafis, N. D., and Lamb, D. Q. 1979, Ap. J. (Letters), 228, L105.
Kylafis, N. D., and Lamb, D. Q. 1982a, Ap. J. (Supp.), in press.
Kylafis, N. D., and Lamb, D. Q. 1982b, Ap. J., in press.
Kylafis, N. D., Lamb, D. Q., Masters, A. R., and Weast, G. J. 1980, Proc. Ninth Texas Symposium on Relativistic Astrophysics, Ann. N.Y. Acad. Sci., 336, 520.
Lamb, D. Q. 1974, Ap. J. (Letters), 192, L129.
Lamb. D. Q. 1979, in Compact Galactic X-Ray Sources, ed. F. K. Lamb and D. Pines (Urbana, Illinois: University of Illinois), p. 27.
Lamb, F. K. 1982, these proceedings.
Lamb, D. Q., and Masters, A. R. 1979, Ap. J. (Letters), in press.
Latham, D. W., Liebert, J., and Steiner, J. 1981, Ap. J., in press.
Linsky, J. 1982, these proceedings.
Margon, B., Lampton, M., Bowyer, S., Stern, R., and Paresce, F. 1976, Ap. J. (Letters), 210, L79.
Martin, C., Basri, G., Lampton, M., and Kahn, S. H. 1982, Ap. J., in press.
Mason, K. O., Lampton, M., Charles, P., and Bowyer, S. 1978, Ap. J. (Letters), 226, L129.
Mason, K., Cordova, F., and Swank, J. 1979, in (COSPAR) X-ray Astronomy, ed. W. A. Baity and L. E. Peterson (Oxford and New York: Pergamon Press), p. 121.
Mason, K. O., Middleditch, J., Cordova, F. A., Jensen, K. A., Reichert, G., Murdin, P. G., Clark, D., and Bowyer, S. 1982, Ap. J., in press.
Masters, A. R. 1978, Ph.D. Thesis, University of Illinois, unpublished.
Masters, A. R., Fabian, A. C., Pringle, J. E., and Rees, M. J. 1977, M.N.R.A.S., 178, 501.
Mewe, R., Heise, J., Gronenschild, E., Brinkman, A., Schrijver, J., and den Boggende, A. 1975, Ap. J. (Letters), 202, L67.
Nather, R. E., and Robinson, E. L. 1974, Ap. J., 244, 269.
Paczynski, B., and Zytkow, A. N. 1978, Ap. J., 222, 604.
Papaloizou, J. C. B., Pringle, J. E., and MacDonald, J. 1982, M.N.R.A.S., 198, 215.
Patterson, J. 1979a, Ap. J. (Letters), 233, L13.
Patterson, J. 1979b, Ap. J., 231, 789.
Patterson, J. 1979b, Ap. J., 234, 978.
Patterson, J. 1980, Ap. J. 241, 235.
Patterson, J. 1981, Ap. J. (Suppl.), in press.
Patterson, J. 1982a, Ap. J., in press.
Patterson, J. 1982b, Ap. J., in press.
Patterson, J., and Price, C. M. 1981, Ap. J. (Letters), 243, L83.
Patterson, J., and Steiner, J. E. 1982, Ap. J. (Letters), in press.
Patterson, J., Branch, D., Chincarini, G., and Robinson, E. L. 1980, Ap. J. (Letters), 240, L133.
Patterson, J., Fabbiano, G., Lamb, D. Q., Raymond, J., Horne, K., White, N., and Swank,

J. 1982, Ap. J., in press.
Patterson, J., Robinson, E. L., and Kiplinger, A. L. 1978, Ap. J., 226, L137.
Patterson, J., Robinson, E. L., and Nather, R. E. 1978, Ap. J., 224, 570.
Patterson, J., Robinson, E. L., and Nather, R. E. 1977, Ap. J., 214, 144.
Patterson, J., Williams, G., and Hiltner, W. A. 1981, Ap. J., 245, 618.
Patterson, J., Fabbiano, G., Lamb, D. Q., Raymond, J., Horne, K., White, N., and Swank, J. 1982, submitted to Ap. J.
Pringle, J. E. 1977, M.N.R.A.S., 178, 195.
Pringle, J. E., and Savonije, G. J. 1979, M.N.R.A.S., 187, 777.
Rappaport, S., Cash, W., Doxsey, R., McClintock, J., and Moore, G. 1974, Ap. J. (Letters), 187, L5.
Raymond, J. C., Black, J. H., Davis, R. J., Dupree, A. K., Gursky, H., Hartmann, L., and Matilsky, T. A. 1979, Ap. J. (Letters), 230, L95.
Robinson, E. L. 1973, Ap. J., 180, 121.
Robinson, E. L. 1976, Ann. Rev. Astron. Ap., 14, 119.
Robinson, E. L., and Nather, R. E. 1979, Ap. J. (Suppl)., 39, 461.
Robinson, E. L., Nather, R. E., and Patterson, J. 1978, Ap. J., 219, 168.
Ross, R. R., and Fabian, A. C. 1980, M.N.R.A.S., 193, 1P.
Rothschild, R. E., et al. 1981, Ap. J., 250, 723.
Schmidt, G. D., Stockman, H. S., and Margon, B. 1981, Ap. J. (Letters), 243, L157.
Shipman, H. 1976, Ap. J. (Letters), 206, L67.
Sion, E. M., Acierno, M. J., and Tomczyk, S. 1979, Ap. J., 230, 832.
Sion, E. M., Acierno, M. J., and Turnshek, D. A. 1978, Ap. J., 220, 636.
Starrfield, S., Sparks, W. M., and Truran, J. W. 1974, Ap. J. (Suppl.), 28, 247.
Starrfield, S., Truran, J. W., and Sparks, 1981, Ap. J. (Letters), 243, L27.
Steiner, J. E. 1981, private communication.
Steiner, J. E., Schwartz, D. A., Jablonski, F. J., Busko, I. C., Watson, M. G., Pye, J. P., and McHardy, I. M. 1981, Ap. J. (Letters), 249, L21.
Stockman, H. S., Schmidt, kG. D., Angel, J. R. P., Liebert, J., Tapia, S., and Beaver, E. A. 1977, Ap. J., 217, 815.
Stockman, H. S., Liebert, J., and Bond, H. E. 1979, in IAU Colloquium 53, White Dwarfs and Variable Degenerate Stars, ed. H. M. Van Horn and V. Weidemann (Rochester, N.Y.: University or Rochester), p. 334.
Stockman, H., Liebert, J., Tapia, S., Green, R., Williams, R., and Ferguson, D. 1981, IAU Circ. No. 3616.
Swank, J. H. 1979, IAU Colloq. No. 53, White Dwarfs and Variable Degenerate Stars, ed. H. M. Van Horn and V. Weidemann (Rochester, NY: Univ. of Rochester Press), p. 135.
Swank, J. H. 1980, private communication.
Swank, J. H. and White, N. 1981, private communication.
Swank, J. H., Boldt, E. A., Holt, S. S., Rothschild, R. E., and Serlemitsos, P. J. 1978, Ap. J. (Letters), 226, L133.
Swank, J., Lampton, M., Bolt, E. M., Holt, S., and Serlemitsos, P. 1977, Ap. J. (Letters), 216, L71.
Swedlund, J. B., Kemp, J. C., and Wolstencroft, R. D. 1974, Ap. J. (Letters), 193, L11.
Szkody, P., and Brownlee, D. E. 1977, Ap. J. (Letters), 212, L113.
Szkody, P., Schmidt, E., Crosa, L., and Schommer, R. 1981, Ap. J., 246, 233.
Tapia, S. 1977a, Ap. J. (Letters), 212, L125.
Tapia, S. 1977b, IAU Circ. No. 3054.
Tapia, S. 1979, IAU Circ. No. 3327.
Tuohy, I. R., Lamb, F. K., Garmire, G. P., and Mason, K. O. 1978, Ap. J. (Letters), 226, L17.

Tuohy, I. R., Mason, K. O., Garmire, G. P., and Lamb, F. K. 1981, Ap. J., 245, 183.
Tylenda, R. 1981, Acta. Astr., 31, 127.
Visvanathan, N., and Wickramasinghe, D. T. 1979, in IAU Colloquium 53, White Dwarfs and Variable Degenerate Stars, ed. H. M. Van Horn and V. Weidemann (Rochester, N.Y.: University of Rochester), p. 330.
Visvanathan, N., Hillier, J., and Pickles, A. 1982, IAU Circ. No. 3658.
Vogt, N., Krzeminski, W., and Sterkin, C. 1980, Astron. Ap., 85, 106.
Wada, T., Shimizu, A., Suzuki, M., Kato, M., and Hoshi, R. 1981, Prog. Theoret. Phys., in press.
Warner, B. 1974, M.N.R.A.S., 168, 235.
Warner, B. 1976, IAU Symposium 73, Structure and Evolution of Close Binary Systems, ed. P. Eggleton, S. Mitton, and J. Whelan (Dordrecht: Reidel), p. 85.
Warner, B., O'Donoghue, D., and Fairall, A. P. 1981, M.N.R.A.S., 196, 705.
Watson, M. G., Sherrington, M. R., and Jameson, R. F. 1978, M.N.R.A.S., 184, 79P.
Weast, G. J., Durisen, R. H., Imamura, J. N., Kylafis, N. D., and Lamb, D. Q. 1979, in IAU Colloquium 53, White Dwarfs and Variable Degenerate Stars, ed. H. M. Van Horn and V. Weidemann (Rochester, N.Y.: University of Rocheter), p. 330.
Weast, G. J., Durisen, R. H., Imamura, J. N., Kylafis, N. D., and Lamb, D. Q. 1982, submitted to Ap. J.
Wesselius, P., and Koester, D. 1978, Astron. Ap., 70, 745.
White, N. E. 1981, Ap. J. (Letters), 244, L85.
White, N. E., and Marshall, F. E. 1981, Ap. J. (Letters), 249, L25.
Young, P., and Schneider, D. P. 1979, Ap. J., 230, 502.

CENTER FOR ASTROPHYSICS

PREPRINT SERIES

No. 1489

RELATIVISTIC THERMAL PLASMAS: PAIR PROCESSES AND EQUILIBRIA

Alan P. Lightman
Harvard-Smithsonian Center for Astrophysics

Submitted to

The Astrophysical Journal
May 1981

Center for Astrophysics

60 Garden St.

Cambridge, Massachusetts 02138

Harvard College Observatory **Smithsonian Astrophysical Observatory**

Center for Astrophysics
Preprint Series No. 1489

RELATIVISTIC THERMAL PLASMAS: PAIR PROCESSES AND EQUILIBRIA

Alan P. Lightman

Harvard-Smithsonian Center for Astrophysics

Abstract

We investigate the equilibria of relativistic thermal plasmas, taking into account electron-positron creation and annihilation and photons produced within the plasma. By including pair-producing photon processes and effects due to the finite size of the plasma, we extend and generalize the earlier work of Bisnovatyi-Kogan, Zeldovich and Sunyaev (1971). In an effectively thin plasma, for each value of $\tau_N = RN\sigma_T$ there is a maximum $T_* = kT/mc^2$, and for each T_* a maximum τ_N, where T, R, N are the temperature, size and proton number density, respectively, and σ_T is the Thomson cross section. For $0.3 \leq \tau_N \leq 10^{-5}$, T_* lies in the range $3 \leq T_* \leq 40$. For each allowed set of parameters (τ_N, T_*) there are two effectively thin equilibria: a high-pair-density solution dominated by photon processes and a low-pair-density solution dominated by particle processes. As luminosity L is increased for fixed τ_N, when $L = L(T^{max}(\tau_N))$ the plasma develops a negative specific heat; T then decreases with increasing L until $T_* \sim 0.1 - 1$ and remains in this transrelativistic range until the plasma becomes effectively thick, eventually radiating as a black body with $T \propto L^{1/4}$. For $L > 10^{41}$ ergs s^{-1} $(N/10^{11}cm^{-3})^{-1}$ in an effectively thin plasma, either $T_* < 3$ or there must be an external source of photons. For an effectively thin plasma with $T_* \gtrsim 3$, the scattering depth never exceeds unity and the "pair absorption" depths to $\gamma + e^+e^-$ and $e + ee^+e^-$ are less than unity.

I. INTRODUCTION

Relativistic thermal plasmas, in which the temperature is above the electron rest mass energy, ar of potential importance to high energy astrophysics. There is ample indirect evidence of relativistic electrons in the synchrotron emission observed from radio galaxies, and the high energy X-rays and γ rays from such sources as NGC 4151, Cen A and 3C273 may be direct evidence of relativistic electrons. This is the second in a series of papers in which we investigate such plasmas. In our first paper (Lightman and Band 1981, hereafter referred to as LB) we studied radiation processes resulting from electrons and positrons with given ultrarelativistic Maxwell-Boltzmann distributions. In this paper we consider processes that create and destroy electron-positron pairs, and determine the equilibrium particle and photon distributions in a thermal plasma as a function of its temperature T, size R, and proton number density N. (Since the emergent photon luminosity L is calculated, the rate of energy input may be specified instead of T as the third independent parameter.) We consider only photons produced internally by the plasma and we consider only ultrarelativistic temperatures, where the asymptotic forms of cross sections permit largely analytic results. The problem is highly nonlinear; pairs produce photons and photons produce more pairs. In addition, some of the reaction cross sections depend on photon energy. For these reasons, the photon distribution and equilibrium pair density must be determined

self-consistently. Previous studies of relativistic thermal plasmas (e.g. Bisnovatyi-Kogan et al. 1971, Pozdnyakov et al. 1977, Stoeger 1977, Liang 1979) have either confined themselves to a small region of parameter space or focused on only a subset of the important reactions. This paper, together with LB, are steps toward a self-consistent and systematic study of relativistic parameter space, determining where various processes dominate and where equilibria exist. In this work we find some qualitatively new phenomena in relativistic plasmas, as well as obtain astrophysically relevant constraints on the sizes, temperatures and luminosities of such plasmas.

There exist no objects of astronomical size that have relativistic temperatures and emit like black bodies - the energy requirements would be prodigious. Even if such plasmas existed, they would be uninteresting to the theorist; the distributions of particles, Fermi-Dirac for electrons and positrons and Planck for photons, follow easily from thermodynamics alone. For convenience we will designate plasmas that are optically thin to photon absorption as effectively thin. In plasmas that are effectively thin and that therefore do not emit as black bodies, the equilibrium particle distributions must be detrmined by the kinetic equations of individual particle reactions. Since there are a variety of pair reactions that occur at temperatures approaching and exceeding the electron mass, one often hears the statement that there

exist no effectively thin thermal plasmas with temperatures satisfying $kT \gtrsim mc^2$. We will investigate the validity of this statement.

One of the pioneering studies of effectively thin relativistic thermal plasmas was that of Bisnovatyi-Kogan, Zeldovich, and Sunyaev (1971), hereafter abbreviated as BKZS. In this work, the equilibrium pair densities were calculated under the assumption that particle-particle processes, cf. equation (14), dominate pair creation. Such an analysis is valid at low photon densities, or, equivalently, at very low values of the scattering depth. BKZS showed that there is a temperature maximum for such a plasma, given by (equation [16] of BKZS with Z = 1)

$$T_e \ln T_e = (\pi/\sqrt{8})\alpha^{-1}, \tag{1}$$

where α is the fine-structure constant and T_e is the dimensionless temperature, written in units of the electron rest mass energy,

$$T_e \equiv kT/mc^2. \tag{2}$$

We will denote the temperature maximum given by equation (1) as T^{BKZS},

$$T_e^{BKZS} \sim 41 . \tag{3}$$

BKZS found that as T approaches T^{BKZS}, the equilibrium electron

density, n_-, approaches infinity. For $T > T^{BKZS}$, pairs are created faster than they can be annihilated and no steady state solutions exist. This result derives from the facts that pair creation by particle-particle interactions is quadratic in theparticle densities, as is pair annihilation, and the rate of annihilation drops rapidly with increasing pair energies in the ultrarelativistic regime. Such a maximum temperature was not found in the subsequent work of Stoeger (1977) or of Liang (1979), which considered only the transrealtivistic regime $T_e \sim 1$, and was not found by Kovner and Milgrom (1981), who considered pair creation only by external photons, leading to a rate linear in the particle density.

Certainly, the assumptions of BKZS must become invalid as $n_- \to \infty$. At the very least theplasma must eventually become thick to absorption (for any given physical size) leading to complete thermodynamic equilibrium and a temperature increasing as the fourth root of the heating rate. Long before this occurs, however, the increasing scattering depth causes the photon density to become sufficiently large that photon-particle and photon-photon interactions dominate particle-particle interactions in creating pairs. Photon processes introduce an essential dependence on the size R of the plasma, a new parameter not present in the BKZS analysis. Intuitively, such photon processes should modify and perhaps lower the temperature maximum found by BKZS. Does there exist at all a temperature maximum T^{max} of an effectively thin plasma, and, if so, what determines n_- at T^{max}? For increasing heating rates and increasing electron densities,

does the temperature of an effectively thin plasma reach and remain near a maximum T^{max} until the plasma becomes effectively thick, or does the temperature reach T^{max} and then decrease until the plasma becomes effectively thick? These are interesting questions that we will address.

Finally, we consider briefly the issue of confining or "trapping" the electrons and positrons within the region where they are created. Evidently, previous considerations of relativistic plasmas with high pair densities (e.g. BKZS, Stoeger 1977, Zhang and Fang 1978, Liang 1979, Eilek 1980, Kovner and Milgrom 1981) have ignored this issue. The problem is that each proton (assumed to be nonrelativistic and confined by gravity or restricted to a small region by inertia) may hold only one electron via charge separation forces. When there are abundant electron-positron pairs, the protons cannot prevent neutral pair clouds from escaping, just as photons escape. Pair clouds or winds produced by hot plasmas could have interesting astrophysical implications; pair "atmospheres" have been previously considered in the context of pulsars (Ruderman and Sutherland 1975). We discuss some mechanisms that may trap the pairs. Plasmas with and without effective pair trapping will have vastly different equilibrium structures.

II. ASSUMPTIONS AND METHODOLOGY

A. Physical Situation and Approximations

We consider a homogeneous plasma of specified temperature T, proton number density N, and size R. For definiteness, we

take the geometry to be spherical, so that R is the radius of the plasma sphere. The problem then is to determine the equilibrium electron, positron and photon distributions self-consistently, subject to the internal processes within the plasma. Since the emergent luminosity L is a by-product of the calculation, equalling in steady state the rate of energy input required to maintain the temperature T, L may be used in place of T as one of the specified parameters. In future work we hope to consider the plasma immersed in an external radiation field or in an external magnetic field.

From R, N, T, three dimensionless parameters may be formed:

$$T_* \equiv kT/mc^2 , \tag{4a}$$

$$\tau_N \equiv R\sigma_T , \tag{4b}$$

$$N_* \equiv N(hc/kT)^3 . \tag{4c}$$

Here σ_T is the Thomson electron scattering cross section. Note that τ_N does not correspond to the scattering depth of the medium when pairs are present; the latter involves the electron and positron densities, which must be determined in the calculation, while the former may be specified in advance. The characteristic denstiy $(kT/hc)^3$ is that of ultrarelativistic particles in full thermodynamic equilibrium at temperature T.

For an effectively thin plasma this density is not relevant, and consequently N_* does not play an independent role. Thus there is only a two-dimensional parameter space for effectively thin plasmas, greatly simplifying the problem. (In a degenerate plasma, the characteristic density $(mc/h)^3$ could combine with N to create a relevant dimensionless parameter, but the plasmas we consider are nondegenerate.

We consider only ultrarelativistic plasmas, $T_* \gg 1$; in practice we consider the region of parameter space $T_* \geq 3$. We will frequently use the ultrarelativistic limit of reaction cross sections. We assume the electrons and positrons have ultrarelativistic Maxwell-Boltzmann distributions:

$$\frac{dn_\pm}{dE} = n_\pm \frac{1}{2(kT)^3} E^2 e^{-E/kT} . \qquad (5)$$

where dn/dE is the number of particles per unit volume per unit energy E and n_- and n_+ are the total number densities of electrons and positrons, respectively. The required conditions for theparticles to maintain thermal distributions are discussed in LB; one requirement is $T_* \lesssim 50$. For such temperatures, the protons are nonrelativistic. We will assume the pairs remain in the plasma, while photons are free to diffuse out. This assumption will be considered again in §IV. We will assume that magnetic fields are negligible. This assumption will be

considered again in §IV. We will consider plasmas that are effectively thin, but not necessarily thin to scattering. We estimate the manner in which the effectively thin equilibria join to those of a plasma in full thermodynamic equilibrium. Finally, we consider plasmas that are neutral, giving the relation

$$n_- - n_+ = N . \qquad (6)$$

B. Reactions Considered

1. Pair production

$$\gamma\gamma \rightarrow e^+e^- \qquad (7a)$$

$$\gamma e \rightarrow ee^+e^- \qquad (7b)$$

$$ee \rightarrow eee^+e^- \qquad (7c)$$

2. Photon production

$$ee \rightarrow ee\gamma \qquad (8a)$$

$$e\gamma \rightarrow e\gamma\gamma \qquad (8b)$$

$$e^+e^- \rightarrow \gamma\gamma \qquad (8c)$$

3. Pair annihilation

$$e^+e^- \rightarrow \gamma\gamma \qquad (9)$$

4. Comptonization

$$e\gamma \rightarrow e\gamma . \qquad (10)$$

In the above reactions e^+ and e^- denote positrons and electrons, respectively, e may be either a positron or an electron, and γ denotes a photon. Reaction (8a) is electron-electron bremsstrahlung and reaction (8b) is double Compton scattering. In choosing the reactions (7) - (10), we considered the possible two-body interactions involving γ and e for each category 1-4, keeping only the lowest order contributions in α, the fine structure constant, for given incident particles. For example, $e^+e^- \rightarrow \gamma\gamma$ is included while $e^+e^- \rightarrow \gamma\gamma\gamma$ is neglected. In category 2 the reaction $\gamma\gamma \rightarrow \gamma\gamma\gamma$ should be included under the stated rules, but it is always negligible. We will show that for the plasmas we consider reaction (8b) may always be neglected relative to (8a) and that the photons produced by reaction (8c), while sometimes contributing to the spectrum, may be neglected for producing pairs.

C. Summary of Procedure

To briefly summarize our procedure:

1. We take asymptotic limits of the cross sections for the above reactions, transform to the plasma rest frame, and average over the electron and positron distributions. The resulting cross sections will be functions of photon energy for some of the reactions.

2. We use equations (8) to write the photon distribution in terms of the temperature and particle densities. To do this, we convert the photon production rate to a photon density by a one-zone approximation to the radiative transfer equation, cf. equation (26), with a dependence on thephysical size of the plasma.

3. We integrate the particle production cross sections over the photon spectra, where appropriate, to obtain the total rate of producing and destroying pairs.

4. We solve for the equilibrium pair densities at each R and T by balancing the rate of pair creation against pair annihilation.

5. We use the equilibrium solution to compute the scattering depth, from which the photon spectra must be modified by the effects of Compton scattering, reaction (10). We repeat steps 2-5 and iterate, until convergence of solutions is achieved.

III. CALCULATION OF EQUILIBRIUM

We henceforth adopt the notation

$$y \equiv n_\gamma/N , \qquad (11)$$

$$x \equiv h\nu/kT , \qquad (12)$$

where ν is a photon frequency. For the photon distribution function, we let n_x be the number density of photons per unit dimensionless frequency x.

A. General Expressions for Pair Creation and Destruction

1. Particle-particle creation

For reaction (7c) the cross section is (Jauch and Rohrlich 1976)

$$\sigma = \frac{3}{8\pi^2}\sigma_T \alpha^2 \left[\ln\left(\frac{E}{mc^2}\right)\right]^3 \qquad (13)$$

in the ultrarelativistic limit, for particles of identical energy E. The threshold energy for a head on collision is $E' = 2m$. Including collisions between electrons and protons, the rate of positron production per unit time per unit volume is (cf. equation [15] of BKZS with $Z = 1$)

$$\frac{dn_+}{dt} \equiv \dot{n}_+ = \frac{3c}{8\pi^2}\sigma_T \alpha^2 (\ln T_e)^3 (n_+ + n_- + N)(n_+ + n_-) \qquad (14a)$$

$$= \frac{3c}{4\pi^2}\sigma_T \alpha^2 (\ln T_e)^3 N^2 y (2y-1). \qquad (14b)$$

2. Particle-photon creation

For reaction (7b), the cross section is (Jauch and Rohrlich 1976)

$$\sigma = 1/3\ \sigma_T \ln (2h\nu/mc^2) \qquad (15)$$

in the ultrarelativistic limit and in the electron rest frame, where ν is the frequency of the incoming photon. Transforming to the plasma rest frame and using the distribution of equation (5), this becomes

$$\sigma = 1/3\ \sigma_T \ln(4T_e^2 x). \qquad (16)$$

The photon energy threshold for this reaction is, in the ultrarelativistic limit,

$$x' = T_e^{-2}. \qquad (17)$$

The rate of positron production via this reaction is

$$\dot{n}_+ = \frac{1}{3}c\sigma_T N(2y-1) n_\gamma \langle \ln(4T_e^2 x)\rangle, \qquad (18)$$

where n_γ is the total photon number density and

$$\langle \ln(4T_e^2 x)\rangle = n_\gamma^{-1} \int_{x'}^{\infty} n_x dx \ln(4T_e^2 x). \qquad (19)$$

$$\equiv \Gamma_{\gamma_e}.$$

3. Photon-photon creation

For reaction (7a), the cross section is (Jauch and

Rohrlich 1976)

$$\sigma = \frac{3}{8}\sigma_T \frac{(mc^2)^2}{h\nu_1 h\nu_2} \ln\left[\frac{4h\nu_1 h\nu_2}{(mc^2)^2}\right] \qquad (20)$$

in the ultrarelativistic limit, where ν_1 and ν_2 are the frequencies of the two interacting photons. The threshold condition is

$$h\nu_1 h\nu_2 \geq (mc^2)^2 . \qquad (21)$$

Thus the rate of positron production via this reaction can be written as

$$\dot{n}_+ = \frac{3}{8} c\sigma_T T_*^{-2} n_\gamma^2 \langle x_1^{-1} x_2^{-1} \ln(4T_*^2 x_1 x_2)\rangle , \qquad (22)$$

where

$$\langle x_1^{-1} x_2^{-2} \ln(4T_*^2 x_1 x_2)\rangle = n_\gamma^{-2} \int_0^\infty x_1^{-1} n_{x_1} dx_1 \int_{\frac{1}{x_1}}^\infty x_2^{-1} n_{x_2} dx_2 \ln(4T_*^2 x_1 x_2) \qquad (23)$$

$$\Gamma_{\gamma\gamma} ,$$

and x' is given again by equation (17).

4. Pair annihilation

For reaction (9), the rate of positron annihilation in the ultrarelativistic limit is (Jauch and Rohrlich 1976 and

equation [12] of BKZS)

$$\dot{n}_+ = -\frac{3}{16} c\sigma_T T_*^{-2} N^2 y(y-1) \ln T_* . \qquad (24.$$

5. Steady-state condition

Combining equations (14), (18), (22) and (24) and demanding that the total $\dot{n}_+$ vanish for equilibrium. we obtain the equation

$$\frac{3}{4\pi^2} \alpha^2 (\ln T_*)^3 y(2y-1) + \frac{1}{3}\alpha (2y-1) (n_\gamma/N) \Gamma_{\gamma e}$$

$$+ \frac{3}{8} T_*^{-2} (n_\gamma/N)^2 \Gamma_{\gamma\gamma} = \frac{3}{16} T_*^{-2} y(y-1) \ln T_* . \qquad (25)$$

BKZS included only the first term on the left hand side of equation (25), leading to the result $y \cdot = as T_* \rightarrow T_*^{BKZS}$, cf. equations (1) and (3). The second and third terms on the left hand side, referring to photon processes that create pairs, are general as they now stand; ir e next section, we will specify the photon distribution created by internal processes; in the future, external photon distributions may be substituted into equation (25).

B. Photon Processes

1. The photon distribution

If $\dot{n}_x$ is the rate of creating photons per unit volume per unit x, then we will initially approximate the photon distribution as

$$n_x = \dot{n}_x (R/c)\ (1+\tau_{th}) \ , \qquad (26)$$

where

$$\tau_{th} \equiv (n_- + n_+)\ R\sigma_T \ . \qquad (27)$$

Equation (26) assumes that the medium is less than one mean free path thick to all photon absorption processes, reactions (7a), (7b) and the inverses of reactions (8a) and (8b). We will justify this assumption below and point out here that, in general, a non Planckian radiation field does not require thinness to all absorption processes. Secondly, equation (26) approximates the effects ofphoton diffusion by the factor $(1 + \tau_{th})$. For $\tau_{th} << 1$, photons leave the medium directly, in a time R/c. For $\tau_{th} > 1$ this time is increased by the factor τ_{th}. For relativistic scatterings, σ_T should be replaced by the photon-energy-dependent Klein-Nishina cross section ; however, our results indicate that τ_{th} never exceeds unity and is greater than 0.5 only for $T_e < 10$. Thus our approximation will not be much in error. Finally, equation (26) neglects the effect of Comptonization, reaction (10), on the photon distribution, an effect that conserves the total number of photons but modifies the spectrum. This effect is non negligible for $T_e \lesssim 20$, is treated in Appendix A, and is incorporated in the G_1 and G_2 factors in equation (38a). Both the diffusion factor $(1+\tau_{th})$ and the effects of Comptonization do not qualitatively

alter the results.

From equations (11) and (63) of LB, combined with equation (26), the bremsstrahlung and pair annihilation contributions to n_x are

$$n_x^B = N_e N_N (4/\pi) y(2y-1) \ln(T_e/x) x^{-1} e^{-x} (1+\tau_{th}) \ , \qquad (28)$$

$$\equiv C^B \ln(T_e/x)\ x^{-1} e^{-x} \ ,$$

$$n_x^A = 0.4\ N_\tau N_N T_e^{-2} \ln T_e\ y(y-1) x e^{-x} (1+\tau_{th}) \qquad (29)$$

$$\equiv C^A x e^{-x} .$$

And, for the total photon distribution, we have the relation

$$n_x = n_x^A + n_x^B \ . \qquad (30$$

The distribution in equation (28) is valid down to a very small x, $x \geq x_t << 1$, at which the medium becomes thick to bremsstrahlung absorption; see equation (15) of LB. As shown in LB, the contribution to n_x from double Compton reactions, equation (8b), may be neglected relative to bremsstrahlung unless $\tau_{th} >> 1$, a condition never satisfied in our solutions. Comptonization will modify the spectrum in equation (28) and is discussed in Appendix A.

2. Averages over the photon distribution

Given the distribution n_x, we must now perform the average for the pair creation cross sections given in equations (19) a (23):

$$\Gamma_{\gamma e} \gtrsim n_\gamma^{-1} C^B \, 4(\ell n T_*)^2 \ell n 4T_* + n_\gamma^{-1} C^A \, 2\ell n 2T_* , \qquad (31)$$

$$\Gamma_{\gamma\gamma} \gtrsim (n_\gamma^{-1} C^B)^2 \, 8T_*^2 (\ell n T_*)^3 \ell n 4 + (n_\gamma^{-1} C^A)^2 \, 2\ell n 2T_* \qquad (32)$$

$$+ n_\gamma^{-2} C^A C^B \, 6(\ell n T_*) T_*^2 \ell n 4 .$$

To obtain theanalytic approximations given in equations (31) - (32), we assume $x_t \ll x' \ll 1$, we evaluate all logarithms at the value of x where the integrand peaks, and we take only the leading terms in exponential-type integrals:

$$\int_{x_{min}}^{\infty} x^{-1} e^{-x} \, dx \gtrsim \ell n (1/x_{min}) , \qquad (33a)$$

$$\int_{x_{min}}^{\infty} \ell n (a/x) e^{-x} x^{-1} dx \gtrsim \ell n \, (a/\sqrt{x_{min}}) \, \ell n \, (1/x_{min}) \qquad (33b)$$

for $x_{min} \ll 1$. In light of the asymptotic approximations to the cross sections, it does not seem justified to obtain more precise evaluations of $\Gamma_{\gamma e}$ and $\Gamma_{\gamma\gamma}$. The ratio of the second to first terms in equation (31), i.e. the ratio of contributions from annihilation photons to bremsstrahlung photons, is

$$\sim 0.1 \, \alpha^{-1} \, (\ell n T_*)^{-1} \, T_*^{-2} \, (y-1)/(2y-1) . \qquad (34)$$

This ratio is always less than unity for $T_* \gtrsim 3$. The ratio of the second to first terms in equation (32) is

$$\sim .02 \, \alpha^{-2} \, T_*^{-6} \, [(y-1), (26-1)]^2 , \qquad (35a)$$

which is always less than unity for $T_* \gtrsim 2$. The ratio of the third to first terms in equation (32) is

$$\sim 0.2 \, \alpha^{-1} \, T_*^{-2} \, (\ell n T_*)^{-1} \, (y-1)/(2y-1), \qquad (35b)$$

which is less than unity for $T_* \gtrsim 3$. We conclude that annihilation photons may be neglected relative to bremsstrahlung photons in producing pairs for $T_* \gtrsim 3$, but are important below this temperature. Henceforth we will restrict ourselves to the region $T_* \geq 3$, neglecting the terms proportional to C^A in equations (31) and (32). Annihilation photons may still dominate the emergent radiation spectrum at $x \sim 1$, as discussed and calculated in LB.

3. Absorption depths

The absorption depth to reaction (7b), for photons above pair creation threshold, $x > x'$, is

$$\tau_{ye}(x) = \tfrac{1}{3}\alpha \, \tau_{th} \, \ell n (4T_*^2 x), \qquad (36)$$

using equations (16) and (27). The absorption depth to reaction (7a) for photons of energy x is

$$\tau_{\gamma\gamma}(x) \approx \frac{3}{2\pi}\alpha\tau_{th}^2\,(1+\tau_{th})(\ln 4)\frac{\gamma}{(2\gamma-1)}\,\ln(T_*^3 x)\,\exp(-\frac{1}{T_* x}), \quad (37)$$

using equations (20), (27) and (28). Equations (36) and (37) indicate that as τ_{th} is increased the medium first becomes thick to $\gamma\gamma$ absorption at a value $\tau_{th} \sim \alpha^{-1/3} \sim 5$, and then becomes thick to γe absorption at a value $\tau_{th} \sim \alpha^{-1}$. In our solutions below, τ_{th} never exceeds unity, so that photon absorption by $\gamma\gamma$ and γe reactions may be neglected. Even when Comptonization is included, as discussed in Appendix A, $\tau_{\gamma\gamma}$ and $\tau_{\gamma e}$ remain small compared to unity.

We mention here that Liang (1979) assumed $\tau_{\gamma\gamma} >> 1$ in his work on $\gamma\gamma \rightleftharpoons e^+e^-$ processes in accretion disks. Liang's physical conditions differ from ours in that he considered transrelativistic plasmas, $T_* \sim 1$, and he assumed a copious source of external photons. In a separate analysis for his conditions, we find $\tau_{\gamma\gamma} < 1$ for the high temperature branch of his solutions.

Absorption of photons by the bremsstrahlung and double Compton processes, the inverses of reactions (8a) and (8b), will always be negligible for the plasmas we consider, as discussed in LB.

C. Analysis of Equilibria

1. The steady-state equation

Substituting equations (31) and (32) with the C^A terms neglected into equation (25), we obtain

$$A(2y-1) + B(2y-1)^2\,(1+\tau_{th})G_1 + Cy(2y-1)^2\,(1+\tau_{th})^2\,G_2 = (y-1)\,, \quad (38a)$$

where

$$A(T_*,\tau_N) = (4/\pi^2)\alpha^2 T_*^2(\ln T_*)^2\,, \quad (38b)$$

$$B(T_*,\tau_N) = (256/9\pi)\alpha^2 T_*^2(\ln T_*)(\ln 4T_*)\,\tau_N\,, \quad (38c)$$

$$C(T_*,\tau_N) = (256\,\ln 4/\pi^2)\alpha^2 T_*^2(\ln T_*)^2\tau_N^2\,. \quad (38d)$$

The functions $G_1(y,T_*,\tau_N)$ and $G_2(y, T_*, \tau_N)$ are modifications that result from changes in the photon spectrum via Comptonization, reaction (10). These functions are given in equations (A-2) and (A-6) and approach unity as $\tau_{th} \to 0$. For $\tau_{th} \sim 1$, G_1 and G_2 make significant corrections. Briefly, Comptonization has two opposing effects on pair creation processes involving photons: low-energy photons are scattered up in energy above pair-creation threshold, increasing the rate of γe and $\gamma\gamma$ pair creation, and the initially bremsstrahlung spectrum above threshold is hardened and partly shifted towards a Wien spectrum, decreasing the rate of the energy-dependent $\gamma\gamma$ interactions.

2. Nature of solutions

Equations (38) must be solved numerically, especially because of the complexity of the G_1 and G_2 functions. Some of the results are given in Figures 1-5.

Much of the character of the solutions may be understood analytically. If the $e^{\pm}e$ interactions dominate the $\gamma\gamma$ interactions in producing pairs, and if the photon trapping factor $(1+\tau_{th})$ and the Comptonization factor G_1 may be set to unity, equation (38) becomes a quadratic equation

$$A(2y-1) + B(2y-1)^2 = y-1, \tag{39}$$

with solution

$$y = \frac{4B + 1 - 2A \pm (4A^2-8B+1-4A)^{1/2}}{8B} . \tag{40}$$

Our results indicate that the above approximations are valid for $T_* \gtrsim 10$. For

$$B > B_{crit}(T_*) = (2A-1)^2/8 \tag{41}$$

there are no real solutions for y. This corresponds to a maximum τ_N for each T_* or a maximum T_* for each τ_N. When $B > B_{crit}(T_*)$, the left hand side of equation (39) is unavoidably larger than the right for all real y, corresponding to production of pairs faster than they can be destroyed. At the critical point given by equation (41),

$$y_{crit} = (3/2-A)/(1-2A) . \tag{42}$$

Note that unless A is near 1/2, y_{crit} has a modest value. For B = 0, we obtain the solution of BKZS

$$y_{BKZS} = (1-A)/(1-2A) . \tag{42}$$

indicating that $y_{BKZS} \to \infty$ as $A \to 1/2$. Indeed, setting $A = 1/2$ just gives the temperature T_*^{BKZS} given by equation (1). For $B < B_{crit}(T_*)$, there are <u>two</u> solutions to the equilibrium equations: a small y solution, in which particle-particle pair creation dominates, and a large y solution, in which photon processes dominate in producing pairs. The small y branch of the solution corresponds to the situation considered by BKZS. Allowing photon processes creates another branch of solutions.

Qualitatively, all of the above holds true for the unapproximated version of equation (38). There exists a maximum τ_N for each T_* and vice versa. We will denote these maximum values by $\tau_N^{max}(T_*)$ and $T_*^{max}(\tau_N)$, respectively. As photon processes create pairs but do not destroy them (except in three-body reactions), $T^{max}(\tau_N)$ is always less than T^{BKZS}, <u>and any external photon sources can only lower $T^{max}(\tau_N)$</u>. The maximum τ_N for each T_* corresponds to a critical buildup of the photon density, cf. equation (26). For each set of parameters (τ_N, T_*) below this critical point, there are two solutions, the larger of which corresponds to the dominance of photon processes in creating pairs. The maximum τ_N at each T_*, as determined exactly by equation (38), is given in Figure 3.

Another feature of the exact equation is readily seen: for $y \gg 1$, the solution can be written as $\tau_{th} = \tau_{th}(T_e)$, since G_1 and G_2 are functions of T_e and τ_{th}, aside from a weak logarithmic dependence on y alone through n_{max} in equation (A-1b) and (A-1c), and B and C enter only as multiplied by y and y^2, respectively. Thus for fixed T_e, the high y branch of solutions has the form $v \propto \tau_N^{-1}$, as can be seen in Figure 1. This asymptotic limit of $\tau_{th}(T_e)$ is actually a maximum, since we have already shown that τ_N has a maximum at each T_e. Again, for the approximations of equation (39), for $y \gg 1$ and A not near 1/2, the asymptotic value of τ_{th} is given by

$$\tau_{th}(T_e) = 0.055\ [\alpha^2 T_e^2\ (\ell n T_e)(\ell n 4T_e)]^{-1}. \qquad (44)$$

This approximation fails for $T_e \to T_e^{BKZS}$ and fails for $T_e \lesssim 10$, where photon-photon processes, Comptonization, and the photon trapping factor must be included. These effects all serve to decrease $\tau_{th}(T_e)$ below the value given by equation (44). The maximum value of the τ_{th} at each T_e, as determined exactly by equation (38), is given in Figure 3. Note that τ_{th} never exceeds unity for $T_e \gtrsim 3$.

Associated with the modest value for the maximum τ_{th} at each T_e, the photon number density never much exceeds the particle number density. From equations (27), (28), (33b) and (A-1c), we obtain

$$n_\gamma/n_- = (4/\pi)\alpha(\ell n 1/x_t)(\ell n T_e/\bar{x}_t)\ \tau_{th}(1+\tau_{th}). \qquad (45)$$

The maximum value of this quantity at each T_e is shown in Figure 3.

Figure 4 shows the significance of various regions of (T_e, τ_N) parameter space. The calculation of BKZS may be considered as 1 dimensional, $\tau_N = 0$, while that of Stoeger $T_e \gg 1$.

The luminosity of the plasma, equal to the heating rate in steady state, may be written as

$$L = 4/3\ \pi R^3 n_- (\dot{\varepsilon}^B + \dot{\varepsilon}^A), \qquad (46)$$

$$\dot{\varepsilon}^B = (4\alpha c \sigma_T m c^2/\pi) N^2 T_e (\ell n T_e) y(2y-1), \qquad (47)$$

$$\dot{\varepsilon}^A = (0.8 c \sigma_T m c^2) N^2 \tau_e^{-1} (\ell n T_e) y(y-1). \qquad (48)$$

Here $a(\tau_{th}, T_e)$, given in equation (45) of LB, is the factor by which Comptonization increases the total energy in the bremsstrahlung emission. As $\tau_{th} \to 0$, $a \to 1$; at $\tau_{th} = 0.1$, $a \sim (2,3)$ for $T_e = (30,3)$; at $\tau_{th} = 1.0$, $a \sim (20,70)$ for $T_e = (30,3)$. Thus Comptonization is important for $\tau_{th} \gtrsim 0.1$. Comptonization has a relatively small effect on the total energy of the pair annihilation spectrum. The energy production rates, per unit volume, by bremsstrahlung and annihilation processes, respectively, are given by $\dot{\varepsilon}^B$ and $\dot{\varepsilon}^A$ from equations (11) and (63) in LB.

Equation (46) may be written in the form

$$L = L_o T_e (\ln T_e)\, \tau_N^3\, y(2y-1)(a + \dot{\epsilon}^A/\dot{\epsilon}^B) \quad , \tag{49a}$$

where $$L_o \equiv \frac{16a}{3}\frac{mc^3}{\sigma_T^2}\frac{1}{N} = 2\times10^{40}\ \text{erg s}^{-1}(N/10^{11}\text{cm}^{-3})^{-1}. \tag{49b}$$

The annihilation contribution to L, $\dot{\epsilon}^A$, is less than the Comptonized bremsstrahlung contribution, $a\dot{\epsilon}^B$, for $T_e > 5$ and is comparable to it for $T_e \lesssim 5$ at intermediate values of τ_N.

For a fixed, representative τ_N, $L(T_e)$ is graphed in Figure 5. The top branch of the curve, labelled "optically thick", will be discussed in 3. below. The dashed portions of the curve lie at temperatures below the ultrarelativistic regime for which detailed calculations have been made.

Several important results are illustrated by Figure 5. First, each luminosity has only one equilibrium associated with it; this fact is closely related to the result that the plasma is thermally stable at fixed luminosity. The stability will be discussed again below. Second, L is a monotonic function of T_e. Thus, as the rate of energy input into the plasma is increased, initially the temperature increases. Eventually the temperature $T_e^{max}(\tau_N)$ is reached, at which point L has a critical value, $L_{crit}(T_e^{max}(\tau_N))$. Further increase in the rate of energy input then decreases the temperature as L increases above L_{crit}, until

the plasma becomes effectively thick. Physically, as L is increased beyond L_{crit}, the nonlinear terms (photon processes) in pair production begin to dominate, cf. equation (38). Additional energy input goes into creating particles at a rapid rate, rather than raising the mean energy per particle. For $T_e \gtrsim 10$, the approximations leading to equations (41) and (42) give the approximation

$$L_{crit}/L_o = \frac{T_e \ln T_e}{8^3}(1-2A)^4\left(\frac{\tau_N}{B}\right)^3(3-2A) \quad , \tag{50}$$

where $A(T_e)$ and $(B/\tau_N)(T_e)$ are given in equations (38).

Consideration of equations (44) and (46)-(49) shows that $L(\tau_N, T_e)$ is maximized at $\tau_N^{max}(T_e)$, and increases for decreasing temperatures. At $T_e=3$, the lowest temperature for which our treatment is valid, L/L_o achieves a maximum of 3.5, at $\tau_N^{max}(3) \approx 0.26$.

3. Effectively thick (black body) solutions

For any plasma of astronomical size and $T_e > 1$, there exists an effectively thick solution in which the photons have a Planck distribution and the electrons and positrons have Fermi-Dirac distributions with equal and opposite chemical potentials. Such a plasma has an enormous pair density and luminosity relative to an effectively thin plasma. For $n_-/N \gg 1$, the electron and positron chemical potnetials may be set to zero. Then, for $T_e \gg 1$,

$$n_-/N \sim 5\times10^{19} T_e^{3} \, (N/10^{11}\ \mathrm{cm}^{-3})^{-1} \ . \qquad (51)$$

The blackbody luminosity, $L = \sigma T^4 4\pi R^2$, where σ is the Steffan-Boltzmann constant, may be written in the form

$$L/L_\odot \sim 10^{22}\, T_e^4\, \tau_N^2\, (N/10^{11}\mathrm{cm}^{-3})^{-1} \ . \qquad (52)$$

The effectively thick electron density, equation (51), is not shown in Figures 1 and 2. In figure 5 the effectively thick solution is shown by the curve labeled "optically thick".

How do the effectively thick and effectively thin curves join? As T_e is lowered to unity and below, equation (51) is no longer a good approximation and the electron density of an effectively thick plasma drops rapidly as $n_- \propto T_e^{3/2}\, e^{-1/T_e}$. At a T_e of order 0.1, dependent only logarithmically on R, the medium must become effectively thin, unless it is effectively thick even for $n_- = N$. We have sketched, although not calculated, the transition from effectively thin to thick by the upper dashed curve in Figure 5. We conjecture that at high luminosity, there is an enormous range of luminosity over which the temperature changes by little, $T_e \sim 0.1$-1. Calculation of the equilibria in this range of parameter space requires trans-relativistic forms for all cross sections as well as the inclusion of three-body processes, and is well outside the scope of the present paper.

4. Negative specific heat

The total thermal energy denstiy, ϵ, is dominated by the electrons and positrons, each of mean thermal energy $\langle E \rangle = 3kT$, cf. equation (5). Thus

$$\epsilon = 3kTN(2y-1) \ . \qquad (53)$$

For $T_e \lesssim 10$ and $y \gg 1$, equation (39) gives $y = B^{-1} \sim [T_e^2 (\ln T_e)(\ln\ln T_e)]^{-1}$, so that the specific heat at constant volume c_v is negative

$$c_v = \left.\frac{\partial \epsilon}{\partial T}\right|_v < 0 \ . \qquad (54)$$

Except at very low temperatures, the specific heat is, in fact, negative along the entire high-y branch of equilibria for the effectively thin plasma under consideration. In Figure 5, for example, the specific heat changes from positive to negative at $T_e = T_e^{max} \sim 35$, $y = 4.1$, and remains negative for increasing y until the plasma begins to become effectively thick.

We conjecture that development of a negative specific heat signals the onset of a "pair-thermal" instability in which the plasma cannot remain homogeneous, but clumps into a two-phase configuration of high-density, low-temperature regions and low-density, high-temperature regions. We hope to pursue this interesting possibility in future work.

5. Stability

As suggested above, the plasma may be unstable to density inhomogeneities. If the plasma remains homogeneous, so that our derived results apply, then it is simple to show that the large y root of equation (38) is unstable at fixed T and R, while the small y root is stable. This follows from the high degree of nonlinearity in the creation rate of pairs when the photon processes dominate.

At fixed L and R, rather than fixed T and R, there is only one equilibrium solution, cf. Figure 5, and it may be shown that this equilibrium is stable.

To calculate the relevant stability conditions for a realistic plasma, a detailed model for the energy input must be specified. It seems unlikely that astrophysically relevant conditions would include a heat bath in thermal contact with the plasma, so that fixed-T perturbations are probably unphysical. Fixed-L perturbations may be more relevant, unless the primary energy source couples to the electrons through an intermediary of different heat capacity. This may be the case in some gravitation accretion problems, in which gravitational energy is first deposited into the ions and then transferred, via Coulomb scatterings, to a cooler population of rapidly radiating electrons.

IV. PAIR TRAPPING AND PAIR-DOMINATED PLASMAS

As mentioned in §I, neutral clouds of electron-positron pairs will escape the plasma like photons unless there exists some

trapping mechanism.

A. Magnetic Trapping

If a magnetic field is present, it provides a "spring" between the protons and pairs, since both classes of particles gyrate about the magnetic field at their respective Larmour radii. If we assume the protons are bound (e.g. by gravity) and at the same time tied to the magnetic field then the pairs will be effectively trapped within the plasma as long as their Larmour radius, r_L, is smaller than the size of the plasma, R. For relativistic electrons of Lorentz factor γ, $r_L = \gamma mc^2/eB$, where e and B are the electron charge and magnetic field, respectively. For an electron distribution of the form of equation (5), we then have

$$\langle r_L \rangle / R = 5.6\times10^{-10}\, T_e\, \left(\frac{R}{10^{13}\,cm}\right)^{-1} \left(\frac{B}{1G}\right)^{-1}. \qquad (55)$$

Thus, only a very small magnetic field is required to ensure $\langle r_L \rangle / R \ll 1$.

What will be the additional effects of such a magnetic field? The synchrotron emission caused by a magnetic field and a population of relativistic thermal electrons peaks at a frequency $\nu_{syn} \approx 0.29\, \gamma^2 eB/mc$. Defining $x_{syn} \equiv \langle h\nu_{syn}/kT \rangle$, where the brackets again denote averaging over a distribution of the form of equation (5),

$$x_{syn} = 4\times10^{-13}\, T_*\left(\frac{B}{1}\right) . \qquad (56)$$

As long as $x_{sync} < x_t$, where x_t is the frequency below which the plasma is thick to bremsstrahlung absorption, the synchrotron emission will have no effect on the previous results. Combining equations (56) and (A-1c), this condition gives

$$B < 3G\left[\tau_{ch}\left(\frac{n_-}{10^{12}\,cm^{-3}}\right)\left(\frac{T_*}{10}\right)^{-5}\frac{\ln(T_*/x_t)}{30}\right]^{1/2} . \qquad (57)$$

For B larger than the value given by equation (57), the photons from synchrotron emission must be considered in addition to those from bremsstrahlung and pair annihilation.

Consideration of equations (55) and (57) shows that there may be a large intermediate range of magnetic field strengths for which pairs are magnetically trapped, but synchrotron emission may still be neglected.

B. Trapping by Collective Plasma Effects

In the event that magnetic fields do not effectively trap the electron-positron pairs, two-stream type plasma instabilities may slow the pairs so that their diffusion time out of the medium is greater than thepair annihilation time. We will consider such effects in a very approximate manner, with one dimensionless parameter.

Plasma oscillations create local net charge accumulations on a Debeye length scale

$$\lambda_D = (kT/4\pi n_- e^2)^{1/2} . \qquad (58)$$

If a fraction q of the pair energy density is put into the electrostatic energy of the plasma oscillations, then each electron, in passing a Debeye sphere, undergoes a scattering angle $\phi \sim \sqrt{q}$. For uncorrelated scatterings, the number of scatterings to achieve a 90° deflection is $N \sim 1/\phi^2 = 1/q$. Thus the mean free path of an electron with respect to plasma scatterings is

$$\lambda_{mf} = \lambda_D/q. \qquad (59)$$

For $\lambda_{mf} << R$, a pair particle must diffuse through the plasma to escape, on a diffusion time

$$t_d = (R/c)(R/\lambda_{mf}) . \qquad (60)$$

If we define the pair annihilation time by

$$t_a = -n_+/\dot{n}_+ , \qquad (61)$$

where $\dot{n}_+$ is given in equation (24), then equations (58) - (61) give

$$t_d/t_a \gtrsim 2\times10^{13}\, q\left(\frac{R}{10^{13}\,cm}\right)^2 T_*^{-5/2}(\ln T_*)\left(\frac{n_-}{10^{12}\,cm^{-3}}\right)^{3/2} . \qquad (62)$$

From equation (62) we conclude that,

at least for values of R and n_- not too different from the normalizations given, only a very small g is required to achieve the pair-trapping condition $t_d/t_a \gg 1$.

C. Pair-Dominated Plasmas

If the total energy density in pairs exceeds the rest mass energy density of the protons, then the plasma as a whole becomes relativistic and cannot be confined gravitationally. Using equation (53), this condition occurs when

$$6yT_*(m/m_p) > 1, \tag{63a}$$

where m_p is the proton rest mass, or

$$y \gtrsim 300\ T_*^{-1}\ . \tag{63b}$$

The relation $y = 300\ T_*^{-1}$ is shown as the dotted line in Figure 2. All equilibria above this dotted line are pair-dominated and may not exist, unless some nongravitational force confines the plasma.

At each T_*, the value of the high y solution increases for decreasing τ_N, so that there is a minimum τ_N, $\tau_N^{\min}(T_*)$, below which equation (63) is satisfied. This minimum τ_N is shown as the dotted line in Figure 4. When the approximation of equation (44) is valid, that equation combined with equation (63) give

$$\tau_N^{\min}(T_*) = 1.7\ [T_*(\ell n T_*)(\ell n 4T_*)]^{-1} \tag{64}$$

In the case where gravitational accretion provides the energy input and gravity is the force that confines the plasma, part or all of the plasma will become unbound and escape when equation (63) is satisfied. Such an event will stop the energy input into the plasma, leading to nonsteady behavior. If the plasma cools sufficiently rapidly, it may become gravitationally bound again and enter a quasi-periodic behavior. Alternatively, the plasma may continue to disperse and cool, in a manner similar to that discussed by Cavallo and Rees (1978).

Even when the plasma as a whole is bound, incomplete pair trapping or simply $\gamma\gamma$ interactions may produce a pair "atmosphere" above the region of proton confinement. If the primary energy deposition is through the protons (eg. gravitational accretion), the pair atmosphere will have to be energized by radiation or by some macroscopic process, as in standard coronae.

V. CONCLUSIONS AND SUMMARY

Bisnovatyi-Kogan, Zeldovich and Sunyaev (1971) considered an effectively thin, relativistic, thermal plasma in which particle processes alone create electron-positron pairs, and found that such a plasma has a maximum temperature $T_* = T_*^{BKZS} \gtrsim 41$, with $n_- \to \infty$ as $T_* \to T_*^{BKZS}$. Here $T_* \equiv kT/mc^2$ and n_- is the electron number density. Clearly the effectively thin assumption

breaks down as $n_- \to \infty$. By consideration of photon processes in addition to particle processes, we have found a second branch of solutions thatself-consistently bridges effectively thin solutions to effectively thick solutions.

When photon processes are included, there are two relevant dimensionless parameters, T_* and $\tau_N \equiv RN\sigma_T$, where R and N are the size and proton number density of the plasma. An effectively thin plasma in equilibrium has maximum values of these parameters, $\tau_N^{max}(T_*)$ and $T_*^{max}(\tau_N)$, with $T_*^{max}(\tau_N) \to T_*^{BKZS}$ as $\tau_N \to 0$. For each set of parameters (τ_N, T_*) allowed, there are <u>two</u> effectively thin equilibria, a low n_- solution in which particle processes dominate in producing pairs and a high n_- solution in which photon processes dominate. As $T_* \to T_*^{max}(\tau_N)$ these two solutions converge, at a modest value of n_-/N. The high n_- equilibria have a <u>negative specific heat</u>, a property that is intimately associated with the approach to effective thickness: as the luminosity L of the plasma (equal to the heating rate in steady state) is continuously increased, the temperature increases until $T = T^{max}(\tau_N)$; at this point the electron density, which is monotonic with L, assumes the values given on the photon-dominated, negative specific heat branch of solutions; further increase of L causes the temperature to <u>decrease</u>, until $T_* \sim 0.1$-1, the temperature then remains in this transrelativistic region with increasing L until the plasma becomes effectively thick, leading eventually to the blackbody law $T \propto L^{1/4}$. Physically, for $L > L(T_{max}(\tau_N))$, additional heat input goes into rapid creation of particles, rather than into raising the mean energy per particle.

Some of our other conclusions follow below. Unless otherwise stated, all results refer to plasmas in which photons are generated internally.

1. The bridge between an effectively thin plasma and an effectively thick plasma occurs in the transrelativistic region, $T_* \sim 0.1$-1; the temperature remains in this region over an enormous range of luminosity.

2. An effectivley thin plasma has maximum values of size and temperature, $\tau_N^{max}(T)$ and $T^{max}(\tau_N)$, as mentioned above.

3. For an effectively thin plasma of sufficiently large luminosity

$$L \gtrsim 10^{41} \text{ erg s}^{-1} \, (N/10^{11} \text{ cm}^{-3})^{-1} ,$$

either the plasma is non thermal, or $T_* < 3$, or there must be an external source of photons impingent on the plasma not considered in the present calculation. Any external source of photons can only decrease the maxima in τ_N and T_* found for internally generated photons, since photons create but do not destroy pairs in the effectively thin limit.

4. A relativistic plasma requires some mechanism to confine the electron-positron pairs; binding the protons is insufficient. Weak magnetic fields or plasma instabilities may be sufficient.

5. Effectively thin relativistic ($T_* \gtrsim 3$) plasmas only have

equilibria that are thin to the pair producing reactions $\gamma\gamma \to e^+e^-$ and $\gamma e \to ee^+e^-$. Such plasmas achieve a maximum depth to scattering $e\gamma \to e\gamma$ of ~ 1, occurring at $T_* = 3$. Heterich (1974) has discussed the consequences of media that are thick to $\gamma\gamma$ reactions, and he and subsequent investigators have derived astrophysical constraints for various sources based on these consequences. Our results indicate that any region thick to $\gamma\gamma$ interactions cannot be in thermal equilibrium at a temperature $T_* \geq 3$ when the photons are produced by the same pairs they create.

6. For $L > L(T^{max}(\tau_N))$ an effectively thin plasma has a negative specific heat. This may indicate the development of a two-phase "pair-thermal" instability.

APPENDIX A: EFFECTS OF COMPTONIZATION ON PAIR PRODUCTION PROCESSES

An approximate analytic treatment of Compton scattering of bremsstrahlung photons by relativistic electrons is given in LB. Here we apply some of those results to pair creation processes.

1. Modification of γe reactions

The rate of production of pairs by γe reactions is only weakly sensitive to the photon spectrum and depends mainly on the number of photons above threshold energy, $x = x' = T_*^{-2}$, cf. equations (18), (19). Comptonization of bremsstrahlung photons increases this number. If we denote by $\mathcal{N}(\tau_{th})$ the number density of photons above threshold energy in a medium with scattering depth τ_{th}, and $\mathcal{N}(0)$ the number of photons above threshold energy in the unComptonized spectrum, then

$$\frac{\mathcal{N}(\tau_{th})}{\mathcal{N}(0)} = \sum_{n=0}^{n_{max}-1} \frac{(n+1)(n+2)}{2} P_n(\tau_{th}) + \frac{1}{2}(n_{max}+1)(n_{max}+2)\left[1 - \sum_{n=0}^{n_{max}-1} P_n(\tau_{th})\right], \quad \text{(A-1a)}$$

where

$$n_{max} = \mathrm{Int}\{\ln(x_t^{-1} T_*^{-2}) / \ln(16 T_*^2)\}, \quad \text{(A-1b)}$$

$$x_t \approx 1\times10^{-11}\left[\tau_{th}\left(\frac{n_-}{10^{12}\,cm^{-3}}\right)\left(\frac{T_*}{10}\right)^{-3}\frac{\ln(T_*/x_t)}{30}\right]^{1/2}, \quad \text{(A-1c)}$$

$$P_n(\tau) = (1-e^{-\tau})^n e^{-\tau}. \quad \text{(A-1d)}$$

By Int(β) we mean the nearest integer to β. These results follow from equations (15), (22), (34), (39) and (41) of LB. The medium becomes thick to bremsstrahlung absorption at the frequency x_t. A nonrelativistic photon increases its energy by a factor $16T_e^2$ upon each scattering; n_{max} is the number of scatterings a photon of frequency x_t undergoes to reach pair creation threshold, $x = T_e^{-2}$. The probability of a nonrelativistic photon undergoing n scatterings before escaping the medium is $p_n(\tau_{th})$. Note the limiting behavior ofthe above equations. for $\tau_{th} \ll 1$, $p_0 \sim 1$ and all other $p_n \sim 0$, so $\eta(\tau_{th})/\eta(0) = 1$. For $\tau_{th} \gg 1$, $p_n \sim 0$ for $n \leq n_{max}$, so $\eta(\tau_{th})/\eta(0) = (n_{max}+1)(n_{max}+2)/2$.

The modification of the γe reaction rate by Comptonization can be written as, cf. equation (38),

$$G_1 = \eta(\tau_{th})/\eta(0) \ . \qquad \text{(A-2)}$$

As an example, if $\tau_{th} = 1$, $T_e = 5$, $x_t = 10^{-10}$, the above reactions give $G_1 \gtrsim 4.5$.

2. Modification of γγ reactions

The Comptonized-bremsstrahlung photon distribution in the region $x > T_e^{-2}$ may be approximated as, cf. equations (37), (40) and (43) of LB,

$$n_x = \eta(\tau_{th}) \left[(1-f) \frac{\ell n(T_e/x) e^{-x} x^{-1}}{(\ell n T_e^2)^2} + \frac{f x^2 e^{-x}}{2}\right] , \qquad \text{(A-3a)}$$

where

$$f = (1-e^{-\tau_R}) \ , \qquad \text{(A-3b)}$$

$$\tau_R = 0.35\, \tau_{th}/\ell n T_e \ . \qquad \text{(A-3c)}$$

For $\tau_{th} \to 0$, this reduces to the unComptonized bremsstrahlung spectrum; for $\tau_{th} \gg 1$ it becomes a Wien spectrum. The quantity τ_R is a frequency-averaged Klein-Nishina scattering depth. Substituting equation (A-3a) into equation (21), we obtain

$$\Gamma_{\gamma\gamma}(\tau_{th}) \propto \frac{|\eta(\tau_{th})|^2}{n_\gamma^2} \left[\frac{1}{2}(\ell n 4)\frac{(1-f)^2 T_e^2}{\ell n T_e} + \frac{3}{4}\frac{f(1-f)(\ell n 4) T_e^2}{\ell n T_e} + \frac{1}{2} f^2 \ell n 2 T_e\right] \qquad \text{(A-4)}$$

Now, as G_2 is defined in equation (38),

$$G_2 = \Gamma_{\gamma\gamma}(\tau_{th})/\Gamma_{\gamma\gamma}(0) \qquad \text{(A-5)}$$

and, noting that $f = 0$ for $\tau_{th} = 0$,

$$G_2 = G_1^2 X \ , \qquad \text{(A-6a)}$$

$$X = \left[(1-f)^2 + \tfrac{3}{2} f(1-f) + f^2 T_e^{-2} \frac{(\ell n 2 T_e)(\ell n T_e)}{\ell n 4}\right] \ . \qquad \text{(A-6b)}$$

For $T_* >> 1$, X is decreasing function of f, corresponding to the fact that the hardening of the spectrum of a given number of photons in the region $x > T_*^{-2}$, via Compton scattering, decreases the energy averaged cross section for $\gamma\gamma$ pair creation. For the same example as before, $\tau_{th} = 1$, $T_* = 5$, $X \gtrsim 0.90$, $G_2 = 18$.

The effect of Comptonization increases the $\gamma\gamma$ absorption depth by less than a factor G_1. As can be seen by equations (37), (A-1) and (A-2), $\tau_{\gamma\gamma}$ will be small compared to unity for the range of our solutions, $\tau_{th} < 1$.

ACKNOWLEDGMENTS

We thank Jonathan Arons, David Band, Douglas Eardley and George Rybicki for useful discussions.

REFERENCES

Bisnovatyi-Kogan, G.S., Zeldovich, Ya.B., and Sunyaev, R.A. 1971, Sov. Astr. - AJ, 15, 17.

Cavallo, G. and Rees, M.J. 1978, M.N.R.A.S., 183, 359.

Eilek, J.A. 1980, Ap. J., 236, 664.

Heterich, K. 1974, Nature, 250, 311.

Jauch, J.M. and Rohrlich, F. 1976, The Theory of Photons and Electrons, Second Edition, (Springer-Verlag: New York).

Kovner, I. and Milgrom, M. 1981, Astr. and Astrophys., in press.

Liang, E.P.T. 1979, Ap. J., 230, 1105.

Lightman, A.P. and Band, D.L. 1981, sub. to Ap. J.

Pozdnyakov, L.A., Sobol, I.M. and Sunyaev, R.A. 1977, Sov. Astr.-AJ, 21, 708.

Ruderman, M.A. and Sutherland, P.G. 1975, Ap. J., 196, 51.

Stoeger, W.R. 1977, Astr. and Astrophys., 61, 659.

Zhang, J. and Fang, L. 1978, Studia Astronomica Sinica, 1, 8; reprinted in 1979, Chinese Astronomy, 3, 141.

FIGURE CAPTIONS

Figure 1: Equilibrium electron densities of an effectively thin plasma as a function of temperature T and size R. Here n_-/N is the electron density divided by proton density and $\tau_N \equiv RN\sigma_T$, where σ_T is the Thomson cross section. Note the maxima $\tau_N^{max}(T)$.

Figure 2: A different representation of Figure 1. The dotted line indicates the value of n_-/N for which the total energy density in electron-positron pairs equals the rest mass energy density of the protons. Plasmas with n_-/N above this line cannot be gravitationally bound. The curve labeled BKZS, $\tau_N = 0$, is the result of Bisnovatyi-Kogan et al. (1971), which neglects photon processes in pair production. Note the maxima $T^{max}(\tau_N)$.

Figure 3: Maximum values of τ_N, of the Thomson depth to scattering $\tau_{th} \equiv R(n_- + n_+)\sigma_T$, and of the total photon density divided by electron density, n_γ/n_-, as a function of temperature. The vertical dashed line is the temperature maximum found by BKZS.

Figure 4: Parameter space study of relativistic, effectively thin plasmas. For temperatures $kT/mc^2 \lesssim 8$ pair production by $\gamma\gamma$ interactions dominates production by γe interactions and vice-versa for $kT/mc^2 \gtrsim 8$. Effects of Comptonization become important for $\tau_{th} \gtrsim 0.1$. The

dotted line is the locus for which the high n_- solution for each T and τ_N has a total energy density in pairs equal to that in protons. For τ_N below this line, the high n_- solution corresponds to plasmas that cannot be gravitationally bound.

Figure 5: Luminosity as a function of temperature for fixed τ_N. Here $L_o \equiv 2\times10^{40}$ erg s^{-1} $(N/10^{11}\ cm^{-3})^{-1}$. Dots indicate the values of dimensionless electron density, n_-/N. The upper curve, labelled "optically thick", is the black body solution $L \propto T^4$, at a greatly increased scale. The dashed portions of the curve, in the transrelativistic range, have not been calculated. For the equilibrium configurations in which T is a decreasing function of L, the plasma has a negative specific heat.

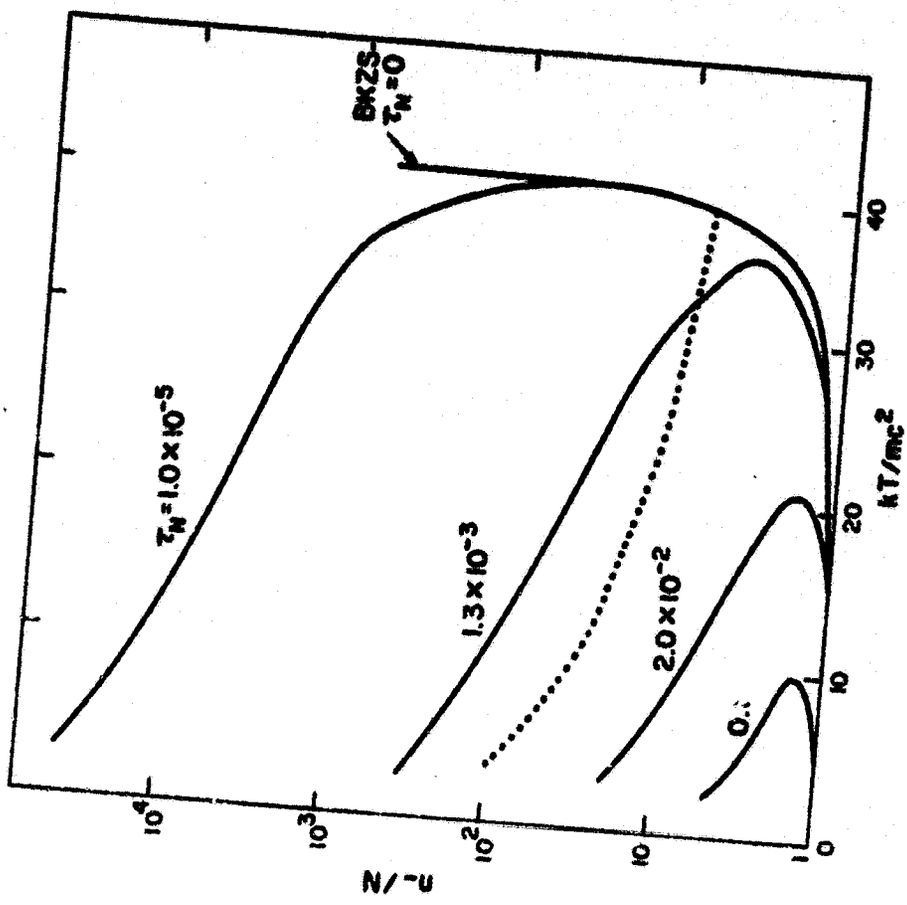

Fig. 2

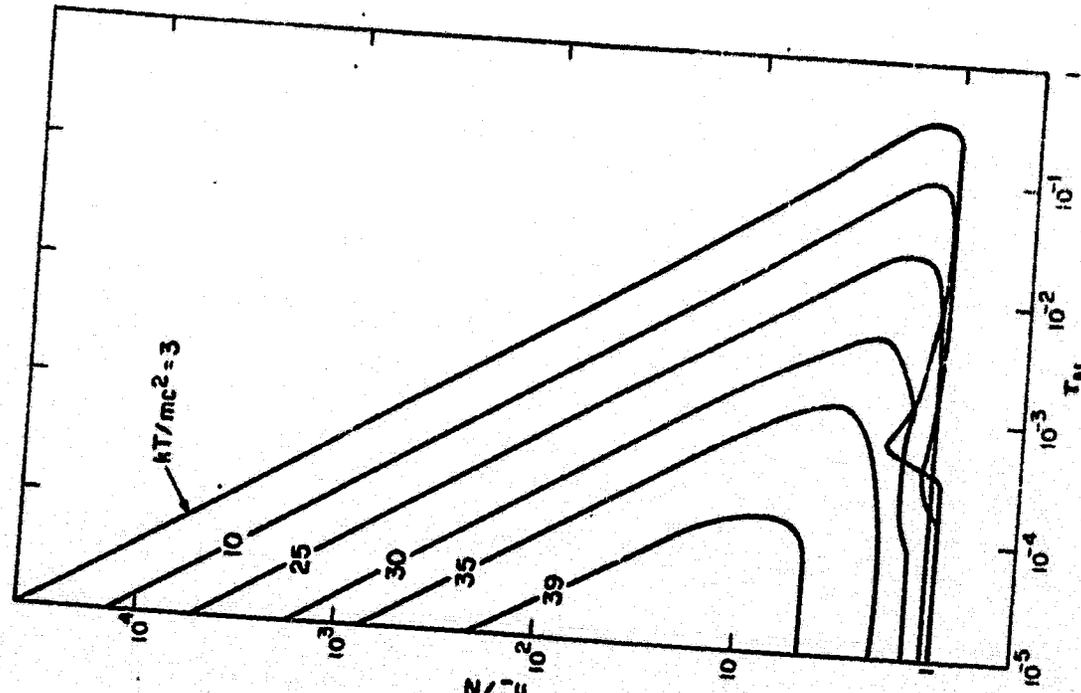

Fig. 1

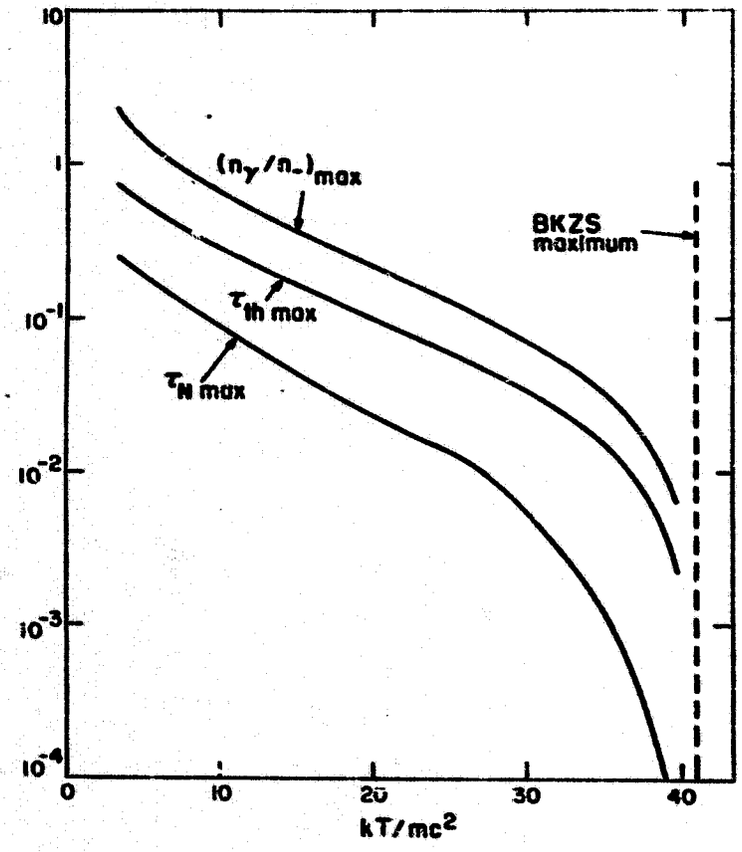
10
1
10^{-1}
10^{-2}
10^{-3}
10^{-4}
0
10
20
30
40
kT/mc^2
$(n_\gamma/n_-)_{max}$
$\tau_{th\,max}$
$\tau_{N\,max}$
BKZS
maximum

Fig. 3

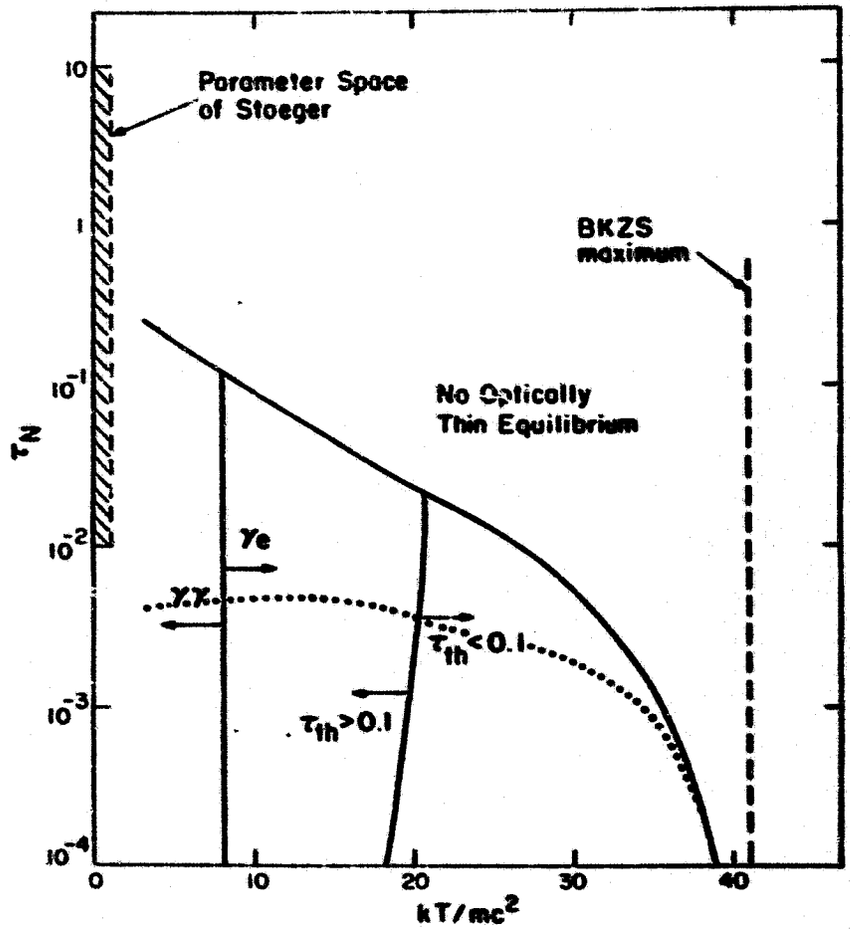
10
1
10^{-1}
10^{-2}
10^{-3}
10^{-4}
τ_N
0
10
20
30
40
kT/mc^2
Parameter Space
of Stoeger
BKZS
maximum
No Optically
Thin Equilibrium
γe
$\gamma\gamma$
$\tau_{th}<0.1$
$\tau_{th}>0.1$

Fig. 4

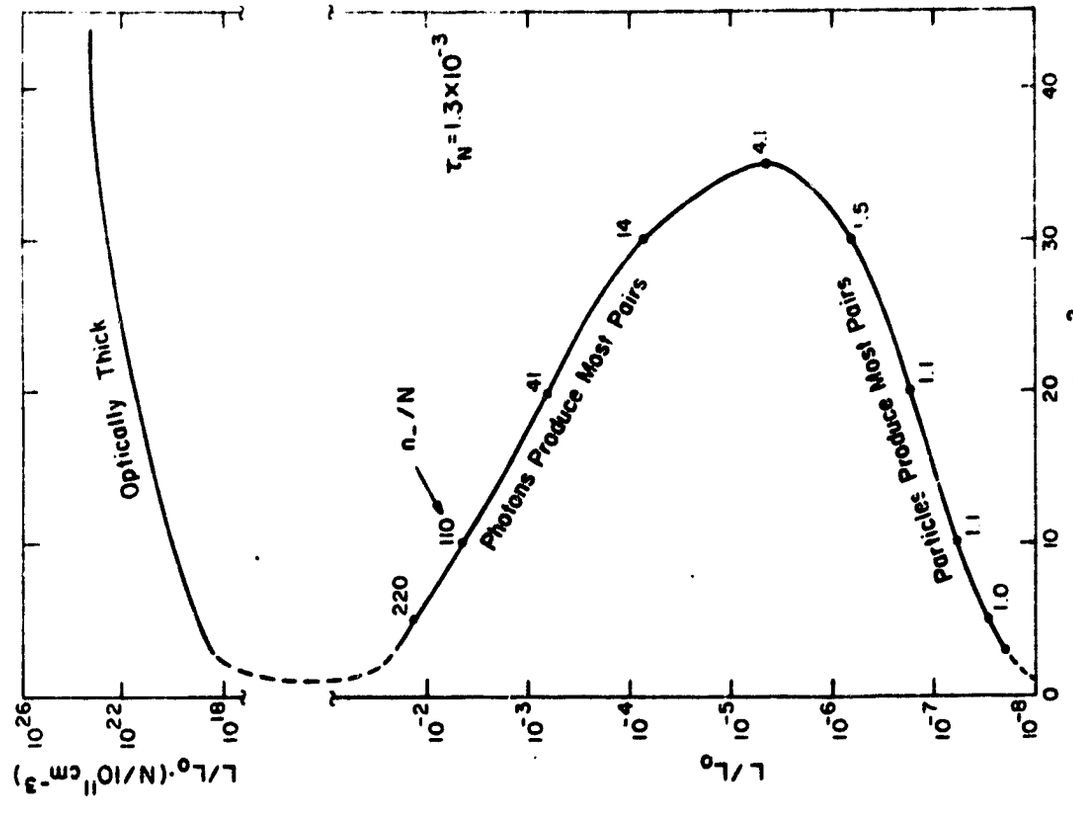

Fig. 5

CENTER FOR ASTROPHYSICS

PREPRINT SERIES

No. 1542

X-RAYS FROM QUASARS AND ACTIVE GALAXIES

Alan P. Lightman
Harvard-Smithsonian Center for Astrophysics

Submitted to
Space Science Reviews

Center for Astrophysics
60 Garden St.
Cambridge, Massachusetts 02138

Harvard College Observatory Smithsonian Astrophysical Observatory

Center for Astrophysics
Preprint Series No. 1542

X-RAYS FROM QUASARS AND ACTIVE GALAXIES

Alan P. Lightman
Harvard-Smithsonian Center for Astrophysics

X-RAYS FROM QUASARS AND ACTIVE GALAXIES*

Alan P. Lightman
Harvard-Smithsonian Center for Astrophysics

I. INTRODUCTION

There is evidently a great deal of activity and commotion in deep space, unrevealed by the naked eye or the delicate twinkling of the stars. As far as we can tell, quasars (QSOs) and "active galactic nuclei" (AGN) have relatively enormous power outputs produced in very small volumes. A typical quasar can produce a hundred to a thousand times the luminosity of a normal galaxy from a region one hundred thousand times smaller in size. Roughly speaking, if the city of Boston were a galaxy in terms of its power output and size, then a quasar would have the power of the entire United States produced in a region the size of a baseball.

At various times, it has been suggested that new kinds of physical laws or phenomena must be required to explain these objects. But more and more evidence has accumulated that shows a continous range of energetic activity, starting with normal galaxies, going through Seyfert galaxies and other AGN, and joining with the less luminous quasars. Moreover, the hypothesized model of gas falling through a deep gravitational well, probably caused by a massive black hole, together with a net angular momentum in the bottom of the well, seems capable of explaining, at least qualitatively, the full range of observed phenomena, from the energetics to the striking, long-lived "jets" of matter observed to emanate from the centers of these objects. In any case, there does seem to be good evidence for some universality in the mechanisms and physical conditions.

*Based on a lecture given at the [illegible] (October 1981).

Among the most important issues in understanding QSOs and AGN are (1) the nature of the power source, (2) the radiation processes, and (3) the mechanism for formation and collimation of the jets. We will discuss these issues in turn, giving a brief, model-independent sketch of some of the important theoretical ideas and observations (with more emphasis on our own interests), and suggesting future work. It is possible that no new observations within the foreseeable future will satisfactorily pin down the above issues.

We will be particularly concerned with phenomena that produce X-rays. The clear association of strong X-rays with QSOs and AGN and the rapid time variability seen in X-rays indicate that this region of the spectrum may contain much information about the conditions near the central region of the objects. Of course, simultaneous observations of all regions of the spectrum may provide important clues to the mechanisms at work.

For some recent reviews of this subject, see e.g. Rees (1977,1978,1980), Fabian and Rees (1979), and Bradt (1980).

II. NATURE OF THE POWER SOURCE: ACCRETION ONTO A MASSIVE BLACK HOLE

A. General Considerations

We will tentatively adopt gas accretion onto a massive black hole as the "standard model" for the power source. The

length scale is then set by the Schwarzschild radius of the black hole, $r_s = 2GM/c^2$, where M is the mass of the hole. We will use the notation $M_8 \equiv M/10^8 M_\odot$. Unless the hole is rotating near maximum angular velocity, we can expect the energy production to peak in the region $r \sim 10 r_s$. The luminosity, L, can be written as

$$L = \epsilon \dot{M} c^2, \qquad (1)$$

where ϵ is the efficiency parameter and $\dot{M}$ is the mass accretion rate. The virial temperature, T_V, set by the proton rest mass energy, is

$$T_V = 10^{12} K \ (r/10 r_s)^{-1}. \qquad (2)$$

The period of a circular orbit, P, also denoted by t_K, in the Newtonian approximation, is

$$P = t_K = 3 \times 10^5 s \ M_8 \ (r/10 r_s)^{3/2}. \qquad (3a)$$

The light travel time across this region is

$$\Delta t_c \equiv r/c = 10^4 s \ M_8 \ (r/10 r_s). \qquad (3b)$$

The total mass accreted, M_{acc}, in the active lifetime, t_{life}, is

$$M_{acc} \equiv \dot{M} t_{life} = 10^7 M_\odot \left(\frac{t_{life}}{10^8 yr}\right)\left(\frac{L}{10^{45} erg\ s^{-1}}\right)\left(\frac{\epsilon}{0.1}\right)^{-1}. \qquad (4)$$

Both the combination of inferred active lifetimes and observed luminosities, and the sizes and velocity dispersions obtained from optical studies, indicate an M_{acc} and an M in the range $10^6 - 10^9 M_\odot$. We denote the ratio of radial velocity, V_r, to Kepler velocity, V_K, by

$$\beta \equiv V_r / V_K. \qquad (5a)$$

The radial infall time, t_r, is then

$$t_r = t_K / \beta. \qquad (5b)$$

Note that β is related to the viscosity parameter α of the

"α-model" disks (Shakura and Sunyaev 1973) by

$$\beta = \alpha (h/r)^2, \qquad (5c)$$

where h is the disk thickness at radius r. In "thick accretion disks" we might expect $h \sim r$, so that $\beta \sim \alpha$. The continuity equation gives an ion number density, N,

$$N = 10^{15} cm^{-3} M_8^{-1} \left(\frac{\epsilon}{0.1}\right)^{-1} (L/L_{Edd})^{-1} (r/10 r_s)^{-3/2}, \qquad (6)$$

where we have normalized L in terms of the Eddington luminosity

$$L_{Edd} \equiv 4\pi G M m_p c / \sigma_T = 10^{46} erg\ s^{-1} M_8.$$

We will denote the mass of the proton and electron by m_p and m, respectively, and σ_T is the Thomson cross section. From equation (6) we obtain the "ion scattering depth"

$$\tau_N \equiv r N \sigma_T = 2 \left(\frac{L}{L_{Edd}}\right)\left(\frac{\epsilon}{0.1}\right)^{-1} \beta^{-1} \left(\frac{r}{10 r_s}\right)^{-1/2}. \qquad (7)$$

The Thomson scattering depth is

$$\tau_T = r (n_- + n_+) \sigma_T \geq \tau_N \qquad (8)$$

where n_- and n_+ are the electron and positron number densities.

Although τ_T might be expected to approach unity in sources radiating at near the Eddington limit, equation (7), the large optical polarization seen in some QSOs and BL Lac objects (Stein, O'Dell, and Strittmatter 1976; Angel 1978), together with the as yet unobserved evidence of strong Comptonization, suggests $\tau_{Th} < 1$. We then obtain an upper limit for the mass in the central, emitting region, M_{em}, (Rees 1977)

$$M_{em} \equiv \frac{4}{3} \pi r^3 n_p m < 4 \times 10^{-4} M_\odot M_8^2 \left(\frac{r}{10 r_s}\right)^2. \qquad (9)$$

Since $M_{em} \ll M$, most of the mass has already collapsed within the emitting region, arguing against some

non-black-hole models for the central power source. Of course, the majority of QSOs and AGN do not show strong optical polarization.

B. Gas flow models

The principal requirements for efficient conversion of gravitational energy into radiation, [illegible], are that (a) the viscous dissipation time scale be comparable to or shorter than the radial infall time scale and that (b) the cooling time of the gas be shorter than the radial infall time scale. When angular momentum is present, an accretion disk forms; most accretion disk models proposed satisfy the above requirements. Even when the infalling gas does not have much net angular momentum, a disk may form out to a radius $r \sim 10^2 r_s$ due to the "dragging of inertial frames" by a rapidly rotating black hole (Bardeen and Petterson 1974). Spherical accretion models require rapid dissipation, since the infalling matter is not delayed by angular momentum.

For a review of the types of α-disk models, see Eardley et. al. (1978). These models differ in whether they are gas or radiation pressure dominated, optically thick or thin, equal or unequal temperatures for electrons and ions, and in the source of photons; they have in common the assumption of a spatially constant value for the viscosity parameter α and the assumption of a thin disk [illegible]. Recently, Lynden-Bell (1978) and Jaroszynski, Abramowicz, and Paczynski (1980) have considered geometricaly thick disks, but without including the effects of viscosity. These thick-disk models are characterized by an unspecified free function, $l(r)$, the non-Keplerian angular momentum distribution along the disk. When more of the internal physics of the disk is included, this funtion may be determined. For some recent spherical accretion models, see Maraschi et. al. (1979) and Maraschi, Roasio and Treves (1981).

An alternative possibility, for both the matter surrounding the hole and the method of energy release, is a disk that anchors a large-scale magnetic field, torquing and spinning down a rapidly rotating black hole (e.g. Blandford and Znajek 1977). In this case the energy is supplied by the rotation of the hole. (At an earlier stage, this energy had to ultimately derive from energy made available in gravitational collapse.) Thermodynamically, this process can provide relatively low-entropy energy that is well suited for accelerating electrons to relativistic velocities.

C. Time Variability

Time variability in the X-rays of $\Delta t \sim 10^3$-10^4 s has now been observed in a number of QSOs and AGN. Some of these results are shown in the Table below, where the observed luminosity L_x is typically in the range 2-10 kev.

Table 1

Source	L_x (erg/s)	$\Delta L_x/L_x$	Δt (s)	$c\,\Delta t$ (cm)
Cen A	1×10^{43}	0.25	7×10^{3}	2×10^{14}
Mk 421	1×10^{44}	2.0	1×10^{5}	3×10^{15}
NGC 6814	1×10^{43}	1.5	2×10^{2}	6×10^{12}
OX 169	1×10^{44}	1.5	6×10^{3}	1.8×10^{14}
3C 273	1.7×10^{46}	0.1	6×10^{3}	1.8×10^{14}
NGC 4151	5×10^{42}	3.0	1×10^{5}	3×10^{13}

The observations for Cen A are from Delvaille et al. (1978), for Mk 421 from Ricketts, Cooke and Pounds (1976), for NGC 6814 from Tennant et. al. (1981), for OX 169 and 3C 273 from Tananbaum (1980), and for NGC 4151 from Tananbaum et. al. (1978). A typical observed fluctuation is shown in Figure 1 for Ox 169.

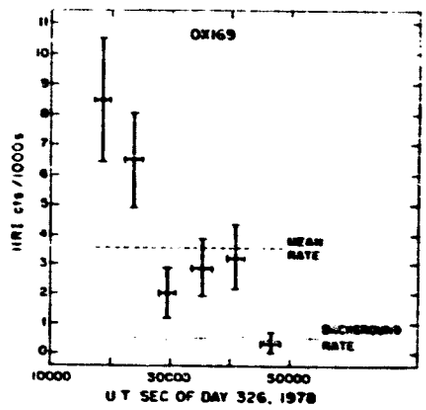

Figure 1: Einstein HRI observations of QSO OX 169, from Tananbaum (1980).

The condition that the size of the emitting region during a fluctuation, ℓ, be smaller than $c\Delta t$ can be written as

$$\left(\frac{\ell}{10r_s}\right) < M_8^{-1}\left(\frac{\Delta t}{10^4 s}\right). \qquad (10)$$

Since many of the fluctuations in Table 1 have $\Delta L \sim L$, we can assume that a large fraction of the steady emission region is involved in the observed fluctuations, $\ell \sim r$. Note that, within the context of the black hole model, equation (10) and Table 1 are consistent for $M_8 \sim 0.1-10$. It is also important to note that if $M_8 \sim 1$, and the fluctuations are produced at a radius $r \sim 10 r_s$, the observed fluctuation timescales are shorter than an orbital period, cf.

equation (3). Since gravitational energy cannot easily be released on a timescale $\lesssim t_K$, the energy in an outburst must have been stored.

Some very general arguments may be given concerning the relation between L, ΔL, and Δt. By assuming that the energy in an outburst is produced by material that is associated with opacity, thereby increasing the light travel time across the emission region, Cavallo and Rees (1978) and Fabian and Rees (1979) have obtained the inequality

$$\Delta L < m_p c^4 \epsilon \Delta t / \sigma_T = 2\times10^{41} \text{erg s}^{-1} \left(\frac{\epsilon}{0.1}\right) \Delta t . \qquad (11)$$

By requiring that the steady luminosity be less than the Eddington limit and using equation (10), Lightman, Giacconi, and Tananbaum (1978) have pointed out the inequality

$$L < 10^{42} \text{erg s}^{-1} \left(\frac{l}{10^5}\right)^{-1} \Delta t . \qquad (12)$$

Fortunately (for theorists), none of the observations in Table 1 violate the above inequalities, although 3C 273 and NGC 6814 push them. That these inequalities seem to have something to do with the actual data suggest both high efficiencies, $\epsilon \gtrsim 0.1$, and an emission region of dimensions determined by the Schwarzschild radius of a black hole.

Clearly, long-term observations with large area detectors and high time resolution are desireable for further testing the above inequalities and related considerations. The proposed Large Area Modular Array of Reflectors (LAMAR) should be quite suitable for this task.

For time resolution sufficient to study a signal of magnitude $\Delta L/L \leq 0.1$, it may be possible to see large blobs of matter spiralling into the black hole. For a circular, non-spiralling orbit, we expect to see angular frequencies $\omega = (GM/r_0^3)^{1/2}$ in the Newtonian approximation, which can be written as

$$\omega = \omega_0 (r/r_0)^{-3/2} \qquad (13a)$$

where $\omega_0 = 2\pi/P_0$ is the angular frequency at radius r_0 and P is given in equation (3). Now, for a radiating blob of matter that slowly spirals inward, the observed angular frequency will increase, seen as a low-Q quasi-periodicity, with decreasing period. To obtain an equation for this spiral, we may specify radius in terms of phase or azimuthal angle ϕ, and then integrate the relation $\omega = d\phi/dt$ along with equation (13a) to obtain $\phi(t)$. Signals would be modulated in proportion to $\cos\phi$.

The type of spiral depends on the local, nongravitational physics, particularly the viscous stresses. As a simple example, the "Archimedes spiral" is of the form

$$r = r_0 \left(1 - \frac{\phi}{2\pi n}\right)$$

where n is a free parameter, and yields

$$\phi(t) = 2\pi n \left[1 - \left(1 - \frac{5\omega_0 t}{4\pi n}\right)^{2/5}\right] \qquad (13b)$$

Another spiral, which can be related to disk models in the literature, derives from equation (5a), $r^{-1}dr/d\phi = \beta$. If we assume that β is a constant (as given by a number of the α-disk models), then equation (5a) gives the logarithmic spiral

$$r = r_0 e^{-\beta\phi}$$

and yields

$$\phi(t) = \frac{2}{3\beta} \ln \left(1 - \frac{3B}{2}\omega_0 t\right)^{-1} . \qquad (13c)$$

We mention that simple analytic solutions may also be obta-

ined when β is a general power law in radius, rather than a constant. The above forms for ϕ are only applicable several Schwarzschild radii away from the black hole; similar general-relativistic expressions could be obtained closer to the hole.

Further theoretical work needs to be done on the time variability to be expected by matter inhomogeneities near the black hole. Accretion instabilites (Pringle, Rees, Pacholczyk 1973; Lightman and Eardley 1974; Shakura and Sunyaev 1976) may contribute to the oberved variability. None of these possibilites has yet been modeled with sufficient detail, in the nonlinear regime, to make quantitative predictions.

D. Gas Supply

A clue to the environment of the power source might be gotten from study of the various sources of "fuel", the required conditions for these sources, and the different implications for luminosity evolution. Some of the models that have been proposed for the source of gas are (a) stellar collisions in a dense star system (e.g. Spitzer and Saslaw 1966), (b) tidal stripping of stars in a dense stellar system by a central massive black hole (Hills 1975), (c) infall of intergalactic gas (Gunn 1979), (d) galaxy mergers (e.g. Roos 1981), (e) intragalactic gas released by normal stellar evolutionary processes. One difficulty with models in which gas originates at large radii from the center is the necessity to dissipate a large amount of angular momentum. If the gas is provided by a dense stellar system, and if [illegible], then it can be shown that the dynamics of the stellar system must be dominated by physical stellar collisions (Shields and Wheeler 1978; McMillan, Lightman, and Cohn 1981).

It seems clear that substantial luminosity evolution occurs in QSOs (e.g. Turner 1979); AGN may be the late time phase of the same evolution. In principle, the gas supply mechanism should have something to do with luminosity evolution. The various mechanisms mentioned above, through their different dependences on the external environment of the QSO or AGN (in (c) and (d)), and on the internal parameters of the black hole and dense stellar system (in (a) and (b)), predict different functional forms for the evolving gas supply rate $\dot{M}(t)$, and hence for the evolving luminosity L(t). A comparison of theoretical models for the gas supply mechanism with a large data set of received fluxes and redshifts might be able to rule out or partly confirm some of the models and clarify the relevant physical conditions. For example, models (a) and (b), with evolution of the stellar-system parameters included, yield late-time asymptotic laws of the form (McMillan, Lightman, and Cohn 1981)

$$\dot{M}(t) \propto t^{-p}, \qquad (14)$$

where p=2 for mechanism (a) and p=1 for mechanism (b).

The test of any theory of luminosity evolution is a statistical problem, requiring a value for the cosmological parameter q_0, some information about the distribution of initial conditions or luminosities (the luminosity function), and some information about the distribution of "turn-on

times" of the objects -- in addition to an evolutionary law of the form of equation (14) for a single object. If additional assumptions can be made about these distributions, they may not need to be completely specified a priori. For example, Turner (1979) assumes the luminosity function maintains its shape in time, which, in our context, would allow determination of a value for p for every assumed value of q_0. Unfortunately, Turner's assumption has little physical justification and seems to require some external clock that determines the physical conditions of each new quasar as it is born. In any case, a very dense X-ray Hubble diagram, with the fluxes and redshifts from many QSOs, will be necessary to solve the essentially statistical problem of luminosity evolution. X-rays seem particularly useful here, since QSOs may be readily identified by their X-ray emission, and this emission may constitute the majority of the total luminosity.

A good determination of the local luminosity function would be quite useful in the above project. Figure 2 below shows a luminosity function calculated for a number of nearby objects.

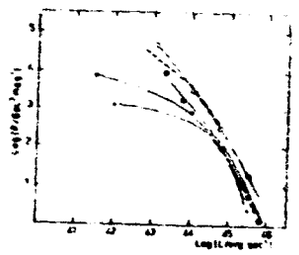

Figure 2: Luminosity function of QSOs and AGN. The dashed line is fit from model (d) and additional assumptions. From Rees (1981).

The universality of the forms in Figure 2, especially above about $L = 3 \cdot 10^{45}$, suggests some universal type of process that establishes the range of conditions for QSOs and AGN.

III. RADIATION PROCESSES

A. Types of Mechanisms

It should be stated at the beginning that, while much of the emission in the radio is easily diagnosed as synchrotron radiation, there is little agreement on how the X-rays and gamma rays are produced. It is almost certain that the conditions in the X-ray emitting region are far from simple. A good fraction of the particles, especially those that ultimately form the observed jets, may be relativistic; there are accretion instabilities; shock waves and magnetic fields

abound; the emission may be part thermal and part nonthermal. The radiation mechanisms we discuss can be divided into two categories: 1. Power-law electron models and 2. Non-power-law electron models. The second category can be further subdivided into thermal (random motions of electrons dominate emission) and nonthermal (bulk motions of eletrons dominate emission) processes.

As will be shown below, the observed X-ray emission is well fit by a power law of the form

$$I_\nu \propto \nu^{-s}, \qquad (15)$$

where I_ν is proportional to the energy per unit frequency ν.

1. Power-law electron models

If the X-ray emission is synchrotron radiation (requiring electron Lorentz factors $\gamma \sim 10^8$ for equipartition magnetic fields of $B \sim 10^{-6}$ G) or relativistic inverse Compton, then a spectrum of the form of equation (15) can be achieved by a power law distribution of electrons of form

$$dn/d\gamma \propto \gamma^{-r} \qquad (16a)$$

where

$$r = 2s+1 . \qquad (16b)$$

For the observed values of the power-law index, $s \sim 0.7$, see below, we require $r \sim 2.4$. A number of groups (Axford, Leer and Skadron 1977, Bell 1978, Blandford and Ostriker 1978) have investigated first order Fermi mechanisms, whereby particles are accelerated into a power law distribution by the converging flows across a shock front. These mechanisms yield values $r \sim 2$-3, and have been applied to cosmic rays. It is also quite possible that such processes accelerate electrons in the central regions of AGN and QSOs, where strong shocks may be present, and evidently produce an electron index in the appropriate range for synchrotron or inverse Compton radiation. If this is the nature of much of the radiation produced, then hign X-ray polarization might be expected. Future X-ray plarization experiments may be quite important in clarifying this possibility.

2. Non-power law electron models

A power law spectrum can also be produced by the scattering of soft photons transmitted through a finite medium of hot electrons, even when these electron do not themselves have a power-law distribution. In this case, a power law results from the absence of an energy scale over a large range of energy. When the electrons have a thermal, nonrelativistic distribution, then s may be related to the Thomson depth τ_{th} and temperature T (Shapiro, Lightman and Eardley 1976, Katz 1976) ($\tau_{th} > 1$)

$$s = -\frac{3}{2} + \left(\frac{9}{4} + \frac{4}{y}\right)^{1/2}, \qquad (17a)$$

where

$$y \equiv 4 T_e \tau_{th}^2 \qquad (17b)$$

$$T_e \equiv kT/mc^2 . \qquad (18)$$

When the electrons have a thermal, relativistic distribution, then the corresponding result is (Pozdnyakov, Sobol and Sunyaev 1976) ($\tau_{th} < 1$)

$$s = \ln \tau_{th}^{-1} / \ln (16 T_e^2) . \qquad (19)$$

We mention that power laws may also be produced by the above process for non-thermal electrons, as long as their distribution is sharply peaked at some "effective temperature." Takahara (1980), Takahara, Tsuruta and Ichimaru (1981) and Maras-

chi, Roasio and Treves (1981) have recently considered models using the above radiation mechanism. The soft photons for this process could be generated by cyclotron radiation (Eardley and Lightman 1976; Takahara, Tsuruta and Ichimaru 1981), produced at perhaps 10^{10} Hz and absorbed up to about the 100th harmonic. Soft photons could also be produced by cold dense clouds in pressure equilibrium with the hot phase of the plasma.

A problem with the Comptonization mechanisms above is that the spectral index depends on the parameters τ_{th} and T, which might be expected to vary from one source to another, in contradiction with the narrow range of s actually observed (see D. below). For a scattering model to work in this context, a "characteristic" geometry or structure is required. For example, if the soft photons are externally incident on a region of hot, thermal electrons with a large scattering depth, then the reflected X-rays have a more universal spectrum. Lightman and Rybicki (1979a) have investigated this process and obtain the universal quasi-power law (for $\nu \gg \nu_0$)

$$s = \frac{3}{2}\left(\ln\frac{\nu}{\nu_0}\right)^{-1}, \qquad (20)$$

where ν_0 is the typical frequency of the soft photon input. This power law extends up to photon energies $h\nu \sim kT$ and into the relativistic domain if the electrons have relativistic random motions.

In the above scattering mechanisms, it is the <u>random</u> motion of the electrons that dominates the emission. A closely related mechanism that depends on the <u>bulk</u> electron motion is the scattering of intially soft photons by the converging flows across a shock front. This process has been investigated by Blandford and Payne (1981a, 1981b) and gives a high energy asymptotic result

$$s = (M^2-1/2,\ (M^2+6),\ (M^2-1)^{-2}, \qquad (21)$$

where M is the Mach number of the shock (not to be confused with a mass). This power law extends up to frequencies such that the photon momentum equals that of the electron. Thus, the bulk motions must be relativistic to produce photons of energies $h\nu \geq mc^2$. Since characteristic bulk velocities are only of the order $v \sim 0.3c$ at $r \sim 10\, r_s$, this scattering process may have difficulty in producing relativistic photons. In any case, Equation (20) gives a value of s a little too small and equation (21), for a strong shock, $M \gg 1$, gives a value of s a little too large. It is possible that refinements of these models might be more satisfactory.

Some general statements may be made. Any thermal process must result in a characteristic thermal (exponential) turnover in the spectrum, and possibly a Wien bump, at $h\nu \sim kT$. A shock mechanism should have a cutoff in the spectrum at energies $h\nu \sim mc(\gamma v)_{shock}$. In almost all cases, no turnovers of any kind have yet been seen. <u>It is important to extend X-ray observations up to higher energies, in search of such a turnover</u>. In any case, it is clear that some turnover must occur, since the observed value of $s \sim 0.7$ indicates an infinite total energy if this power law continues to arbitrarily high frequencies.

Changes of the spectrum during luminosity fluctuations

may also provide some information about the emission mechanism. In any scattering model in which soft photon are scattered up to high energies, one expects the spectrum to harden during a fluctuation if the temperature remains constant. Rybicki and Lightman (1979b) and Payne (1980) have investigated the time-dependent versions of Comptonization by thermal electrons within this context. Some attempts have been made to model the observed (or absence of) spectral evolution in outbursts by such processes (e.g. Tennant et. al. 1981). If the Compton cooling time is much shorter than the energy input time, it may be the soft photon source rather than the temperature that remains constant during fluctuations. Guilbert, Ross and Fabian (1981) have investigated this possibility and find that the spectrum first hardens and then softens as the temperature decreases. Over a range of parameters with $y \gtrsim 1$, the time-averaged spectrum has a quasi power-law shape, with $0<s<1$, and a thermal cutoff (with no Wien hump) at the initial electron temperature. It is possible that in many cases, steady state spectra are not relevant and we should always be considering time averages of nonsteady processes. Better spectral resolution during luminosity fluctuations will be helpful here.

There are various pocesses that may be involved in producing the electron distribution, if it is not thermal. In addition to the shock acceleration already mentioned, large scale magnetic and electric fields may be present (Blandford 1976, Lovelace 1976, Blandford and Znajek 1977). Cavaliere and Morrison (1980) have pointed out that the electrons must

be reaccelerated in crossing the emission region. Defining a parameter q by

$$q = \left(\begin{array}{c}\text{probability} \\ \text{of scattering}\end{array} \times \begin{array}{c}\text{fractional energy loss} \\ \text{per scattering}\end{array}\right) \qquad (22)$$

$$= (\sigma_T n_\gamma R) \times (4h\nu/\gamma mc^2) .$$

Here n_γ is the photon density

$$n_\gamma = L/(4\pi R^2 c h\nu) , \qquad (23)$$

so that

$$q \sim 70 \left(\frac{L}{L_{Edd}}\right)\left(\frac{R}{10 R_S}\right)^{-1} . \qquad (24)$$

In any source where q exceeds unity, reacceleration is necessary. Note that q is about equal to the Kepler time divided by the Compton cooling time.

B. Thermalization Time Scales

A principal uncertainty is whether any of the observed X-ray emission from QSOs and AGN is thermal. Such emission requires that the electrons be able to thermalize, via two-body collisions or perhaps collective plasma motions, on a time scale shorter than energy is deposited or radiated and shorter than pair creation when the latter is important. We will consider two-body thermalization below, keeping in mind that collective effects may always be faster.

First we consider the ion thermalization time. The bulk of the released gravitational energy is probably intially deposited into the ions. Taking a value of 25 for the Coulomb logarithm, the ion thermalization time, t_{ii}, via ion-ion scattering is, cf. Spitzer (1962)

$$t_{ii} \sim \frac{T^{3/2} m_p^{1/2}}{(5.6\pi N e^4 \ln\Lambda)} = 5\times 10^{12} N^{-1} \left(\frac{T}{10^{12} K}\right)^{3/2} . \qquad (25a)$$

Substituting equation (6) into equation (25a), and taking T=

10^{12} K, we obtain

$$t_{ii} = 5\times10^{2} c \left(\frac{L}{L_{EDD}}\right)^{-1} \beta \left(\frac{\epsilon}{0.1}\right) M_8 , \qquad (25a)$$

and using equations (3) and (5b), we obtain

$$t_{ii}/t_r = 1.6\times10^{2} \left(\frac{L}{L_{EDD}}\right)^{-1} \beta^{2} \left(\frac{\epsilon}{0.1}\right) . \qquad (25c)$$

Here and elsewhere in this section, all quantities will be evaluated at $r = 10 r_s$ for simplicity, unless otherwise stated. Since energy is deposited into the ions on a timescale t_r, the last ratio must be less than unity for ion-ion collisions to thermalize the ions. Ions may also thermalize by scattering with the electrons. If we denote this timescale by t_{ie}, then

$$t_{ii}/t_{ie} \sim \left(\frac{m}{m_p}\right)^{1/2} \left(\frac{n_- + n_+}{N}\right) \left(\frac{m}{m_p} + \frac{T_e}{T_i}\right)^{-3/2} ; \qquad (26)$$

where T_i and T_e denote the ion and electron temperature, respectively. (If the particles are not thermal, then temperatures should be replaced by mean energies.) For $T_i = 10^{12}$K and $T_e = mc^2 = 6\times10^{9}$K, equation (26) gives $t_{ii}/t_{ie} \sim 50(n_- + n_+)/N$. Thus, a relatively low electron mean energy and the presence of many electron positron pairs may allow the ions to thermalize.

Next we consider electron thermalization via electron-electron scattering. For relativistic electrons, $T_* > 1$, this timescale, t_{ee}, is

$$t_{ee} = T_*^2 (n_- + n_+)^{-1} (c\sigma_T \ln \Lambda)^{-1} \qquad (27)$$

$$= 2.4\times10^{2} c\, T_*^2 \left(\frac{n_- + n_+}{N}\right)^{-1} \left(\frac{L}{L_{EDD}}\right)^{-1} \beta \left(\frac{\epsilon}{0.1}\right) M_8 .$$

The electron cooling time, t_{cool}, may be evaluated in a model-independent way:

$$t_{cool} = \frac{3}{2} [illegible] (n_- + n_+) [illegible] T_* \left(\frac{n_- + n_+}{N}\right) \left(\frac{m}{m_p}\right) (\beta c)^{-1} t_K . \qquad (28)$$

We then obtain the ratio

$$t_{ee}/t_{cool} \sim 0.1 [illegible] \left(\frac{[illegible]}{n_- + n_+}\right)^{2} \left(\frac{L}{L_{EDD}}\right)^{-1} \beta^{2} \left(\frac{\epsilon}{0.1}\right)^{2} , \qquad (29)$$

which must be less than unity for the electrons to thermalize. Equation (29) suggests that in some cases we might expect thermal electrons and in some cases not. As long as the electrons are only marginally relativistic, the electrons should be able to thermalize unless the luminosity is very much below the Eddington limit and there are few electron positron pairs. It seems likely, however, that a fraction of the electrons will be accelerated up to very relativistic energies by some of the processes mentioned above. In this case we would not expect the electrons to be able to sustain a thermal distribution. In any event, as is discussed below, the copious production of e^+e^- pairs prevents the temperature of an optically thin thermal medium from becoming very relativistic.

The time scale for electrons to receive energy from ions, t_{ei}, satisfies

$$t_{ei} = t_{ie} \left(\frac{T_e}{T_i}\right) \left(\frac{n_+ + n_-}{N}\right)$$

Since electrons can cool relatively efficiently, faster than they receive energy from the ions, we may expect the electron mean energy to be much lower than that of the ions, as suggested by Shapiro, Lightman and Eardley (1976).

The conclusion is that there may well be two populations of electrons: a marginally relativistic, thermal population and a highly relativistic, nonthermal population. Unfortunately, it is difficult to calculate the relative proportions of these two populations at the present time.

C. Pair Effects

With the high virial temperatures available, cf. equation (2), much exceeding the electron rest mass, it seems likely that some sizeable fraction of the electrons will be at least marginally relativistic, and most detailed models in the literature (e.g. Shapiro, Lightman and Eardley 1976; Maraschi, Roasio and Treves 1981; Takahara, Tsuruta and Ichimaru 1981) do indeed have this character. In such a situation, the effects of electron-positron pair production must be included. When pairs are present, the distributions of radiation and pairs must be solved for self consistently, since photons produce pairs, pairs produce photons, and all the cross sections are, in general, energy dependent. Some recent work in these processes has been done for steady plasmas by Stoeger (1977), Liang (1979), Lightman and Band (1981), Lightman (1981), and Svensson (1981), and in the context of a time-dependent cooling "fireball" by Cavallo and Rees (1978).

As an example, we consider production of pairs by the reaction

$$e^{\pm} + \gamma \longrightarrow e^{\pm} + e^{+} + e^{-},$$

which may dominate when a large photon density is present and the electrons are energetic. This reaction gives a positron production rate

$$\dot{n}_{+} \sim c \sigma_T \alpha_f n_\gamma (n_+ + n_-) \qquad (30)$$

(where α_f is the fine structure constant), only logarithmically sensitive to the particle and photon distributions, as long as the threshold condition

$$h\nu \gg m_e c^2$$

is strongly satisfied. The pair production time scale for this process, t_{pair}, is

$$t_{pair} \equiv \tau_{\gamma\gamma}^{-1} = .06\, t_{\nu B} \left(\frac{h\nu}{m_e c^2}\right) \left(\frac{L}{L_{Edd}}\right)^{-1} \left(\frac{r}{10 r_S}\right)^{1/2} \left(\frac{n_e}{n_{e,m}}\right), \qquad (31)$$

where we have used equations (23), (5b) and (3), and the L refers to the luminosity in those photons above threshold. In sources that are not too far below the Eddington limit, we therefore expect this process to have ample time to produce pairs. Since pairs produce more pairs, there may be a non-steady behavior in which, for a short period of time (and with $\tau_{\gamma\gamma}$ varying rapidly perhaps), an overabundance of pairs is produced.

It is also of interest to compare the time scale, t_{ann}, for the pair annihilation process

$$e^{-} + e^{-} \longrightarrow 2\gamma$$

to the cooling time. (In a steady state the creation time would equal the annihilation time.) If pairs cool before they annihilate, then we might expect to see a feature in the spectrum at the electron rest mass energy, as has been seen (redshifted by 20%) in the March 1979 gamma ray burst event. For QSOs at redshift z, this feature would be at the energy 511 kev/(1+z). For electrons of Lorentz factor γ,

$$t_{ann} = 16\gamma^2/(27 \sigma_T c n_-). \qquad (32)$$

In addition to comparing equation (32) to equation (28) we can assume a specific cooling mechanism. For example, the time scale for synchrotron cooling, t_{syn}, is

$$t_{syn} = 6\pi m c / (\gamma^2 \sigma_T) \qquad (33)$$

Then, using the expression for the gas and magnetic pres-

sures, P_G , and P_B , respectively,

$$P_G = \frac{1}{3}\gamma mc^2 (n_- + n_+) \qquad (34)$$

$$P_B = B^2/8\pi , \qquad (35)$$

we can obtain the ratio

$$t_{syn}/t_{ann} = 3\gamma^{-4} (P_G/P_B) . \qquad (36)$$

For equipartition magnetic fields, $P_B \sim P_G$, pairs will evidently cool before they annihilate as long as $\gamma \gtrsim 2$. The absence of an observed annihilation line may indicate the magnetic fields are below their equipartion value. When relativistic pairs annihilate before substantial cooling, the photons produced will at most yield a broad feature at $h\nu \sim \gamma mc^2$, and even this may be dominated by Comptonized bremsstrahlung radiation (Lightman and Band 1981).

Recent work (Lightman 1981; Svensson 1981) has shown that there is a maximum temperature that can be achieved by a thermal, optically thin plasma in equilibrium, dependent on the value of the ion scattering depth, equation (7). A maximum temperature comes about because the pair annihilation rate decreases with increasing temperature and the pair production rate increases as the photon density increases (which increases with τ_N). This maximum (or, equivalently, the maximum τ_N possible for each value of T) is shown in Figure 3. Furthermore, there is generally an enormous range in luminosity over which the temperature remains in the narrow range $0.1 \lesssim T_e \lesssim 1$, with copious pair production at the high end and threshold effects at the low end serving as a thermostat.

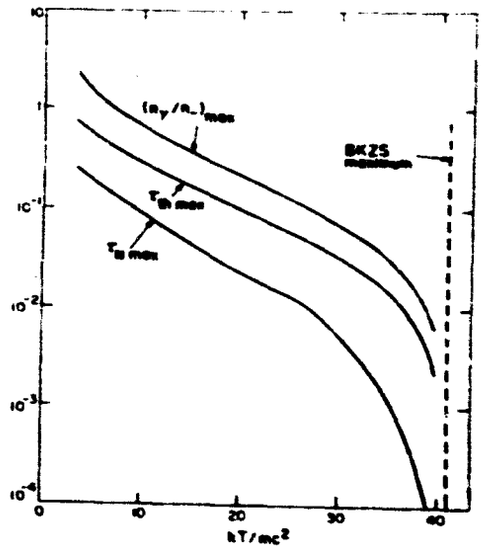

Figure 3: Maximum ion scattering depth, Thomson depth, and photon to electron ratio that can be achieved at each temperature in an optically thin, steady thermal plasma. From Lightman (1981).

Earlier work by Bisnovatyi-Kogan, Zeldovich, and Sunyaev (1971), which did not include finite size effects and neglected photon processes, obtained the maximum temperature $kT = 4mc^2$. The magnitude of this maximum is set by the reciprocal of the fine structure constant. In the calculations resulting in Figure 3, only internal sources of photons were included (bremsstrahlung, double Compton, and annihilation). Any additional source of photons, e.g. a soft photon source, must lower the maximum T at each value of τ_A, since photons

produce but do not destroy pairs in an optically thin plasma. Thus, the maxima shown in Figure 3 are upper limits. Observed spectra with power laws extending above $h\nu > kT_{max}$ indicate that either the plasma is nonthermal or nonsteady.

Another constraint on the mean energy and number density of the pairs arises from requiring that the total system of ions and pairs must be gravitationally confined. This leads to the inequality

$$\gamma\left(\frac{n_- + n_+}{N}\right) < \frac{1}{4}\left(\frac{m_p}{m}\right)\left(\frac{r}{r_s}\right)^{-1} \qquad (37)$$

When equation (37) is violated, magnetic confinement requires magnetic fields above equipartition strength. Equation (37) must be satisfied on average, but could be violated for short times or over small regions.

We finally mention that photon-photon pair production

$$\gamma + \gamma \rightarrow e^+ + e^-$$

may limit the presence of hard gamma rays. If $h\nu_s$ is the energy of a soft photon and $h\nu_h$ is the energy of a hard photon, then the threshold condition for pair production is

$$\left(\frac{h\nu_s}{mc^2}\right)\left(\frac{h\nu_h}{mc^2}\right) \geq 2$$

The scattering depth to the above reaction is

$$\tau_{\gamma\gamma} = n_s \sigma_T r \qquad (38)$$

where n_s is the number density of "field" photons in a bandwidth $2\nu_s$ around ν_s. Some constraints may be placed on sources for which strong gamma emission is seen, by requiring that the number density n_s be sufficiently small to achieve $\tau_{\gamma\gamma} < 1$, (Herterich 1974). For example, Fabian and Rees (1979) have shown that the observed gamma and X-ray emission

from 3C 273 (see Figure 4) require that the gamma rays be emitted in a region $r > 3 \times 10^{16}$ cm, much larger than the X-ray emitting region. We mention, however, that the above constraint may be violated if the produced pairs themselves produce more gamma rays that are not substantially downgraded in energy. Since the various reactions that would redistribute the spectrum, e.g. Compton scattering, are energy dependent, it is not clear how large $\tau_{\gamma\gamma}$ can be before the gamma rays would certainly be cut off. This is an area in which more research is needed.

D. Observed Spectra

The composite spectrum of the QSO 3C 273 is shown in Figure 4.

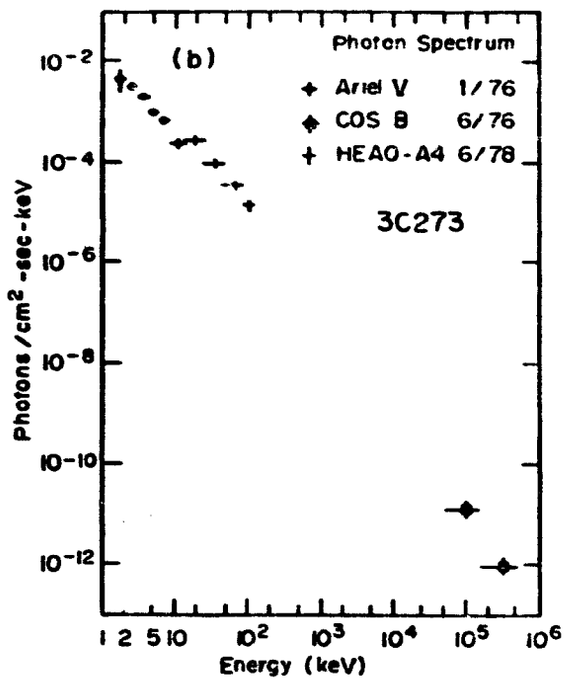

Figure 4: Spectrum of 3C 273. From Eradt (1980)

The portion of this spectrum from 13 to 120 kev is well fit by a power law with s=0.67. This spectrum is actually fairly characteristic of many AGN and QSOs. In Figure 5, we see a histogram of spectral indicies that describe power laws seen in Seyfert galaxies. (The index α in Figure 5 is the same as the s given in equation (15).)

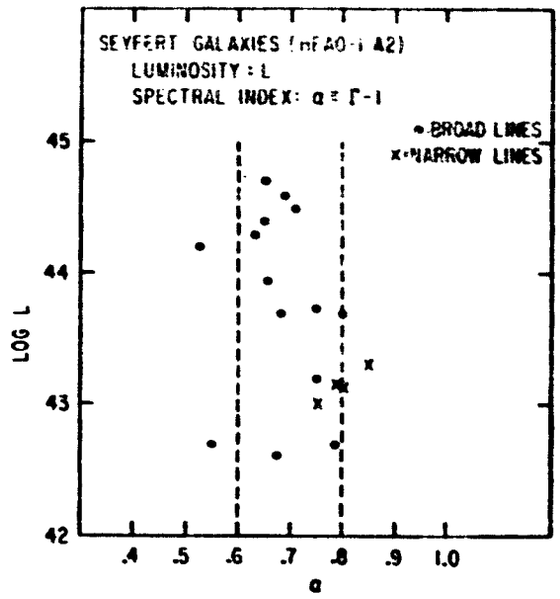

Figure 5: Histogram of spectral indicies observed for Seyfert galaxies. α is the energy index. From Mushotzky (1981).

The data, over an observed range 1-100 kev, are well fit with an s $\sim$ 0.69, and a small scatter about this mean $\sigma \sim 0.15$. This result has been reported by Mushotzky (1981) and by Maccacaro, Perola and Elvis (1981). The universality of these spectra is striking and suggests a universal type of emission mechanism, as discussed above. Emission above 1 Mev has also been seen in a few other objects, e.g. NGC 4151 (Schonfelder 1978). It is crucial to obtain spectra of as many QSOs as possible, to confirm the similarity of their spectra to those

of AGN. For this purpose large area detectors like LAMAR should be useful.

From all the above considerations, there is a clear need for observations at higher energies, going into the gamma rays. There may be a wonderland of interesting physics waiting to be learned at $h\nu \geq mc^2$. The proposed satellite GRO should have such a capability. To summarize the needs for such observations:

(1) With a spectral index of s=0.7, most of the total luminosity has yet to be observed! Look back at all the go-or-no-go formulae that contain an L. Until the observations are pushed to sufficiently high energies to see a turnover in the spectrum, we only have lower limits on that L.

(2) When a break, or turnover, in the spectrum is seen at high energies, we will have a much better idea of whether the emission is thermal or nonthermal.

(3) As suggested by the discussion in C. above, a number of interesting effects associated with electron-positron pairs may be seen at energies $h\nu \geq mc^2$. These features and the physical effects they represent may be completely hidden at lower energies.

Observations of the spectra at low energies, especially near the soft X-ray absorption cutoff, $h\nu \leq 1$ kev, are also important. Lawrence and Elvis (1981) have recently found good evidence for a correlation between total X-ray luminosity and the ratio of hard ($h\nu$ 2-10 kev) to soft ($h\nu$ 0.5-4.5 kev) components. They interpret this result to indicate that the covering factor of the broad line emission region over the continuum X-ray source is a monotonically decreasing function of X-ray luminosity. Two possible explanations are that brighter sources, either through radiation pressure or hydrodynamic effects, are able to "blow away" the surrounding absorbing gas, or that the accumulation of absorbing gas is associated with ageing (e.g. through stellar evolutionary processes) and older objects are in the declining phase of their activity (see luminosity evolution in II D. above).

IV. BEAMS AND JETS

It is impossible to consider the subject of QSOs and AGN without mentioning the dramatic, well collimated streams of matter seen emanating from the centers of these objects. These "jets" have been detected in a variety of different objects and in several different wavelengths. Recently, they have been seen in the X-ray band also (e.g. Schreier et. al. 1979, Feigelson et. al. 1981). The opening angle of a jet is typically $\theta \leq 10^\circ$, the velocity of the matter $300 km s^{-1} < v < c$, and the jet lifetime $t_{life} \geq 10^6 yr$. See Rees (1980) and Begelman, Blandford and Rees (1981) for recent reviews of the physics of jets.

Since jets are ubiquitous in QSOs and AGN, whatever produces a jet should be a commonly occuring phenomenon, not requiring special conditions. Furthermore, the jet "remembers" its directionality for a million years or more, so the fundamental beaming mechanism must be associated with a long-lived and stable axis of symmetry. Most researchers feel that net

angular momentum is a key ingredient in defining the required axis, but the detailed mechanism for accelerating matter along this axis is not yet understood.

One of the earliest suggestions was the "twin-exhaust" hydrodynamic model of Blandford and Rees (1974), in which a heat source at the center of a rotating gas cloud, in an external gravitating potential, creates a low density channel of gas that burrows a tunnel along the path of least resistance, the rotation axis. The first detailed hydrodynamical calculations to test the validity of this suggestion have recently been completed by Norman et. al. (1981), and some of their results are shown in Figure 6.

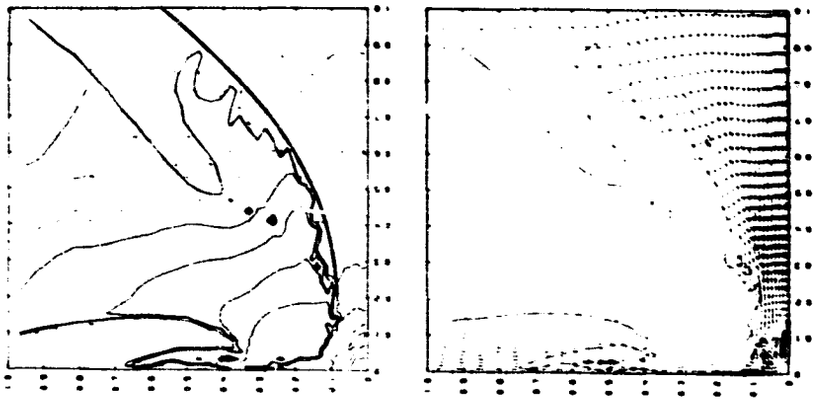

Figure 6a: Density contours of the cloud jet structure at t= 1.6. The solid line is the jet wall. The rotation axis is vertical. Units given in the text. From Norman et. al. (1981).

Figure 6b: The velocity vector field for the jet in 6a. Note the central shock. From Norman et. al. (1981).

The unit of length here is GM/c^2, where M is the mass of the confining cloud and c^2 is the internal energy per unit mass of the hot, light gas introduced at the center. The unit of time is $GM/c^{3/2}$. The central cavity is at a radius R=0.15. The gas accelerates smoothly to supersonic velocity, terminating in a shock front at R=0.1, at which point collimation begins. These results indicate a cavity-nozzle structure more compact than that suggested by Blandford and Rees (1974). The calculations of Norman et. al. (1981) assume a flat bottomed gravitational potential, rather than a point source potential that would be generated by a central black hole. Future such calculations, perhaps more applicable to the AGN and QSO context, will yield one of the first reliable estimates for the amount of collimation that may be achieved by this mechanism.

Another idea, suggested by Lynden-Bell (1978), is that radiation pressure may accelerate matter along the interior funnel formed by a thick accretion disk (e.g. Jaroszynski, Abramowicz and Paczynski 1980). Some recent kinematical studies by Abramowicz and Piran (1980) suggest that the disk funnel must be extremely narrow for this method to yield adequate collimation, with a ratio of outer to inner disk radii of at least 10^4. No calculations have yet been done to self consistently determine the parameters of the funnel, or to test whether such a narrow funnel is stable in the presence of radiation and matter.

It is quite possible that none of the above mechanisms are able to achieve the observed collimation, and that much

of the collimation is actually achieved far from the black hole, perhaps by large scale magnetic fields. Blandford and Payne (1981c) have recently investigated such a model, in which angular momentum is removed from an accretion disk by magnetic fields that extend to large radii. An outflow of matter along the rotation axis is then possible. At large distances from the disk, the toroidal component of the magnetic field may collimate the matter.

V. CONCLUSIONS

We conclude by recapping some of the important future observations that may clarify the physics of QSOs and AGN.

1. Temporal Resolution. (a) The various theoretical constraints on L, ΔL, and Δt, when pushed to their limits, may provide our best handles on the efficiencies and emission-region sizes. (b) Spectral changes during fluctuations may help specify the radiation mechanism. (c) Signatures of spiralling matter or accretion instabilities may be revealed by high time resoltuion.

2. Large Sample of QSO Spectra, Intensities, and Redshifts. (a) It is important to learn whether a single universal spectrum describes QSOs as well as AGN. (b) With a large X-ray Hubble diagram for QSOs, we can begin to test luminosity evolution against theoretical models of the gas supply mechanism.

3. X-ray Polarization. Synchrotron radiation typically produces large polarization. Most other mechanisms produce a small polarization.

4. High Energy Measurements $h\nu \sim 1\text{-}10$ MeV. (a) With an observed spectral index $\alpha \sim 0.7$ for AGN, we now have only a lower bound on the total luminosity of most of these objects. (b) The shape of the turnover in the spectrum, at high energies, should tell us about the emission mechanism. (c) A good deal of physics associated with pair production (maximum temperatures of thermal, steady plasmas; annihilation features) can only be observed at energies $h\nu \geq .5$ MeV.

To end with a note of caution: Most of the ideas have been presented as if there were one universal framework for all QSOs and AGN, one basic scenario of gas accretion onto a massive black hole, one dominant radiation process, one mechanism for producing and collimating the jets. I think sometimes, especially in astronomy, we tend to use Occam's razor too much. We should be receptive to the possibility that a number of different processes and mechanisms may be operating in different objects, or perhaps going on simultaneously in the same object -- even though the net results of luminosities, spectra, and variabilities can be squeezed into a common framework.

Acknowledgments

We thank D. Eardley, M. Elvis, P. Gorenstein, J. Grindlay, D. Payne, G. Rybicki, and H. Tananbaum at the Harvard-Smithsonian Center for Astrophysics for useful comments. This work was supported in part by NASA grant NAGW 246.

REFERENCES

Abramowicz, M.A. and Piran, T. 1980, Ap. J. Lett., 241, 17.

Angel, R. 1978, in Proc. Pittsburg Conference on BL Lac Objects, ed. A.M. Wolfe

Axford, W.I., Leer, E., and Skadron, G. 1977, Proc. 15th Int. Cosmic Ray Conference (Plovdiv, Bulgaria).

Bardeen, J. and Petterson, J.A. 1974, Ap. J. Lett., 195, L65.

Begelman, M.C., Blandford, R.D. and Rees, M.J. 1981, Ann. N.Y. Acad. Sci., in press.

Bell, A.R. 1978, M.N.R.A.S., 182, 147.

Bisnovatyi-Kogan, G.S., Zeldovich, Ya.B., and Sunyaev, R.A. 1971, Sov. Astr.-AJ, 15, 17.

Blandford, R.D. 1976, M.N.R.A.S., 176, 465.

Blandford, R.D. and Ostriker, J.P. 1978, Ap. J. Lett., 221, L29.

Blandford, R.D. and Payne, D.G. 1981a, M.N.R.A.S., 194, 1033.

Blandford, R.D. and Payne, D.G. 1981b, M.N.R.A.S., 194, 1041.

Blandford, R.D. and Payne, D.G. 1981c, preprint.

Blandford, R.D. and Rees, M.J. 1974, M.N.R.A.S., 169, 395.

Blandford, R.D. and Znajek, P.L. 1977, M.N.R.A.S., 179, 433.

Bradt, H.V. 1980, Ann. N.Y. Acad. Sci., 336, 59.

Cavaliere, A. and Morrison, P. 1980, Ap. J. Lett., 238, L63.

Cavallo, G. and Rees, M.J. 1978, M.N.R.A.S. 183, 359.

Delvaille, J.P., Epstein, A. and Schnopper, H.W. 1978, Ap. J. Lett., 219, L81.

Eardley, D.M. and Lightman, A.P. 1976, Nature, 262, 196.

Eardley, D.M., Lightman, A.P., Payne, D.G. and Shapiro, S.L. 1978, Ap. J., 224, 53.

Fabian, A.C. and Rees, M.J. 1979, in X-ray Astronomy, ed. W.A. Baity and L.E. Peterson (Pergamon).

Feigelson, E.D., Schreier, E.J., Delvaille, J.P., Giacconi, R., Grindlay, J.E. and Lightman, A.P. 1981, Ap J., in press.

Guilbert, P.W., Ross, R.R. and Fabian, A.C. 1981, M.N.R.A.S. in press.

Gunn, J.E. 1979, in Active Galactic Nuclei, ed. C. Hazard and S. Mitton (Cambridge University Press).

Heterich, K. 1974, Nature, 250, 311.

Hills, J.G. 1975, Nature, 254, 295.

Jaroszynski, M., Abramowicz, M.A. and Paczynski, B. 1980, Acta Astr., 30,

Katz, J.I. 1976, Ap J., 206, 910.

Lawrence, A. and Elvis, M. 1981, Ap. J., in press.

Liang, E.P.T. 1979, Ap. J., 234, 1105.

Lightman, A.P. 1981, Ap. J., in press.

Lightman, A.P. and Band, D. 1981, Ap. J., in press.

Lightman, A.P. and Eardley, D.M. 1974, Ap. J. Lett., 187, L1.

Lightman, A. P., Giacconi, R. and Tananbaum, H., 1978, Ap. J., 224, 375.

Lightman, A.P. and Rybicki, G.B. 1979a, Ap J. Lett. 229, L15.

Lightman, A.P. and Rybicki, G.B. 1979b, Ap. J., 232, 882.

Lovelace, R.V.E. 1976, Nature, 262, 649.

Lynden-Bell, D. 1978, Phys. Scripta, 17, 185.

Maccacaro, T., Perola, G.C., and Elvis, M. 1981, Ap. J., in press.

Maraschi, L., Perola, G.C., Reina, C. and Treves, A. 1979, Ap. J., 230, 243.

Maraschi, L., Roasio, R. and Treves, A. 1981, Ap. J., 1981, in press.

McMillan, S.L.W., Lightman, A.P. and Cohn, H. 1981, Ap. J., in press.

Mushotzky, R.F. 1981, Ap. J., in press.

Mushotzky, R.F., Holt, S.S. and Serlemitsos, P.J. 1978, Ap. J. Lett., 225, L115.

Norman, M.L., Smarr, L. Wilson, J.R. and Smith, M.D. 1981, Ap. J., 247, 52.

Payne, D.G. 1980, Ap. J., 237, 951.

Pozdnyakov, L.A., Sobol, I.M. and Sunyaev, R.A. 1976, Sov. Astron. Lett., 2, 55.

Pringle, J.E., Rees, M.J. and Pacholczyk, A.G. 1973, Astr. Ap., 29, 179.

Rees, M.J. 1977, Ann. N.Y. Acad. Sci., 302, 613.

Rees, M.J. 1978, Phys. Scripta, 17, 193.

Rees, M.J. 1980, in Origin of Cosmic Rays, ed. G. Setti, and A. Wolfendale (Reidel).

Ricketts, M.J., Cooke, B.A. and Pounds, K.A. 1976, Nature, 259, 546.

Roos, N. 1981, PhD thesis, Uinversity of Leiden.

Schonfelder, V. 1978, Nature, 274, 344.

Schreier, E. et al. 1979, Ap. J. Lett., 234, L30.

Shakura, N.I. and Sunyaev, R.A. 1973, Astr. and Ap., 24, 337.

Shakura, N.I. and Sunyaev, R.A. 1976, M.N.R.A.S., 175, 613.

Shapiro, S.L., Lightman, A. P. and Eardley, D.M. 1976, Ap. J., 204, 187.

Shields, G.A. and Wheeler, J.C. 1978, Ap. J., 222, 667.

Spitzer, L. 1962, Physics of Fully Ionized Gases, (John Wiley and Sons: new York)

Spitzer, L. and Saslaw, W.C. 1966, Ap. J. 143, 400.

Stein, W.A., O'Dell, S.L. and Strittmatter, P.A. 1976, Ann. Rev. Astr. Ap., 14, 173.

Stoeger, W.R. 1977, Astr. Ap., 61, 659.

Svensson, R. 1981, preprint.

Takahara, F. 1980, Prog. Theo. Phys., 63, 1551.

Takahara, F., Tsuruta, S. and Ichimaru, S. 1981, Ap. J., in press.

Tananbaum, H. 1980, in X-ray Astronomy, ed. R. Giacconi and G. Setti (Reidel).

Tananbaum, H., Peters, G., Forman, W., Giaconni, R. and Jones, C. 1978, Ap. J., 223, 74.

Tennant, A.F., Mushotzky, R.F., Boldt, E.A. and Swank, J.H. 1981, Ap. J., in press.

Turner, E. 1979, Ap.J., 231, 231.

Winkler, P.F. and White, A.E. 1975, Ap. J. Lett., 199, L139.

CENTER FOR ASTROPHYSICS

PREPRINT SERIES

No. 1578

X-RAY ILLUMINATION OF GLOBULAR CLUSTER PUZZLES

A. P. Lightman and J. E. Grindlay
Harvard-Smithsonian Center for Astrophysics

To appear in
The Astrophysical Journal

Center for Astrophysics
60 Garden St.
Cambridge, Massachusetts 02138

Harvard College Observatory Smithsonian Astrophysical Observatory

Center for Astrophysics
Preprint Series No. 1578

X-RAY ILLUMINATION OF GLOBULAR CLUSTER PUZZLES

Alan P. Lightman and Jonathan E. Grindlay

Harvard-Smithsonian Center for Astrophysics

To appear in The Astrophysical Journal

Abstract

We enumerate many of the infamous puzzles presented by globular clusters, regarding their gross features, their internal dynamics, and their X-ray emission. We then focus on the latter puzzles; in particular, why do globular clusters provide a favorable environment for forming discrete X-ray sources, are X-ray emitting globular clusters (XEGC) unusually near the galactic center and, if so, why, and why do the observed clusters never contain more than a single discrete X-ray source. A statistical analysis of the data allows plausible explanations of these puzzles. Adopting the model that globular cluster X-ray sources consist of binary systems formed by two-body tidal interactions, we find a significant positive correlation between the two-body binary formation time scale, t_{B2}, and the distance from the galactic center, R, for globular clusters in general. We offer possible physical explanations of this result. XEGC are found to have significantly small values of R and t_{B2}. Furthermore, t_{B2} and the inferred lifetime of X-ray sources may be used to estimate the probability of observing an X-ray source in a cluster, and in the galaxy in general. We obtain rough quantitative agreement with the observed rate of occurrence of X-ray sources in globular clusters. If clusters are classed according to either R or t_{B2}, the probability of finding more than one X-ray source in a single cluster is less than 50%. Our data set consists of 116 clusters for which R is known, of which 8 are XEGC, and 84 clusters for which t_{B2} can be computed, of which 7 are XEGC.

I. Globular Cluster Puzzles

Because they are thought to be among the oldest objects in the galaxy, globular clusters provide important clues for determining the age and process of formation of the galaxy, as well as for verifying theories of stellar evolution. Furthermore, globular clusters are a theorist's paradise for the study of stellar dynamics, with a number of stars (10^5-10^6) large enough to eliminate the importance of highly stochastic effects and small enough to allow time for interesting gravitational evolution, such as energy equipartition and core collapse. In short, there is a great deal to be learned from globular clusters, and the task is, in principle, within our reach.

Despite our continued attack, however, there remain quite a few unsolved puzzles regarding globular clusters. In this paper, we address those puzzles relating to the x-ray emission of globular clusters:

Why do globular clusters provide a particularly favorable environment for the formation of galactic x-ray sources, as first pointed out by Katz (1975)? The ~100 known globular clusters in our galaxy contain only ~10^{-4} of the mass of the galaxy; yet ~10 of the ~100 known galactic x-ray sources lie in globular clusters.

Is it true that x-ray emitting globular clusters (XEGC) are located unusually near the galactic plane and/or galactic center and, if so, why?

Why is there never more than one compact x-ray source observed in a globular cluster?

In addition to these puzzles, one can list: why are globular clusters so weakly gravitationally bound compared to galaxies? Why are globular clusters remarkably similar in size and mass, considering the large range of scales between galaxies and globular clusters? Why is there a large variation in the numbers of clusters in otherwise similar galaxies? Why do globular clusters differ systematically in metal abundance from one galaxy to another? Why are binaries so rare in globular clusters? Why do observed spatial distributions of stars in globular clusters show no evidence of the core collapse predicted by dynamical, theoretical models? What is the explanation for the strikingly smooth and simple distribution observed for central relaxation times in globular clusters?

Almost certainly some of these puzzles are intimately related, with a common resolution, and it is for this reason that we have collected them together. We hope that a probe of the first three puzzles, those involving the XEGC, may ultimately bring us closer to an understanding of globular clusters in general.

II. X-RAY EMITTING GLOBULAR CLUSTERS

The reader may consult the recent reviews by Lewin and Clark (1980) and by Grindlay (1981) for a comprehensive summary of observational data and ideas regarding the XEGC.

A. Model of X-ray Sources in Globular Clusters

There are several independent lines of evidence to suggest that the globular cluster X-ray sources are close binary star systems, in which gas is transferred from a normal star to a compact companion, probably a neutron star. This model was suggested by Katz (1975) and by Clark (1975). (1) The binary nature of a number of X-ray sources outside of globular clusters has long been known. (2) The generally accepted nuclear flash model for X-ray bursters (e.g. Joss 1978 and references therein), many of which are in globular clusters, employs gas accumulation onto a neutron star. (3) Analysis of the observed black-body-like spectrum during X-ray bursts (Swank et al. 1977, van Paradijs 1978) indicates a characteristic emitting radius of ∿10 km, typical of the size of neutron stars. (4) Finally, a statistical analysis of the positions of the X-ray sources within the XEGC, assuming energy equipartition and employing the method of Lightman, Hertz and Grindlay (1980), indicates the mass of a typical globular cluster X-ray source is between 2 and 11 times the mean mass of a star, at the 10% likelihood level (Grindlay 1981, Grindlay et al. 1982).

The absence of observed peridicities and eclipses from the globular cluster X-ray sources imposes certain requirements on the above model. The absence or periodicities, normally assiciated

with a strong magnetic field inclined with respect to the neutron star rotation axis, may simply result from the decay of the magnetic field (e.g. Gunn and Ostriker 1970). Since globular clusters are old systems, most of their neutron stars might be expected to be quite aged. (However, recent results showing that X-ray bursters radiate above the Eddington limit, e.g. Grindlay et al. 1980, may require strong magnetic fields to confine the radiating gas.) The absence of eclipses could be due to the geometry of the binary systems, particularly if the compact object is fueled by Roche lobe overflow from a low-mass companion star (e.g. Joss and Rappaport 1979).

We will tentatively adopt the above model for globular cluster X-ray sources.

B. Formation, Lifetime and Probability of Occurrence

As Clark (1975) has pointed out, the great age of globular clusters suggests that globular cluster X-ray binaries are formed through the capture of stars in the cluster by single compact remnants of massive (cluster) stars, rather than by the evolution of primordial binaries. The preferred mechanism here for binary formation is the two-body, tidal-interaction process first suggested by Fabian, Pringle and Rees (1975). This process for forming binaries occurs at least 100 times more rapidly than the dissipationless three-body process, for parameters typical of globular clusters (see, e.g. Lightman and Shapiro 1978), and automatically produces a close binary of the type required to produce an X-ray source.

If we require a pericenter separation $\ell = 3r_*$ between the two approaching stars in order to dissipate sufficient orbital energy for forming a binary (e.g. Press and Teukolsky 1977), the time scale for two-body binary formation per globular cluster is calculated to be

$$t_{B2} = 7\times10^{13}\ \text{yr.}\ \left(\frac{v_c}{1\ \text{km s}^{-1}}\right)^{-2}\left(\frac{n_c}{1\ \text{pc}^{-3}}\right)^{-1/2}\left(\frac{f}{.03}\right)^{-1}\left(\frac{r_*}{R_\odot}\right)^{-1}\left(\frac{m_*}{M_\odot}\right)^{1/2}. \quad (1)$$

Here v_c and n_c are the central values of the root mean square velocity dispersion and stellar density in the globular cluster, r_* and m_* are the radius and mass of the captured field star, and f is the fraction of core stars that are compact remnants. Henceforth, we will set r_* and m_* to their solar values. To obtain equation (1) we included the effects of gravitational focussing (cross section goes as r_* and not r_*^2), used the virial theorem, and set the rate of binary formation per star averaged through the core equal to a tenth the rate at the center of the cluster. We refer the reader to the review of stellar dynamics in Lightman and Shapiro (1978).

The quantities v_c and n_c, or equivalently core radius and n_c, may be measured for each cluster. The fraction f is unknown, but may be estimated on the basis of the globular cluster mass function or by fitting dynamical models to the observed light distribution (Da Costa and Freeman 1976, Illingworth and King 1977, Gunn 1980). In a fit to the cluster M3, Gunn (1980) obtains remnant fractions f = .03 for the dominant mass classes. In a fit to M15, Illingworth and King (1977) obtain a value $f \sim 0.01$ for the neutron star population. Hills (1976) has pointed out

that exchange encounters are likely, in which a compact remnant would replace a member of a binary composed of normal stars. This process would increase the effective value of f. In any case, we will make the simplifying assumption that f is the same for all globular clusters and treat all compact remnants as neutron stars.

We will roughly approximate the lifetime of the X-ray source, τ_x, as the time to transfer 1 $M_\odot$ from the normal star to its compact companion. If we assume the efficiency of mass to energy conversion is $\sim$10% (appropriate for a neutron star) and all of the energy produced is observed in the X-ray luminosity, L_x, then

$$\tau_x = 7\times10^{8}\ \text{yrs}\ \left(\frac{L_x}{10^{37}\ \text{erg s}^{-1}}\right)^{-1}. \quad (2)$$

The probability P_x of observing an X-ray source in a given globular cluster is then, for $P_x \leq 1$,

$$P_x \sim \tau_x / t_{B2}\ . \quad (3)$$

When $P_x > 1$, that quantity may be interpreted as the expected number of X-ray sources in the cluster. The expression given in equation (3) is closely related to, but more general than, Clark's (1975) estimate for the expected number of observed globular cluster X-ray sources, N_x. Letting N_R be the total number of binaries that have been formed and ξ be the fraction of normal stars that are now overflowing their Roche Lobes,

Clark obtains $N_X = N_R \xi$. If we make the identification $\xi = \tau_x / t_o$, where t_o is the age of the cluster, and $N_R = t_o / t_{B2}$, then the two expressions become equivalent. If we assume that the available population of normal stars and hence τ_x does not vary much between clusters, then equation (3) yields $P_x \propto t_{B2}^{-1}$, an hypothesis that can be tested.

Finally, we will compute the probability that no single clusters contain more than one X-ray source. Let there be n globular clusters in the same class, defined by some common value of a significant parameter such as the two-body-binary formation time scale or the distance from the galactic center. Let there be m X-ray sources independently distributed with equal probability among these n clusters. Then the probability $P(m,n)$ that every X-ray source be located in a different cluster is, for $m \leq n$,

$$P(m,n) = \frac{n!}{n^m (n-m)!} . \qquad (4)$$

We will use this expression to confront puzzle 10.

III. DATA ANALYSIS

Table 1 presents the data used in our analysis. The data for the distances R from the galactic center were taken from Harris and Racine (1979), with the exception of the last three clusters, where we made our own estimates using the observed angular coordinates and an assumed distance from earth of 10 kpc. There are 116 clusters in all with tabulated R. The data for

the central velocity dispersions, central number densities, and central relaxation times t_{rc}, were taken from Peterson and King (1977), with the exception of Liller 1 and Terzan 2, where the data were taken from Malkan, Kleinmann and Apt (1980) using the most metal rich (conservative) values. The central relaxation times appear in column 2. From the data for v_c and n_c and equation (1) we computed the two-body binary formation time for each cluster, given in the fourth column. There are 84 clusters in all with tabulated t_{rc} and t_{B2}. Blank spaces indicate no data is available.

The last 8 clusters in the data set are those we have designated as X-ray emitting globular clusters, XEGC. Specifically, all such clusters have X-ray luminosities $L_x \geq 10^{36}$ erg $s^{-1} \equiv L_e$ in the 0.5 - 4.5 keV energy band. The luminosity L_e was chosen to be higher than the highest upper limit assigned by the Einstein satellite to clusters for which no positive X-ray detection has been made (see, e.g. Grindlay 1981). (NGC 2419 has the largest upper limit, $L_x < 0.9\ L_e$.) Data for L_x were taken from Grindlay (1981) and are given in the fifth column, only for the 8 XEGC. (NGC 104 has a positive X-ray detection $L_x = 0.03\ L_e$, but is not one of the XEGC by our definition.) All of the XEGC contain a single discrete X-ray source (see Grindlay et al. 1982 for methods of verification and details of the X-ray images). Excluded from our set of XEGC are Terzan 1 and Terzan 5, with R values of 1.1 kpc and 1.2 kpc, respectively. These clusters have been tentatively identified with X-ray burst sources (Grindlay 1981, Makishima et al.

1981), but the persistent X-ray emission and source identification have not been ascertained with the Einstein satellite.

A. Distribution in R

We first test the hypothesis that the XEGC are unusually near the galactic center, an oft-stated premise. There is an important selection effect that must be removed in testing correlations between X-ray emission and distance to galactic center. Because of obscuration and confusion, it is more difficult to detect clusters near the galactic center than far from the galactic center, at optical wavelengths. To eliminate this bias in a conservative manner, all XEGC first identified by X-ray emission must be excluded from the data analysis. In practice, this eliminates Liller 1 and Grindlay 1, reducing the effective number of XEGC for this analysis from 8 to 6. (For the analyses in C. and D. below, not explicitly subject to this selection effect, the full data set will be used.)

We have computed the probability distribution $P_6(\bar{R})$ of the mean value of R of a random subset of 6 clusters drawn from the population of 108 non-XEGC. $P_6(\bar{R})d\bar{R}$ is the probability this mean would lie between R and $\bar{R}+d\bar{R}$. $P_6(\bar{R})$ is shown in Figure 1 and was computed by filtering the Fourier transform $\phi_6(k)$, defined by

$$\phi_6(k) \equiv \int e^{\frac{ik}{6}(R_1+R_2+..R_6)} \; p(R_1)p(R_2)...p(R_6) \; dR_1dR_2...dR_6 \; . \tag{5a}$$

Here p(R), the distribution in R, is taken to be a normalized sum of delta functions centered on the observed values of R, $\bar{R}_i$, for the non XEGC,

$$p(R) = \frac{1}{108} \sum_{i=1}^{108} \delta(R-\bar{R}_i) \; . \tag{5b}$$

Filtering $\phi_6(k)$, i.e. imposing $\phi_6(k) = 0$ for $k > k_{max}$, serves to smooth out features arising from the delta functions in p(R). Inverting the filtered $\phi_6(k)$ then yields $P_6(\bar{R})$. In Figure 1 we have used $k_{max} = (0.25 \text{ kpc})^{-1}$, but our results are not sensitive to this value, as confirmed by a number of different trials.

Note the strong bimodal characteristic of $P_6(\bar{R})$, indicating distinct "bulge" and "halo" populations. Application of the central limit theorem to estimate $P_6(\bar{R})$ would have been disastrous here, yielding a Gaussian distribution centered on 11.7, the mean R of the 108 non-XEGC. (Of course, $P_6(\bar{R})$ also has a mean $\bar{R}$ of 11.7.)

The mean R of the 6 XEGC is $\bar{R}_x = 5.8$. From $P_6(\bar{R})$ we compute that the probability $\bar{R}$ could be this small or smaller is 0.12. Thus, on this basis, it is unlikely the XEGC are part of the same population as the non-XEGC. (This test, when applied to the full set of 8 XEGC, yields a probability of 0.018.)

We also used a completely independent statistical test, the Kolmogorov-Smirnov test (see e.g., Lehman 1975) and ranked all 114 clusters according to R. If the XEGC clusters are typical of all clusters in their values of R, then their ranks should be uniformly distributed between 1 and 114. The cumulative, normalized distribution in ranks of the XEGC have a maximum deviation of 0.44 from a uniform distribution; the probability of this value, for 6 objects

drawn randomly from a uniform distribution, is 0.071. This test again confirms the fact that the XEGC have significantly smaller values of R than the non-XEGC. (This test, when applied to the full set of 8 XEGC, yields a probability of 0.005. A similar probability is obtained if Terzan 1 and Terzan 5 are included instead of Liller 1 and Grindlay 1.)

We performed the same K-S test on the globular clusters in M31, using optical data from Battistini et al. (1980) and Sargent et al. (1977) and X-ray data from van Speybroeck (1981). In M31 there are 323 globular clusters identified, 20 of which contain discrete X-ray sources. The XEGC have significantly small values of projected radius, R_p; the K-S test gives a probability of 9.8×10^{-3} their ranks could have been drawn from a uniform distribution.

B. Distribution in z

We also performed the K-S test for the distribution in height above the galactic plane, z (data not shown in Table 1), yielding a probability of 0.22. Finally we performed a Komogorov-Smirnov test on the distribution of a "flatness-parameter" $P \equiv 3z^2/R^2$ and found that the XEGC do not have an abnormal distribution of this parameter.

From these tests, we conclude that the XEGC are indeed correlated with small R, and that their small values of z are probably a consequence of the first correlation.

C. Correlations Between R and t_{B2}

Evidently, there is something about proximity to the galactic center that favors creation of an XEGC out of an ordinary globular cluster. To test the hypothesis that a relatively low value

of t_{B2} is also correlated with the XEGC, and with small R in general, we consider the location of clusters in the t_{B2}-R plane, shown in Figure 2. It is clear that the XEGC have relatively low values of t_{B2}. A Kolmogorov-Smirnov test on the ranks of t_{B2} for the XEGC shows the probability they could have been drawn from a uniform distribution is .036. More generally, there is a positive correlation of R with t_{B2} for all 84 globular clusters for which data are available. Using a Spearman's rank correlation test (see, e.g. Lehman 1975) for R vs. t_{B2}, we find that the probability the observed correlation could be accidental is $1 - \mathrm{erf}(2.2) \simeq 2 \times 10^{-3}$, where erf(x) is the error function of x. (The Spearman's test assigns a rank in R and a rank in t_{B2} to each cluster, defines a function of the square of the difference in these two ranks, summed over all clusters and then computes the probability this function could be as large and positive or as large and negative as it is for arrays of ranks chosen randomly.)

D. Correlations Between R and t_{rc}

It was originally pointed out by Bahcall and Ostriker (1975) that the XEGC (only 4 were known at that time) had relatively low values of the central relaxation time, t_{rc}. In terms of v_c and n_c, t_{rc} may be written as (setting the logarithm term to a constant)

$$t_{rc} = 6 \times 10^9 \text{ yrs.} \left(\frac{v_c}{1 \text{ km s}^{-1}}\right)^3 \left(\frac{n_c}{1 \text{ pc}^{-3}}\right)^{-1} , \qquad (6)$$

and is the time for energy exchange via cumulative two-body gravitational scatterings. Core collapse of a self-gravitating system occurs on a time scale $\sim 100\ t_{rc}$ and such a collapse could produce conditions favorable for forming an X-ray source. Bahcall and Ostriker argued that clusters that had undergone core collapse were those likely to have formed massive black holes, which they took as a model for globular cluster X-ray sources. For a variety of reasons (see §II.A.) such a model now seems unlikely, but core collapse does very definitely decrease the time scale for two-body binary formation, as both v_c and n_c increase in core collapse. This would promote formation of an X-ray source according to our adopted model.

To test the hypothesis of a correlation between R and t_{rc} for globular clusters in general, we consider the location of clusters in the t_{rc}-R plane, shown in Figure 3 (van den Bergh, 1980, considered a similar diagram.) There is a positive correlation. A Spearman's test for R vs. t_{rc} reveals that the probability the observed correlation could be accidental is $1 - \mathrm{erf}(3.4) \gtrsim 2 \times 10^{-6}$.

IV. DISCUSSION AND CONCLUSIONS

A. Bulge Population Association

The first of our analyses reveals that the XEGC are significantly nearer the galactic center than the average globular cluster. If we define the "galactic bulge" as the region $R \leq 4$ kpc, then 4 out of 34

globular clusters in the galactic bulge are XEGC (again using the reduced, optically-selected sample that excludes Liller 1 and Grindlay 1). If all of the bulge clusters were equally likely to harbor an X-ray source, then the probability that every X-ray source be located in a different cluster, as observed, is from equation (4), $P(4,34) = 0.83$.

If it is only the value of R, rather than some other parameter such as t_{B2}, that determines the probability of forming an XEGC, then one must search for an acceptable physical explanation associated only with R. One possibility is that clusters with small apocenter pass near the galactic center more frequently than other clusters, and that each passage may somehow create an X-ray source, e.g. by forming a binary or accumulating gas. However, if such sources are binary systems, then their lifetime, cf. equation (2), is longer than an orbital period for many clusters outside of the bulge, so we should expect to see many XEGC in that region also, and we do not.

Another possibility is that the relatively high metal abundances found in clusters nearer to the galactic center (e.g. van den Bergh 1980) are associated with likelihood of forming an X-ray source. This might be the case if such higher abundances indicate a higher initial population of massive stars and possibly a higher number of compact remnants (Grindlay 1981).

B. Two-Body Binary Formation Rate Association

If the model for X-ray sources in globular clusters discussed in §II.A and B is relevant, then the probability of observing an

X-ray source in a cluster, P_x, should vary inversely with t_{B2}, cf. equation (3). Small number statistics make it difficult to reliably test this expectation, but we have made an attempt by binning the data into half decade logarithmic intervals, shown in Table 2. In each range of t_{B2}, the observed P_x is the number of XEGC divided by the total number of clusters. It can be seen that the data are not inconsistent with $P_x \propto t_{B2}^{-1}$.

There is a further quantitative check on P_x. The last column in Table 2 computes the "theoretical" value of P_x, using equation (3), a typical L_x of 10^{37} erg s^{-1} in equation (2), and an average value of t_{B2} for each range in the first column of Table 1. The values of f and L_x are not arbitrary, but consistent with observations, so the theoretical values of P_x cannot be freely scaled. That these values do not differ substantially from the observed values, cf. columns 4 and 5 of Table 2, gives further support to our adopted model for the nature and formation of X-ray sources in clusters. For example, binary formation by the three-body process alone yields less than one expected XEGC.

Table 2 also explains, within the adopted model, why two X-ray sources are never seen in the same cluster, in answer to one of our puzzles. If the probability of forming an X-ray source is uniform for all clusters in each range of t_{B2}, then equation (4) gives P(3,8) = 0.66 for clusters in the next to last row, and higher values for the others. Thus either by this analysis, or the analysis treating all bulge clusters on equal footing as in A. above, it is not surprising that two X-ray sources are not found in any one cluster.

We can attempt to push the two-body-binary-formation model one step further. If all the X-ray sources in the galactic bulge region outside of globular clusters are also formed by this process, then the expected number observed should be, cf. equation (3), $N_{XG} \sim \tau_x / t_{B2G}$. Here t_{B2G} is the two-body binary formation time scale for the galactic bulge as a whole, and can be computed to be

$$t_{B2G} \sim 4\times10^8 \text{ yrs } \left(\frac{n}{0.1 \text{ pc}^{-3}}\right)^{-1} \left(\frac{v}{250 \text{ km s}^{-1}}\right) \left(\frac{N}{10^{11}}\right)^{-1} \left(\frac{f}{.03}\right)^{-1}, \quad (7)$$

where N is the total number of stars and n and v are characteristic densities and velocities, normalized to their expected values. (In equation (1), appropriate for globular clusters, the virial theorem was used to express N in terms of n and v.) Using $L_x = 10^{37}$ erg s^{-1} again as a characteristic value in τ_x, we obtain from equations (2) and (7), $N_{XG} \sim 1$. That this computed number, at least based on the assumed values of the parameters, is considerably smaller than the observed value of ~ 30 suggests that most bulge X-ray sources may require a mechanism of formation other than capture of a general field star by a compact remnant. For example, the evolution of white dwarf binary systems, e.g., cataclysmic variables, into compact neutron star binary systems does not produce a system with the high X-ray luminosities observed, as shown by Rappaport, Joss and Webbink (1981). The origin of the galactic bulge X-ray sources outside globular clusters constitutes another puzzle. Such sources may, in fact, originate in globular

clusters. In any case, this analysis and equation (7) do give some semi-quantitative explanation for the fact that globular clusters, relative to their total mass, provide a favorable environment for the formation of X-ray sources, in answer to one of our puzzles.

C. Influence of the Galactic Center

The positive correlations of t_{B2} and t_{rc} with R, cf. Figures 2 and 3, motivate a physical explanation in which proximity to the galactic center produces a cluster with relatively low values of t_{B2} and t_{rc}. We offer two possibilities, involving either the initial conditions or the initial dynamical evolution. The relatively high densities of matter near the galactic center, at the initial time of formation of the clusters, may have produced clusters with relatively low values of t_{B2} and t_{rc}. Alternatively, the relatively strong shock heating of clusters passing near the galactic center could have hastened the rate of collapse of such clusters by increasing the initial rate of core contraction, cf. Spitzer (1975). In either of these possibilities, the effective initial distributions of t_{B2} and t_{rc} among the clusters would have been R-dependent, thus modifying the analysis of Lightman, Press and Odenwald (1978) regarding the distribution of central relaxation times.

In any case, the observed correlation of R with t_{B2} for globular clusters in general, together with our adopted model for globular cluster X-ray sources, affords an explanation to one of our puzzles.

In conclusion, the positive correlation found between distance from galactic center and two-body binary formation time for

globular clusters in general, plausible cause and effect explanations for this correlation, and the strongly supported hypothesis that X-ray sources in globular clusters require binary star systems give a possible explanation of several of the puzzles regarding X-ray emitting globular clusters.

Acknowledgments

We thank y. Avni, G. Rybicki and L. van Speybroeck for useful discussions and G. Clark for comments on the manuscript. This work was supported in part by NASA grants NAGW 246 and NAS 8-30751.

TABLE 1

CLUSTER	t_{rc} (yrs)	R (kpc)	t_{B2} (yrs)·f	L_x/L_*
104	8.3E+07	8.20	9.4E+07	
286	1.2E+09	12.30	8.0E+10	
362	7.1E+07	10.20	1.3E+08	
1261	4.9E+08	16.10	3.1E+09	
PAL 1		52.00		
1904	1.4E+08	20.00	1.4E+09	
2298	2.3E+08	17.90	9.8E+09	
2419	1.2E+10	101.30	2.3E+10	
2808	1.6E+08	11.50	7.1E+07	
PAL 3	4.2E+09	29.40	1.1E+13	
3201	2.9E+08	9.70	3.4E+09	
PAL 4	6.9E+09	96.30	4.5E+12	
4147	1.3E+08	20.20	1.2E+10	
4372		7.80		
4590	4.7E+08	10.20	3.2E+09	
4833	6.3E+08	7.60	2.6E+09	
5024	1.1E+09	18.10	2.5E+09	
5053	5.4E+09	16.20	6.8E+11	
5139	3.5E+09	7.10	4.7E+08	
5272	4.3E+08	12.40	6.8E+08	
5286	7.1E+07	7.50	2.5E+08	
5466	2.8E+09	15.30	1.5E+11	
5634		17.50		
5694	1.6E+08	26.10	1.3E+09	
4499	2.5E+09	15.40	1.6E+11	
5824	4.7E+07	17.10	8.7E+07	
PAL 5		16.50		
5897	3.0E+09	6.90	4.1E+10	
5904	2.4E+08	6.70	5.6E+08	
5927	2.2E+08	5.00	8.7E+08	
5946		5.30		
5986	4.4E+08	4.50	8.2E+08	
PAL 14		60.00		
6093	2.5E+07	3.20	1.4E+08	
6101		8.60		
6121	1.2E+08	7.00	1.6E+09	
6139		3.00		
6144	1.8E+08	2.80	1.4E+10	
6171	2.0E+08	4.30	1.3E+10	
6205	3.1E+08	9.10	1.0E+09	
6218	2.8E+08	5.10	4.4E+09	
6229	2.3E+08	30.60	2.7E+09	
6235		2.80		
6254	1.5E+06	5.50	1.1E+09	
6266	8.0E+07	3.20	1.5E+08	
6273	3.6E+07	2.40	5.3E+08	
6284	6.8E+06	2.00	3.4E+08	
6287	5.7E+07	1.70	4.9E+09	
6293	1.5E+07	2.00	2.8E+08	
6304	1.3E+08	3.70	1.3E+09	
6316		3.50		
6325	1.4E+08	2.50	2.4E+09	

6333	9.6E+07	2.70	6.2E+08	
6341	6.6E+07	10.90	2.5E+08	
6342		6.70		
6352	2.2E+08	4.30	5.7E+09	
6355		2.30		
6356	3.5E+08	8.60	3.3E+08	
6362	1.3E+09	5.60	1.5E+10	
6366		5.60		
6388	1.3E+08	6.30	2.7E+07	
6397	2.3E+07	7.10	1.1E+09	
6401		2.30		
6402	1.6E+09	4.40	2.0E+09	
PAL 6		6.10		
6426	3.1E+08	9.60	1.1E+11	
6440	3.0E+07	6.60	2.5E+07	
6453		2.10		
6496		2.40		
6517	1.7E+07	3.20	6.4E+07	
6522	1.4E+07	2.60	1.2E+08	
6528	3.5E+07	1.40	3.0E+08	
6535		5.30		
6539		6.90		
6541	6.7E+07	3.00	2.5E+08	
6544		4.40		
6553	3.4E+08	3.30	4.5E+08	
6558		1.00		
PAL 7		5.80		
6569	8.1E+07	1.60	6.6E+08	
6584		7.30		
6626	5.2E+07	3.10	2.4E+08	
6637	7.0E+08	2.20	6.5E+08	
6638	1.3E+09	1.90	1.5E+09	
6642		3.20		
6652		6.40		
6656	5.5E+08	6.10	4.3E+08	
PAL 8		22.00		
6681	2.3E+07	2.90	2.0E+08	
6715	1.4E+08	13.00	6.0E+07	
PAL 9		7.50		
6723	6.0E+08	2.70	4.1E+09	
6752	8.9E+07	6.00	3.6E+08	
6760	2.1E+07	6.30	1.2E+09	
6779	5.4E+08	9.70	4.4E+09	
PAL 10		7.90		
6809	9.6E+08	4.60	7.1E+09	
PAL 11		6.70		
6838	8.1E+07	7.60	9.6E+09	
6864	7.8E+07	11.70	1.9E+06	
6934	4.2E+08	12.00	1.2E+09	
6981	7.2E+08	12.90	1.6E+10	
7006	1.2E+09	32.10	1.1E+10	
7089	4.2E+08	10.50	2.2E+08	
7099	1.5E+07	7.60	2.0E+08	
PAL 12		15.60		
PAL 13		25.70		
7492	9.6E+08	21.30	5.3E+11	
1851	3.0E+07	16.40	9.6E+07	1.0
6441	7.6E+07	1.90	4.4E+07	3.7
6624	2.5E+07	1.40	2.5E+08	52
6712	3.5E+08	4.00	2.3E+09	1.2
7078	1.2E+08	10.30	9.6E+07	3.0

TER 2	1.0E+07	0.70	8.0E+08	3.1
LIL 1	2.5E+07	0.90	1.1E+08	8.8
GRI 1		0.90		12

Table 2

$t_{B2} \cdot (\frac{f}{0.03})$	Total Number of Clusters	Number of X-ray Clusters	P_x Observed	P_x Theoretical
$>10^{11}$ yrs	24	0	0	<.007
3.2×10^{10}-10^{11}yrs	16	1	.063	.011
10^{10}-3.2×10^{10}yrs	17	1	.059	.033
3.2×10^{9}-10^{10}yrs	17	2	.12	.11
10^{9}-3.2×10^{9}yrs	8	3	.38	.33
$<10^{9}$ yrs	2	0	0	>1

REFERENCES

Bahcall, J.N. and Ostriker, J.P. 1975, Nature, 256, 23.

Battistini, P., Bonoli, F., Braccesi, A., Fusi Pecci, F. Malagnini, M.L., and Marano, B. 1980, Astr. Ap. Suppl., 42, 357.

Clark, G.W. 1975, Ap. J. Lett., 199, L143.

Da Costa, G.S. and Freeman, K.C. 1976, Ap. J., 206, 128.

Fabian, A.C., Pringle, J.E. and Rees, M.J. 1975, M.N.R.A.S., 172, 15P.

Grindlay, J.E. 1981, in X-Ray Astronomy with the Einstein Satellite, ed. R. Giacconi (D. Reidel).

Grindlay, J.E., Hertz, P., Steiner, J., Murray, S. and Lightman, A.P. 1982, in preparation.

Grindlay, J.E., Marshall, H., Hertz, P., Soltan, A., Weisskopf, M., Elsner, R., Ghosh, P., Darbro, W. and Sutherland, P. 1980, Ap. J. (Letters), 240, L-121.

Gunn, J.E. 1980, in Globular Clusters, ed. D. Hanes and B. Madore, (Cambridge University Press).

Gunn, J.E. and Ostriker, J.P. 1970, Ap. J., 160, 979.

Harris, W. and Racine, R. 1979, Ann. Rev. Astron. Astrophys., 17, 241.

Hills, J.G. 1976, M.N.R.A.S., 175, 1P.

Illingworth, G. and King, I. 1977, Ap. J. (Letters), 218, L109.

Joss, P.C. 1978, Ap. J. Lett., 225, L123.

Joss, P.C. and Rappaport, S. 1979, Astron. Astrophys., 71, 217.

Katz, J.I. 1975, Nature, 253, 698.

Lehman, E.L. 1975, Nonparametrics: Statistical Methods Based on Ranks, (Holden-Day, Inc., San Francisco).

Lewin, W. and Clark, G. 1980, Ann. N.Y. Acad. Sci., 336, 451.

Lightman, A.P., Hertz, P. and Grindlay, J.E. 1980, Ap. J., 241, 367.

Lightman, A.P., Press, W.H. and Odenwald, S. 1978, Ap. J., 219, 629.

Lightman, A.P. and Shapiro, S.L. 1978, Rev. Mod. Phys., 50, 437.

Makishima, K., et al. 1981, Ap. J. (Letters), 247, L23.

Malkan, M., Kleinmann, D. E., and Apt, J. 1980, Ap. J., 237, 432.

Peterson, C. J., and King, I. R. 1977, unpublished revision of 1975, A. J., 80, 427.

Press, W.H. and Teukolsky, S.A. 1977, Ap.J., 213, 183.

Rappaport, S., Joss, P. C., Webbink, R. 1981, Ap. J., in press.

Sargent, W. L. W., Schechter, P. L., Boksenberg, A., and Shortridge, K. 1977, Ap. J., 212, 326.

Spitzer, L. 1975, in Dynamics of Stellar Systems, ed. A. Hayli (D. Reidel).

Swank, J.H., Becker, R.H., Boldt, E.A., Holt, S.S., Pravdo, S.H., and Serlemitsos, P.J. 1977, Ap. J. Lett., 212, L73.

van den Bergh, S. 1980, in Globular Clusters, ed. D. Hanes and B. Madore, (Cambridge University Press).

van Paradijs, J. 1978, Nature, 274, 650.

van Speybroeck, L.P. 1981, in preparation.

FIGURE CAPTIONS

Figure 1: Probability distribution of the mean value of distance to galactic center $\bar{R}$ of a random subset of 8 globular clusters. This distribution is calculated from the 108 non X-ray emitting globular clusters, according to the filtered Fourier transform method described in the text. The mean value of R of the 8 X-ray emitting globular clusters is $\bar{R}_x = 4.6$.

Figure 2: Scatter diagram of the two-body formation time versus distance from the galactic center, R, for 84 globular clusters. The positions of the X-ray emitting clusters and non X-ray emitting clusters are indicated by + and ·, respectively. For this diagram we used a value f = 0.1 in equation (1).

Figure 3: Scatter diagram of the central relaxation time versus distance from the galactic center, R, for 84 globular clusters. The positions of the X-ray emitting clusters and non X-ray emitting clusters are indicated by + and ·, respectively.

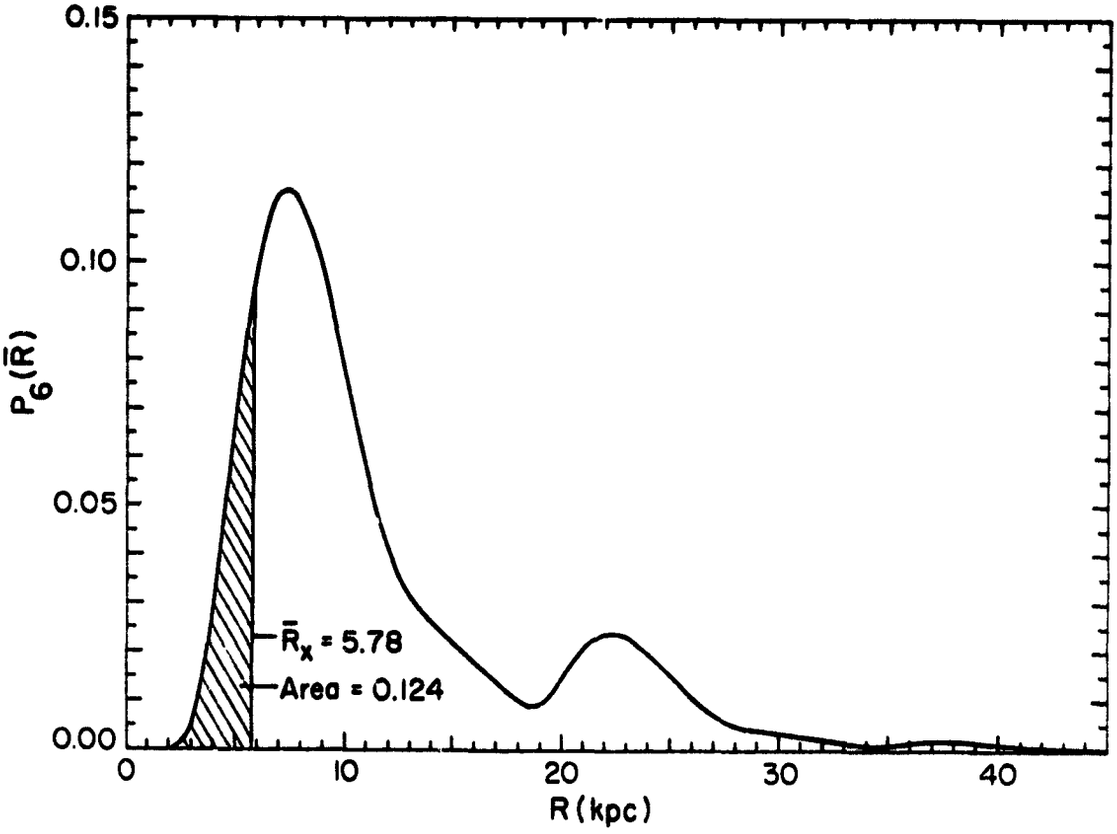

FIGURE 1

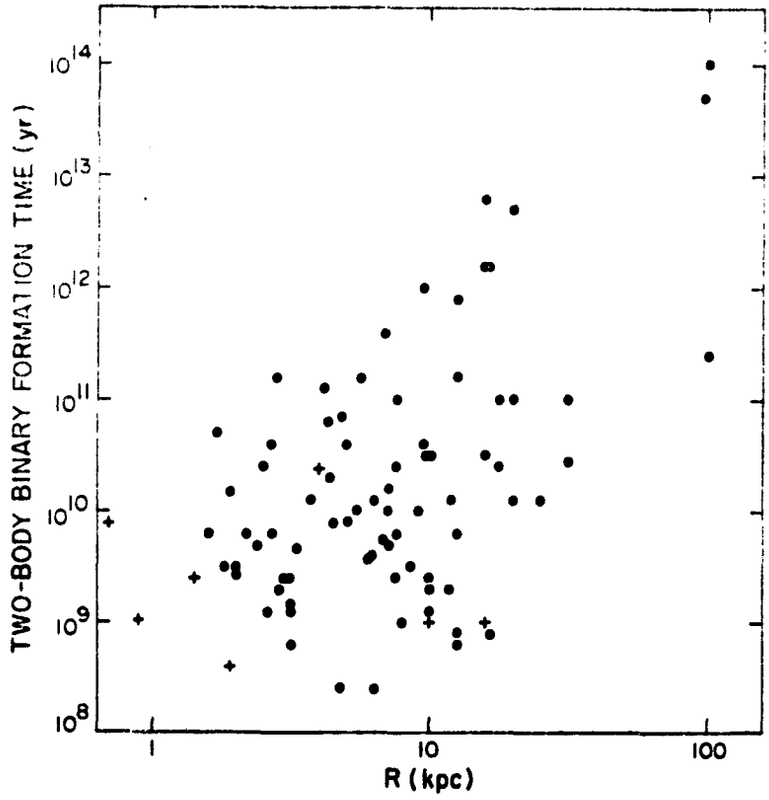

Figure 2.

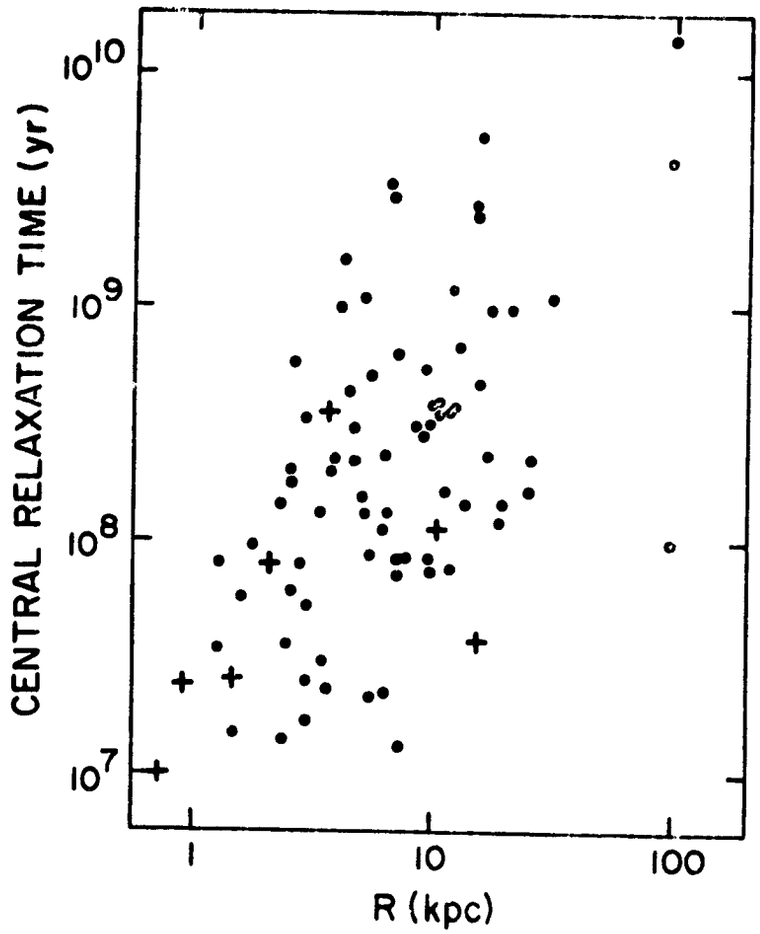

Figure 3.